Numerical Simulation of Entrainment and Recirculating Flow at the Base of a Truncated Aerospike Nozzle with Supplementary Base Flow

by

Venkatraman Nagarajan

A Thesis Presented in Partial Fulfillment
of the Requirements for the Degree
Master of Science

Approved July 2017 by the
Graduate Supervisory Committee:

Daniel B White, Co-Chair
Werner Dahm, Co-Chair
Huei-Ping Huang

ARIZONA STATE UNIVERSITY
August 2017

ABSTRACT

The aerospike nozzle belongs to the class of altitude compensating nozzles making it a strong candidate for Space Shuttle Main Engines. Owing to their higher efficiency compared to conventional bell nozzles, the aerospike nozzles are being studied extensively and are being used for many Single State to Orbit (SSTO) designs. A rocket engine nozzle with altitude compensation, such as the aerospike, consumes less fuel than a rocket engine with a bell nozzle. Aerospike nozzles are huge and are often difficult to construct and have to be truncated in order to make them feasible for application in a rocket propulsion system. Consequently, truncation of the aerospike leads to pressure loss under the base, which in-turn decreases the overall thrust produced by the rocket nozzle. To overcome this loss, a technique called base bleed is implemented in which a secondary jet is made to flow through the base of the truncated portion. This thesis uses dynamic pressure contour plots to find out the ideal base bleed mass flow rate to avoid base recirculation in 10 %, 20 % and 30 % truncated aerospike nozzles.

ACKNOWLEDGMENTS

I would like to thank Dr Daniel B.White for guiding me through this thesis work and helping me get a clear idea of the subject in hand. Furthermore, I would like to thank him for his encouragement and his valuable inputs throughout.

I would like to thank Dr Werner Dahm for agreeing to be my co-chair for this thesis.

Finally, I would like to thank Dr Huei-Ping Huang and Dr Werner Dahm for agreeing to be a part of my committee for this thesis.

TABLE OF CONTENTS

Page

LIST OF FIGURES

Figure Page

Figure Page

Figure Page

Figure Page

CHAPTER 1

ROCKET ENGINE NOZZLE

A rocket engine nozzle is used in a rocket engine to expand and accelerate the combustion gases produced by burning propellants so that the exhaust gases exit the nozzle at hypersonic velocities. In other words the nozzle is responsible for accelerating high pressure high temperature gas to a very high velocity thereby producing a large amount of thrust. There are quite a few different types of nozzles in use namely the conical nozzles, bell nozzles, expansion deflection nozzles, plug nozzles (aerospike) and annular & linear aerospike nozzles.

Nozzle Thermodynamics(Barrere, Jaumotte, Fraeijs de Veubeke, & Vandenkerckhove, 1960; Farley & Campbell, 1960; Frey & Hagemann, 1999; Hagemann, Immich, Nguyen, & Dumnov, 1998; HOFFMAN, 1987; Knauber, 1996; Koelle, 1961; LILLEY, 1986, 1987; Muss et al., 1997; Rao, 1958, 1961; Shapiro, 1954; Sutton, 1998; Sutton & Biblarz, 2016; Williams, Barrere, & Huang, 1969)

The ideal rocket nozzle works on the principal of conservation of energy and processes are assumed to be adiabatic. There is no change in entropy change in a rocket nozzle arising from shocks or friction. One term associated with fluid flow is the enthalpy which comprises of internal energy plus work from the flow. The enthalpy of an ideal gas can be directly expressed as a product of specific heat at constant pressure and absolute temperature T. The enthalpy conversion happens in a rocket when the enthalpy of flow appears as an increase in kinetic energy between any two sections x and y, according to the following equation.

$$(hx - hy) = \left(0.5 * \left((vy^2) - (vx^2)\right)\right) = \left(cp(Tx - Ty)\right) \quad (1)$$

The ideal rocket follows laws of conservation of mass. Considering a single inlet and a single outlet, the fluid flowing in will have a constant mass flow rate:

$$\dot{m}=\dot{m}_x=\dot{m}_y=\text{Area}*\text{velocity}/\text{Volume}=A\upsilon/V \quad (2)$$

The volume V can be found at any point x using the perfect gas law which is: $p_xV_x=RT_x$ where R is the gas constant, which is the quotient when we divide the universal gas constant R' by the molecular mass. Specific heat at constant volume, c_v, and the same at constant pressure, c_p, are related by the following equation:

$$c_p-c_v=R, \quad (3)$$

where R is the gas constant obtained by dividing universal gas constant R' by the molecular mass. Two points x and y have their absolute temperature T related by

$$\frac{Tx}{Ty}=\left(\frac{px}{py}\right)^{\frac{k-1}{k}}=\left(\left(\frac{Vy}{Vx}\right)^{k-1}\right) \quad (4)$$

If a flow is brought to a halt isentropically it is referred to as a stagnation condition. The parameters associated with the condition are represented with the subscript 0. The stagnation enthalpy is just the sum of static enthalpy and fluid kinetic energy. The stagnation temperature T_o, the absolute temperature T and specific heat are related by,

$$To=T+\frac{v^2}{2c_p} \quad (5)$$

And the stoagnation pressure and local pressure can be related by,

$$\frac{P0}{p}=\left(\left(1+\frac{v^2}{2c_pT}\right)^{\frac{k}{k-1}}\right)=\left(\left(\frac{V}{Vo}\right)^{k}\right) \quad (6)$$

And similarly for absolute temperature,

$$\frac{To}{T}=\ 1+\ 0.5*(k-1)*(M^2) \quad (7)$$

If the local velocity gets to zero, the local temperature and pressure will approach the stagnation conditions. Ina combustion chamber the velocity is negligibly small, so the combustion pressure can be taken as the total or stagnation pressure.

Another important parameter entailing nozzle thermodynamics is the Mach number M. At the throat the flow is usually sonic, that is, the Mach number becomes unity. The Mach number, absolute temperature and stagnation temperature are related by the equation:

$$M=\sqrt{\left(\frac{2}{k-1}\right)*\left(\left(\frac{T_0}{T}\right)-1\right)} \quad (8)$$

The local pressure, stagnation pressure and Mach number are related by:

$$\left(\frac{p_0}{p}\right)=\left(1+0.5*(k-1)*(M^2)\right)^{\frac{k}{k-1}} \quad (9)$$

And similarly for absolute temperature,

$$\frac{T_o}{T}=\ 1+\ 0.5*(k-1)*(M^2) \quad (10)$$

There is one more relationship involving cross-sectional area A, Mach number M and k which is:

$$\left(\frac{A_y}{A_x}\right) = \left(\frac{M_x}{M_y}\right) * \sqrt{\left(\frac{\left(1+\left(\frac{k-1}{2}\right)\right)*M_y^2}{\left(1+\left(\frac{k-1}{2}\right)\right)*M_x^2}\right)^{\frac{k+1}{k-1}}} \quad (11)$$

Conical nozzles(Sutton & Biblarz, 2016)

The cone nozzle is one of the oldest nozzles and gets its name from the fact that it resembles a cone. An ideal nozzle directs all of its exhaust axially thereby producing the maximum possible thrust. Cone nozzles are usually associated with a correction factor, λ, which is the ratio of momentum of exhaust gases coming out from an ideal nozzle and the momentum of exhaust gases coming out from a nozzle with half angle α.

$$\lambda = 0.5*(1+\cos\alpha) \quad (12)$$

For a rocket nozzle with a divergence cone angle of 45°(α=22.5°), the exit momentum will be 96% of the ideal momentum. Nozzles with a small divergence angle α yield a higher value of λ and therefore yield a near ideal thrust. However, such nozzles have to be made longer and this adds up to the rocket mass and complexity. On the other hand, a high divergence angle yields a shorter nozzle but the thrust output is low. Thus cone nozzles usually have optimum divergence angles between α=12°& α=18° to achieve high thrust output with a minimum length.

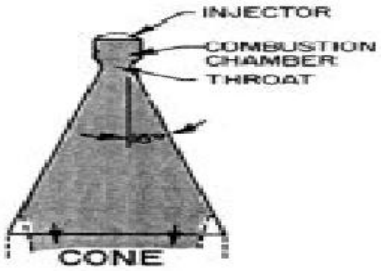

Figure 1.1. 2D Cross Section of a Conical Nozzle
(courtesy :http://www.aerospaceweb.org/design/aerospike/shapes.shtml)

Bell nozzle

The bell nozzle is the most widely used type of rocket nozzle and overcomes the drawbacks of a cone nozzle. Unlike the cone nozzle, the walls of the bell nozzle diverge up to a point and then begin to straighten out downstream. The diverging portion of the nozzle provides sufficient space for the incoming gas to expand and the straight portion directs high speed exhaust axially thereby producing optimum thrust. The large expansion section near the throat causes expansion shock waves and the straightening of the walls to drive the exhaust axially causes compression shock waves. In this way, the bell nozzle overcomes the drawbacks of a cone nozzle by minimizing weight and maximizing performance.

Figure 1.2. Bell Nozzle (courtesy
https://space.stackexchange.com/questions/1171/efficient-types-of-nozzles-used-in-rockets)

Expansion-Deflection nozzle

The expansion deflection nozzle is an improved version of a bell nozzle wherein the gases coming out from the throat are redirected towards the wall by a center body called pintle. The exhaust gases in this nozzle expand outward more rapidly thereby favoring shorter nozzles. Furthermore, altitude compensation is achieved with an expansion deflection nozzle as the exhaust gases interact with the ambient air forming an atmospheric boundary.

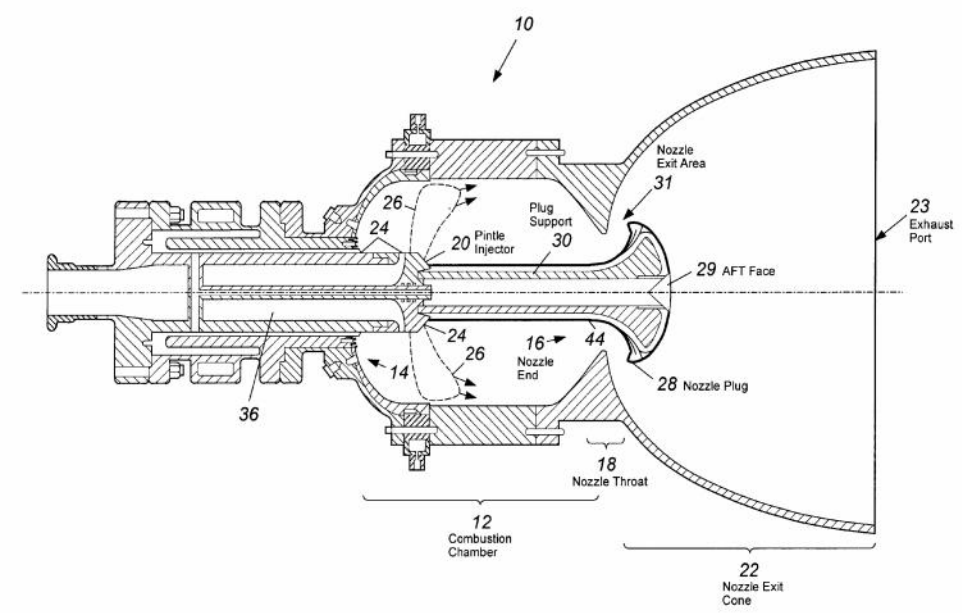

Figure 1.3. Expansion-Deflection Nozzle(courtesy:google images)

Aerospike nozzle

The aerospike nozzle belongs to the group of altitude compensating nozzles and is designed to provide altitude compensation (optimum thrust at all altitudes).Unlike the

bell and cone nozzles, the exhaust is not constrained by the walls of the nozzle but rather flows over the wall surface as shown in Fig 1.4. Altitude compensation is achieved as the ambient air controls the rocket exhaust expansion thereby having a control over the exit ratio. At lower altitudes, the ambient pressure is high enough to press the exhaust against the aerospike wall thereby forming a pattern as shown in the Fig 1.4. As we go higher the ambient pressure decreases and as a result the exhaust starts expanding a bit further away from the nozzle walls. At very high altitudes, the nozzle flow becomes under-expanded and starts to expand a lot further away from the walls as shown in the Fig 1.4. Aerospike nozzles are the most favored for Single State to Orbit (SSTO) designs which makes the rocket lighter and easy to design.

Altitude compensation: Bell nozzle versus Aerospike Nozzle(Lash, 2015)

Altitude compensation refers to the technique used to obtain optimum pressure thrust at all altitudes by letting the ambient air form an atmospheric boundary over the exhaust. The purpose of any nozzle in a rocket engine is to direct all of its gases axially to obtain optimum thrust.

In case of bell nozzles, the pressure thrust produced is not optimum for all altitudes and thus does not qualify as an altitude compensating nozzle. At low altitudes where the ambient pressure is low, the flow is over-expanded giving rise to flow separation within the nozzle walls leading to a reduction in overall thrust produced. At high altitudes, the exhaust continues to expand inefficiently outside of the bell contour even after leaving the nozzle. Since there is no external pressure acting on the exhaust to redirect it back axially, there is a reduction in overall thrust produced. At intermediate

altitudes, where the exhaust pressure and ambient pressure are nearly the same the thrust produced is at an optimum level.

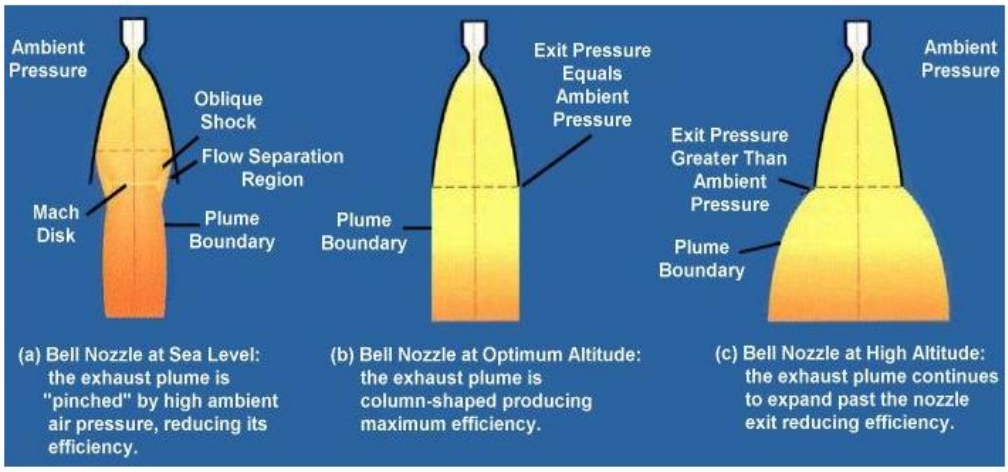

Figure 1.4. Altitude Compensation in a Bell Nozzle(Lash, 2015)

On the other hand, aerospike nozzles provide maximum thrust at all altitudes because the exhaust flow is external to the nozzle wall as opposed to case in bell nozzles. At lower altitudes where the ambient pressure is high, the atmospheric boundary formed over the nozzle exhaust directs all of the exhaust momentum axially and gives no room for boundary separation to occur. At higher altitudes, where the ambient pressure is low, the ambient air pressure constrains the exhaust to flow along the nozzle contour with the help of expansion/compression waves thereby making the exhaust axial and producing optimal thrust.

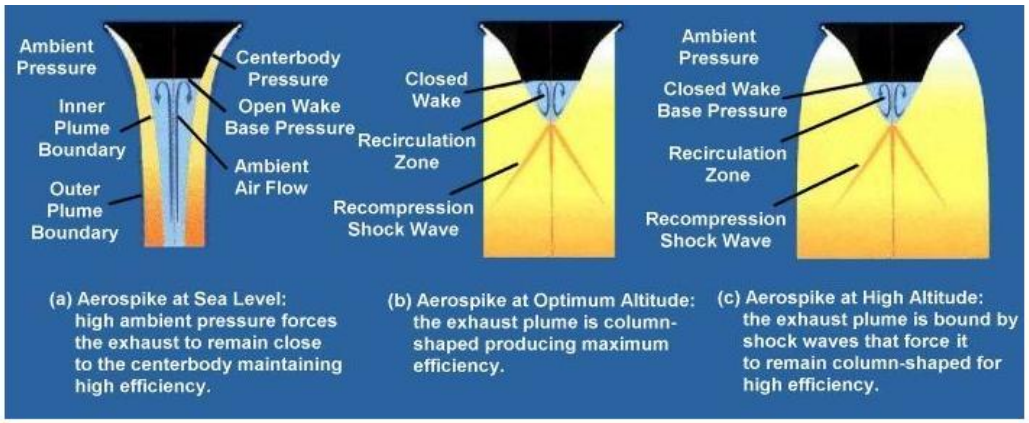

Figure 1.5. Altitude Compensation in an Aerospike Nozzle(Lash, 2015)

Literature review

Aerospike nozzles have been researched upon and studied in countries like USA, Japan, Europe, Russia and China since late 1950.(Baftalovskii, Kraiko, & Tillyayeva, 1999; Dumnov, Nikulin, & Ponomaryov, 1993; Onofri et al., 2006; Ryan, Solano, Holland, & Rahman, 2001; Sakamoto et al., 1999; Tomita et al., 1997; C. H. Wang, 2005; C.-H. Wang, Liu, & Qin, 2009)The aerospike nozzle would have replaced the conventional nozzles in the Space Shuttle Main Engine if not for the technological difficulties associated with its construction. Fig 1.6 below shows the XRS-2200 Aerospike engine (built for the X-33 program) being tested at NASA's Stennis Space Center located at Mississippi. Unfortunately the X-33 program was called off eventually because of overweight composite cryogenic fuel tank and high cost.During late 1990s, both real life experiments and numerical simulations were carried out in China to determine the performance based on flow field behavior.

Figure 1.6. XRS-2200 Being Tested for the X-33 Reusable Launch Vehicle RLV(Courtesy: google images)

Research about aerospike nozzles started first in the early 1970s within the USA in the form of projects taken up by Rocketdyne, NASA and the U.S. Air Force.One such project was taken up by Rocketdyne to develop and test an annular aerospike thrust chamber in 1973 and the same was fabricated and tested the following year. One of the first studies about linear aerospike engine for Single State to Orbit (SSTO) was done in the year 1977 by Rocketdyne. From the studies conducted, Rocketdyne came to a conclusion that aerospike engine was a strong contender for SSTO rockets and aerospike nozzles were versatile for a wide range of altitudes.(HUANG, 1974; KIRBY & MARTINEZ, 1977; LAMONT, 1973; Lash, 2015a)

Another experiment conducted on the aerospike nozzle was the LASRE (Linear Aerospike SR-71 experiment) by NASA at California, in the year 1998. A scaled model (20 %) of a half-span X-33 fore-body, with a linear aerospike engine at the rear, was used for the test. The objective of this experiment was to evaluate the aerodynamic

performance of combination of the X-33 lifting body and the linear aerospike engine and to document information for future reusable launch vehicles.(Gibbs, 2014; Lash, 2015)The LASRE was mounted on the back of an SR-71 to simulate a flying supersonic wind tunnel. There was even a reflection plane placed between SR-71 and the model, parallel to the axis of the SR-71, to prevent the flow field coming from the SR-71 from interfering with the model's flow-field. The objective of the experiment was to find out how speed and altitude affects the aerodynamics of a reusable launch vehicle like the X-33.(Calzada, 2015; Lash, 2015; "NASA - Dryden Flight Research Center - News Room," 1997)

The tests conducted by NASA inspired universities around the world to research about aerospike nozzles and their advantages over conventional nozzles for SSTO flight. Japan's National Aerospace Laboratory showed interest in aerospike nozzles by studying the thrust performance of the linear aerospike engine and their results indicated a way to predict the thrust co-efficient of an aerospike engine. Between 2001 and 2003 the Beijing University of Aeronautics and Astronautics laid the groundwork for experimental and numerical methods of aerospike design and aerospike solid-propellant optimization.The same university researched about an alternative tile shaped nozzles.(Dai, Liu, Cheng, & Ma, 2003; Lash, 2015b; Liu et al., 2001; Wuye, Yu, Xianchen, & Haibin, 2001)

In the year 2009, a project done by the California Polytechnic State University aimed at integrating a hybrid rocket motor with an aerospike nozzle. According to their study, aerospike nozzles suffer from throat ablation because of the way they work. The project focused on reducing the throat ablation for aerospike nozzles when integrated with hybrid rocket motors(Lemieux, 2010).A university in Italy researched about how it

would be optimal if exhaust expansion occurs in two stages, primary expansion accomplished by a cluster of bell nozzles and secondary expansion accomplished by the linear aerospike nozzle.(Geron, Paciorri, Nasuti, & Sabetta, 2007a) German National Technology Programme and Russian National Programme contributed towards research about losses encountered with clustering and also tested the round to square modules used for primary expansion.(Geron, Paciorri, Nasuti, & Sabetta, 2007b; Hagemann, Immich, & Dumnov, n.d.; Lash, 2015c).Through clustered nozzles they were able to get rid of the problems faced by an annular nozzle while retaining the advantages from the aerospike nozzle like altitude compensation, shorter nozzle lengths and base area utilization. In addition to that, clustered modules favored stable combustion, lower thermal loads, easier manufacturing and thrust vectoring.(Fick & Schmucker, 1996; Nasuti & Onofri, 1999; T.-S. Wang, Droege, D'Agostino, Lee, & Williams, 2004).In 2007, University of Tokyo researched about the performance of linear aerospike nozzle with clustered modules.(Tsutsumi, Yamaguchi, Teramoto, & Nagashima, n.d.)The first ever liquid propellant aerospike nozzle was tested by California State University in the year 2004(Besnard& Garvey, 2004).The same university went on to develop a high expansion rocket engine which could be used to validate aerospike performance and try out nozzle curvature in the circumferential and longitudinal section.(Meiss&Besnard, 2013).

CHAPTER-2

NUMERICAL SIMULATIONAND SETUP

The simulations were done using ANSYS-Fluent module under Workbench 17.1. A simple 2D model of a linear plug (aerospike) nozzle was designed as shown in the Fig 2.1. There were separate designs for a full length spike and the spikes plug-truncated by 10, 20 and 30 percent. The nozzle is contained in a rectangular enclosure, the sides of which serve as atmospheric boundaries. The axis of the inlet is parallel to the spike. The entire 2D geometry is symmetric along the y-axis. The exhaust flow coming from the inlet(which is the portion of the nozzle downstream after the throat) is supersonic. The fluid parameters used in all the simulations were taken from NASA CEARUN which was calculated for a rocket with a chamber pressure of 7Mpa, with Rp-1 as the fuel and liquid oxygen as oxidizer. The O/F ratio chosen was 2.26 and the ratio of chamber pressure to exit pressure was 175. An absolute convergence criteria of 0.001 was chosen for all the simulations.

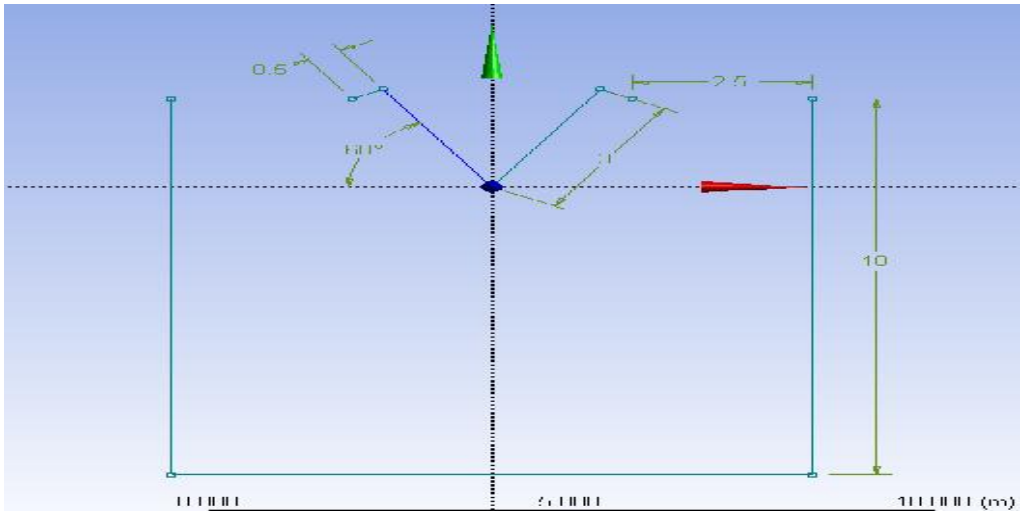

Figure 2.1. 2D Model of the Aerospike Nozzle

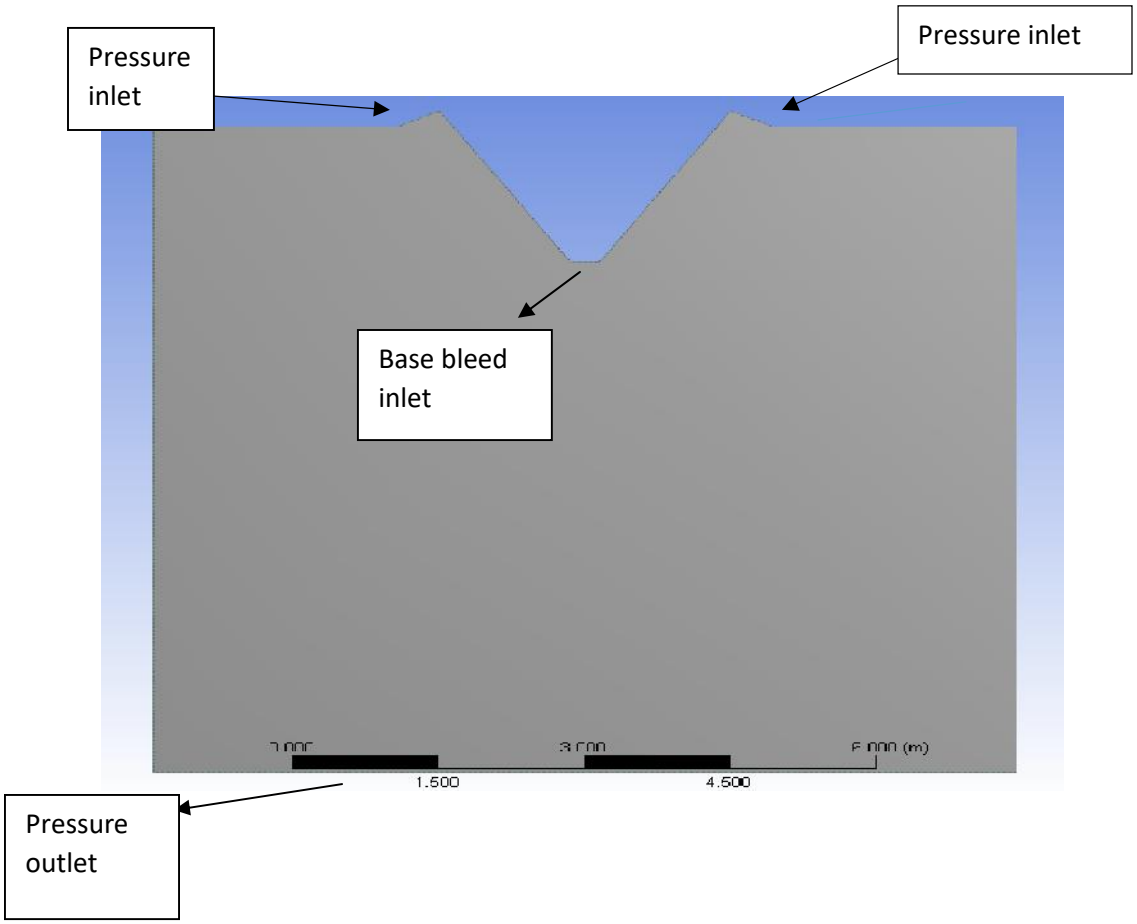

Figure 2.2 2D Geometry of the Model

Geometry module

The 2D properties were selected in the geometry module to start off with and the design was done within the same module. The inlets are 0.5m wide and the spike is 3m long and makes an angle of 60^{o} between the spike and the x axis. After designing and dimensioning, a 2D surface was created using the 'surface from sketches' option within the geometry module.

Meshing module

A face mesh was inserted into the 2D structure along with a refinement. The mesh relevance center was set to 'Fine' and the smoothing was set to 'High'. The mesh generated had a skewness of about 0.4.The boundary types were labelled as shown in figure 2.2 (for the truncated cases the base of the truncation was labelled as 'base bleed inlet', not shown in the figure).

Setup module

- The set up was started with double precision checked off. Inside the setup module, under the 'General' tab, the mesh was 'Checked'. The solver was set to 'Pressure based', velocity formulation was set to 'Absolute', Time was set to 'Steady', and the 2D space was set to 'Planar'. 'Gravity' was unchecked.
- Inside models tab 'Energy' was set to 'On' and under 'viscous model', realizable k-epsilon model was chosen.
- Inside 'Materials' tab, air was chosen as the fluid. The density of the air was set to 'ideal gas' because the fluid used for simulations was compressible air. The specific heat was set to 5500 J/KgK.
- Inside 'Boundary Conditions', pressure inlet boundary was first chosen and it had to be initialized with total and static pressure.The chamber pressure (7MPA) was taken to be the total Pressure because the gas velocity is very low at the chamber(Sutton & Biblarz, 2016). Since the inlet was intended to be supersonic, a velocity of 1500 m/s was chosen for the

velocity of the fluid at the inlet. From this information static pressure was calculated from the formula;

Total pressure = Static pressure + 0.5*density*(velocity^2)

The density was obtained from NASA-CEARUN. The static pressure came out to be (4.85*10^6) pascals. Following this, 'Gauge Total Pressure' was set to 7*10^6 pascals and 'Supersonic/Initial Gauge pressure' was set to 4.85*10^6 pascals. Turbulence specification method was 'Intensity and Hydraulic diameter'. The turbulent intensity was set to 5% and the Hydraulic Diameter was set to 0.5m.(Formula for hydraulic diameter for a circular tube is

$$4A/L = 4 * pi * r * r/2 * r = 2 * r = d \quad (12)$$

The hydraulic diameter is the actual diameter of the inlet, which is 0.5m according to our design).

- Inside 'Boundary Conditions' the next boundary type modified was 'base bleed inlet'. The boundary type chosen for this named selection was 'Mass Flow Inlet'. The mass flow rate was chosen according to the simulation. For all simulations, the 'Initial Gauge Pressure' was set to (0.4*10^5) pascals. The Initial Gauge Pressure refers to the static pressure and for a given mass flow rate a low value of static pressures yields a higher value of flow velocity. With this in mind, the value of (0.4*10^5) was chosen for the base bleed inlet. The turbulence specification was 'Intensity and Hydraulic Diameter'. The turbulent intensity was set to 5% and 'Turbulent Diameter' was given the value of base bleed inlet width (The width changes for each level of truncation, that is, the width is 0.3m for 10%

truncated spike, 0.6m for 20% truncated spike and 0.9m for 30 % truncated spike).

- The next boundary was the 'Pressure outlet'. The back pressure was set to atmospheric pressure (101325 Pascals) and the 'Turbulence specification' was 'Intensity and Hydraulic Diameter'. The intensity was set to 5% and value of Hydraulic diameter was set to 8.86m as per the design.
- The last step in 'Boundary conditions' tab was setting the operating pressure to 0.
- Inside 'Solution Methods', 'Turbulent Kinetic Energy' and 'Turbulent Dissipation Rate' were set to 'Second Order Upwind'.
- Inside 'Solution Controls', the Courant number was varied according to the stability of the solution (value varied from 3 to 5 depending upon convergence). Inside 'Limits', 'Maximum Absolute Pressure was increased to an order of (10^10) Pascals, the 'Maximum Static Temperature' was set to 5000K and 'Maximum Turbulent Viscosity Ratio' was set to (10^9).
- Inside Monitors, the absolute criteria for continuity was (10^-3). This value can be changed to higher values for better accuracy.
- Inside 'Solution Initialization', 'Standard Initialization' was chosen and the setup was initialized from 'Pressure Inlet'.
- The calculations were then run from the setup until convergence was obtained.
- The contour & vector plots were then taken from the 'Graphics' tab.

CHAPTER 3

RESULTS AND CONCLUSION

The contour plots are obtained for dynamic pressure in Pascals, velocity magnitude in m/s, enthalpy in J/kg, turbulent kinetic energy in m^2/s^2, turbulent dissipation rate in m^2/s^3 and finally a vector plot of velocity magnitude in m/s.Simulations were done for a full length aerospike, a 10 percent truncated aerospike, a 20 percent truncated aerospike and a 30 percent truncated aerospike nozzle with and without base bleed (for the truncated cases). For each aerospike configuration, different values of base bleed mass flow were tried and are listed below.

For 10 percent truncation, the mass flow rates (kg/s) for base bleed inlet were:

50, 60, 70, 80, 90, 100, 110, 120, 130, 140 and 150

For 20 percent truncation, the mass flow rates (kg/s) for base bleed inlet were:

200, 220, 240, 260, 280 and 300

For 30 percent truncation, the mass flow rates (kg/s) for base bleed inlet were:

380, 400, 420, 440, 460 and 480

To better understand the effect of plug truncation, a separate image of each contour plot zoomed-in near the base truncation (base bleed inlet) has been presented to the right of each contour. For example, the page after the next one contains contour plot of dynamic pressure, contour plot of dynamic pressure zoomed in near the base truncation, contour plot of enthalpy, contour plot of enthalpy zoomed in near the base truncation, contour plot of turbulent dissipation rate, contour plot of turbulent dissipation rate zoomed in near the base truncation.

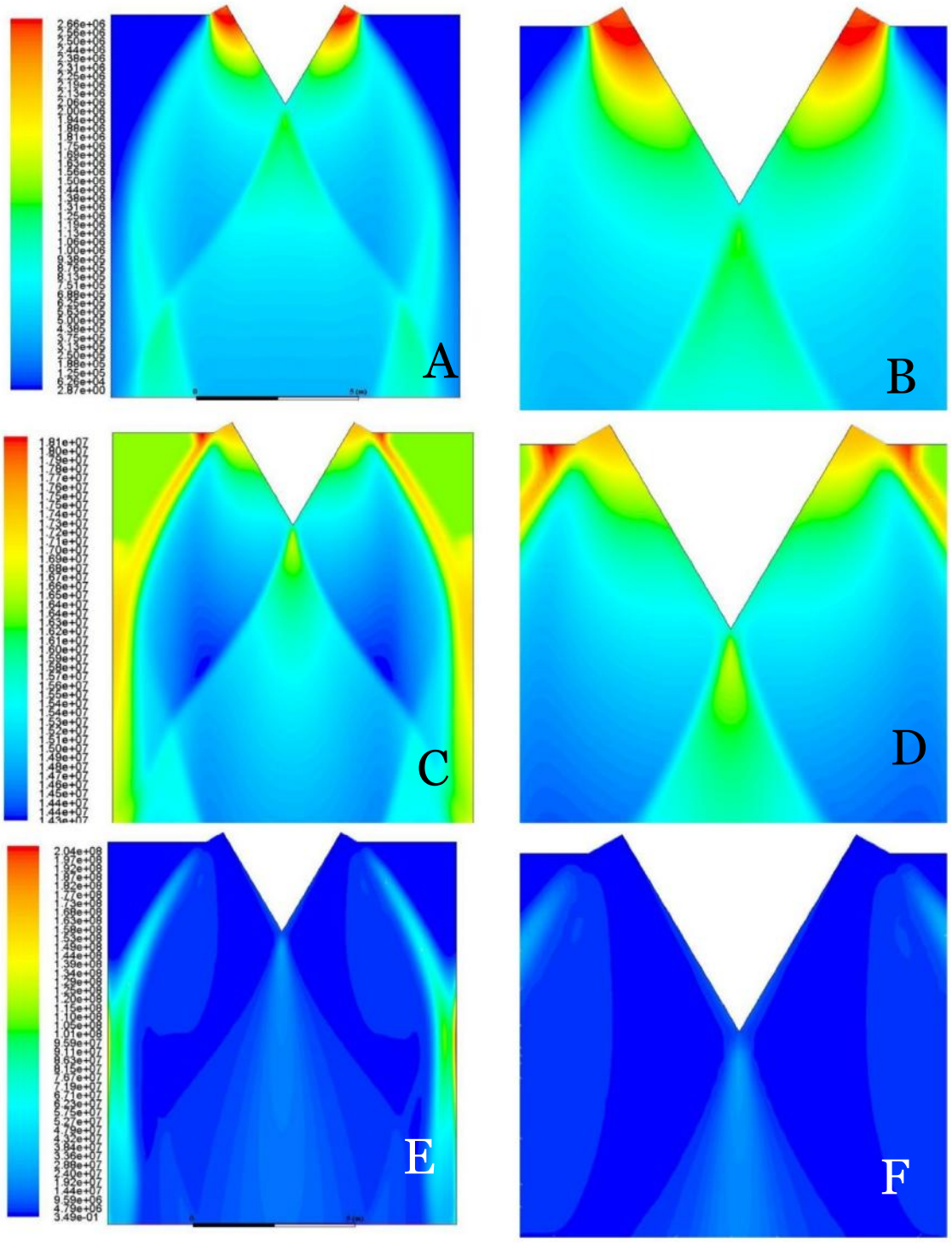

Figure3.1. Contours of: Dynamic Pressure(A,B), Enthalpy (C,D) & Turbulent Dissipation Rate (E,F) for Full Length Spike.

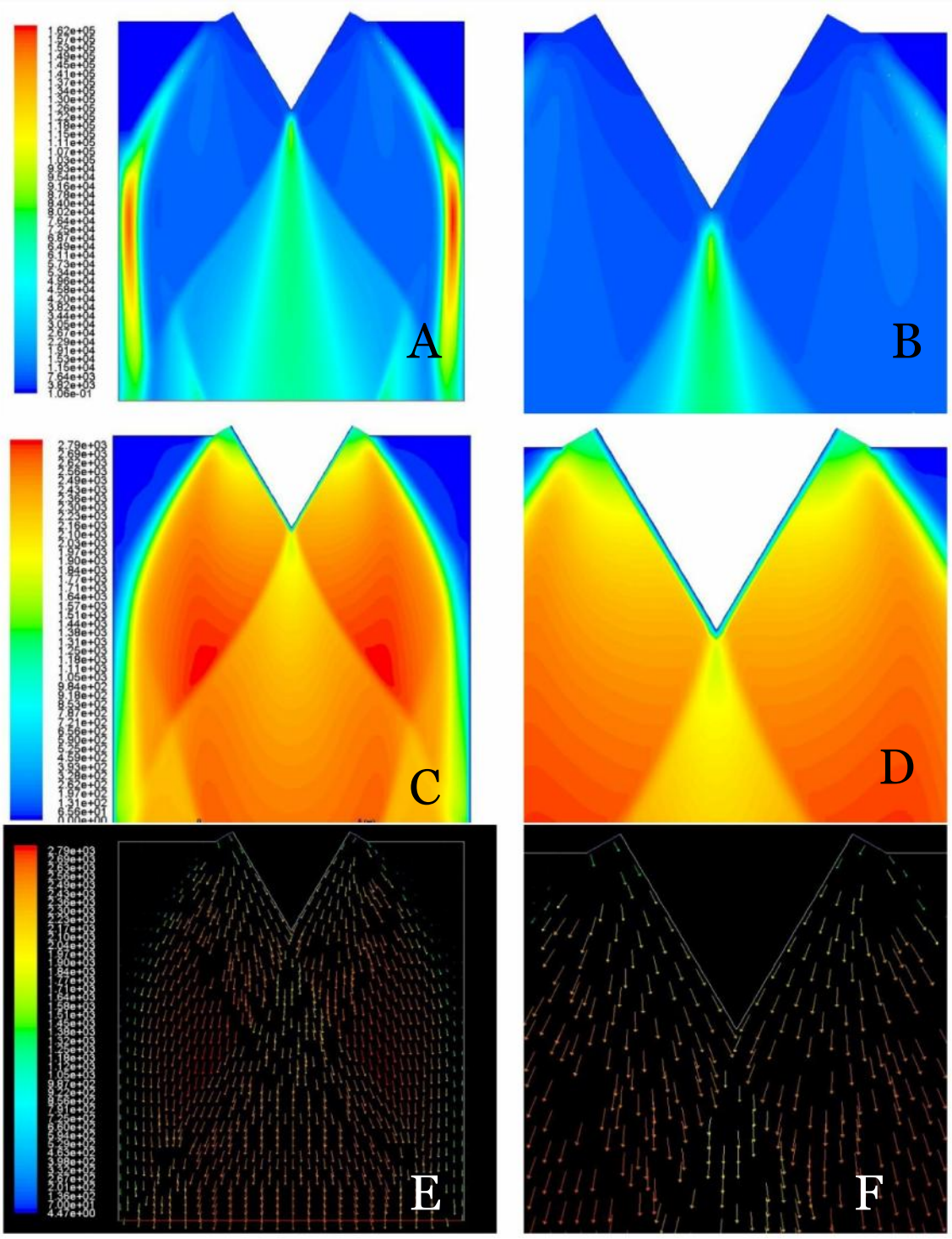

Figure 3.2. Contours of Turbulent Kinetic Energy (A,B) ,Velocity Magnitude (C,D) & Velocity Vector (E,F) for Full Length Spike.

The above two images contain the contour plots for the full length case. Looking at the dynamic pressure contours, we observe that the pressure field is uniform without giving rise to any kind of recirculation just below the spike. Although a full length spike produces near ideal thrust, the spike has to be truncated to make the nozzle lighter, more compact and easy to construct.

The following two pages contain the contour plots for the 10% truncated case without base bleed. Looking at the contour plot of dynamic pressure, we see a portion just below the truncation (near base bleed, refer figure 2.2 to understand the location of base bleed in the geometry), having an extremely low value of dynamic pressure. This is the root cause of base recirculation and is highly undesirable and contributes to a loss of thrust, making the nozzle inefficient.

The goal of the base bleed analysis was to find the optimum base bleed mass flow rate for which the dynamic pressure profile is uniform just below the truncation. The subsequent pages (25-46) contain contours for the 10 % truncation case with base bleed. Looking at the contour plots of dynamic pressure for the cases with base bleed, we see the base recirculation getting suppressed as we increase the base bleed mass flow rate. For the 10 percent truncated case, the dynamic pressure profile is almost uniform near the base of the truncation when the base bleed mass flow rate is 150 kg per sec. In other words, the base recirculation is completely suppressed, and the thrust produced is close to ideal.

.

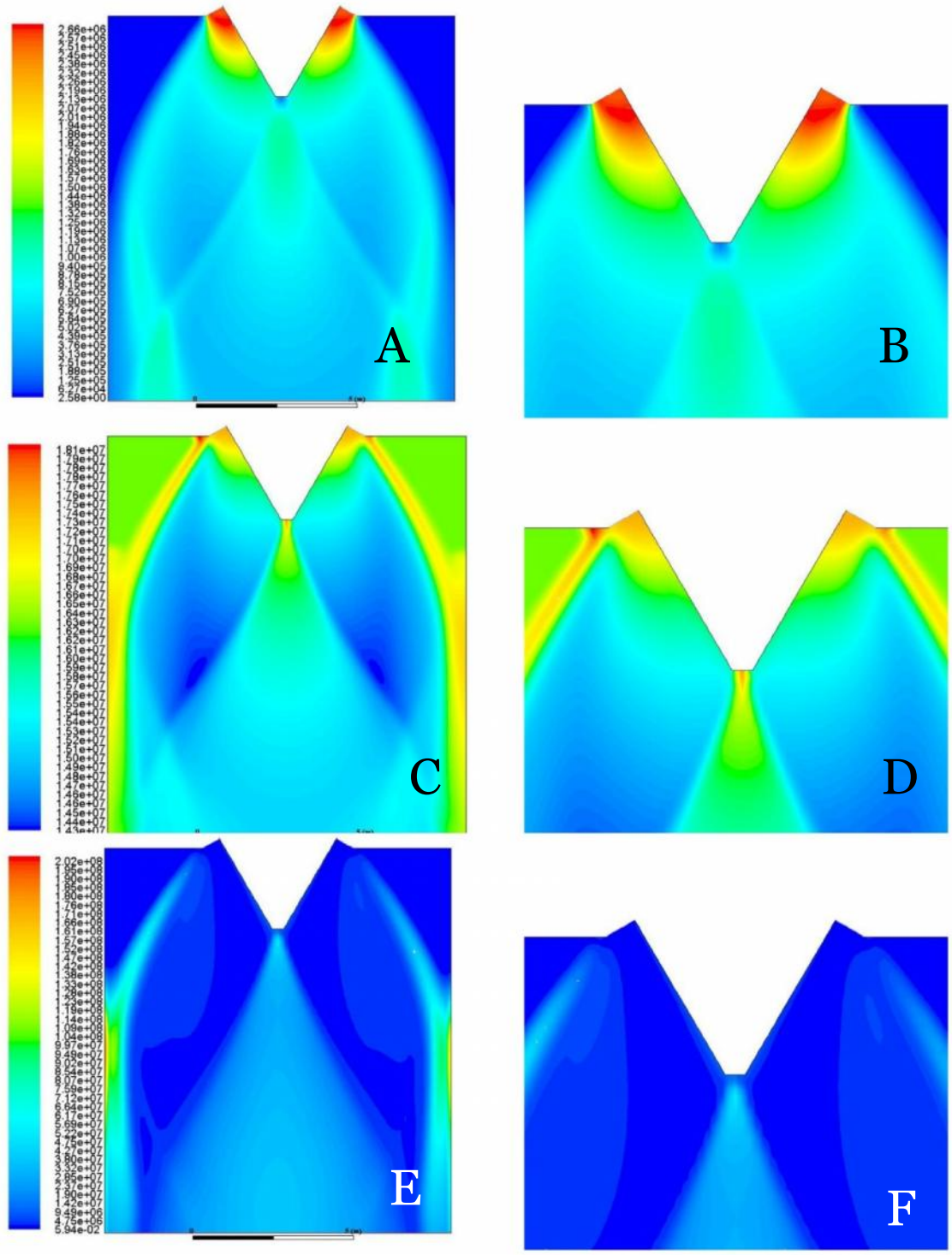

Figure3.3. Contours of Dynamic Pressure (A,B) , Enthalpy (C,D) & Turbulent Dissipation Rate(E,F) for 10 % Truncation Without Base Bleed.

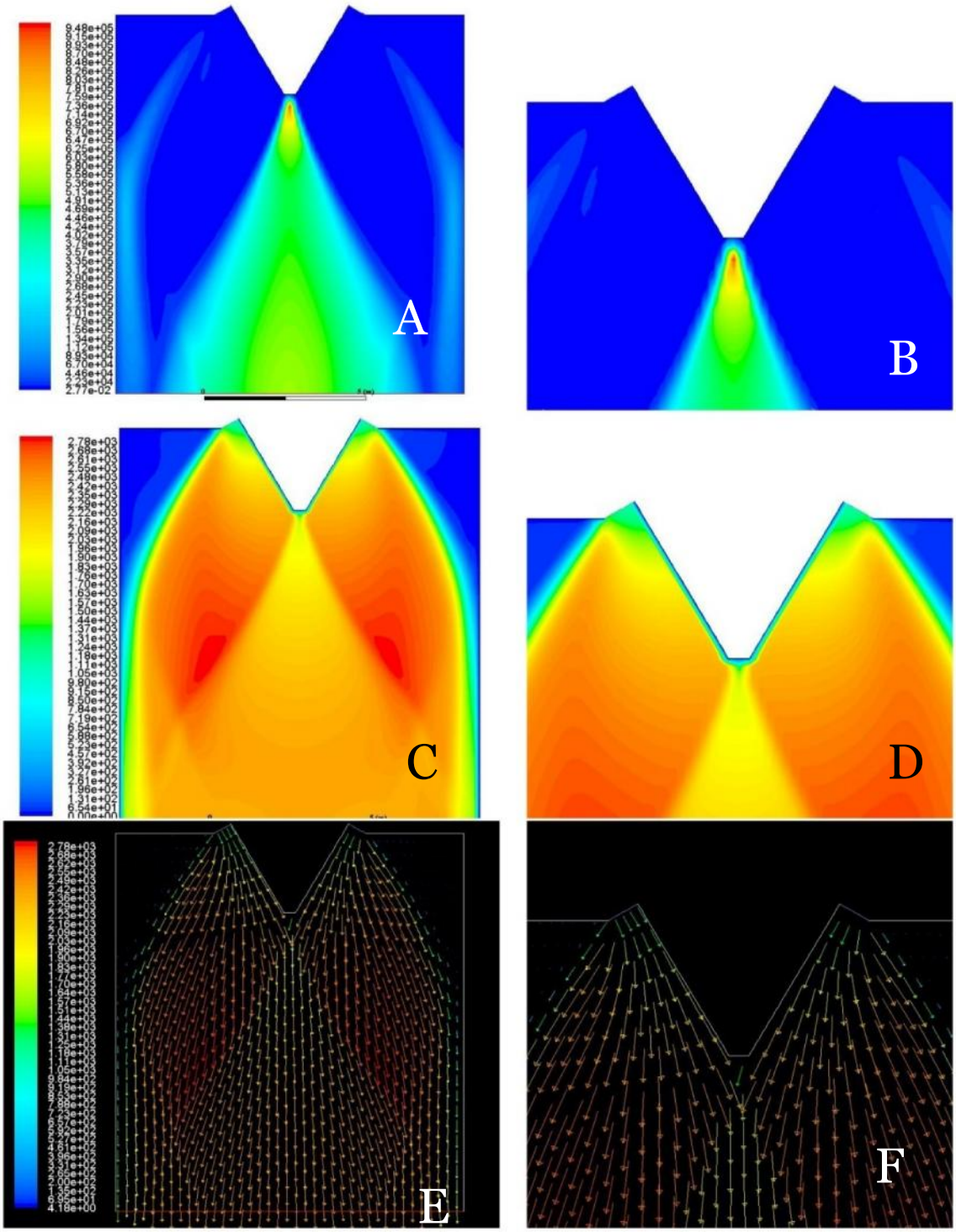

*Figure3.4.*Contours of Turbulent Kinetic Energy (A,B) , Velocity Magnitude (C,D) & Velocity Vector (E,F) for 10 % Truncation Without Base Bleed.

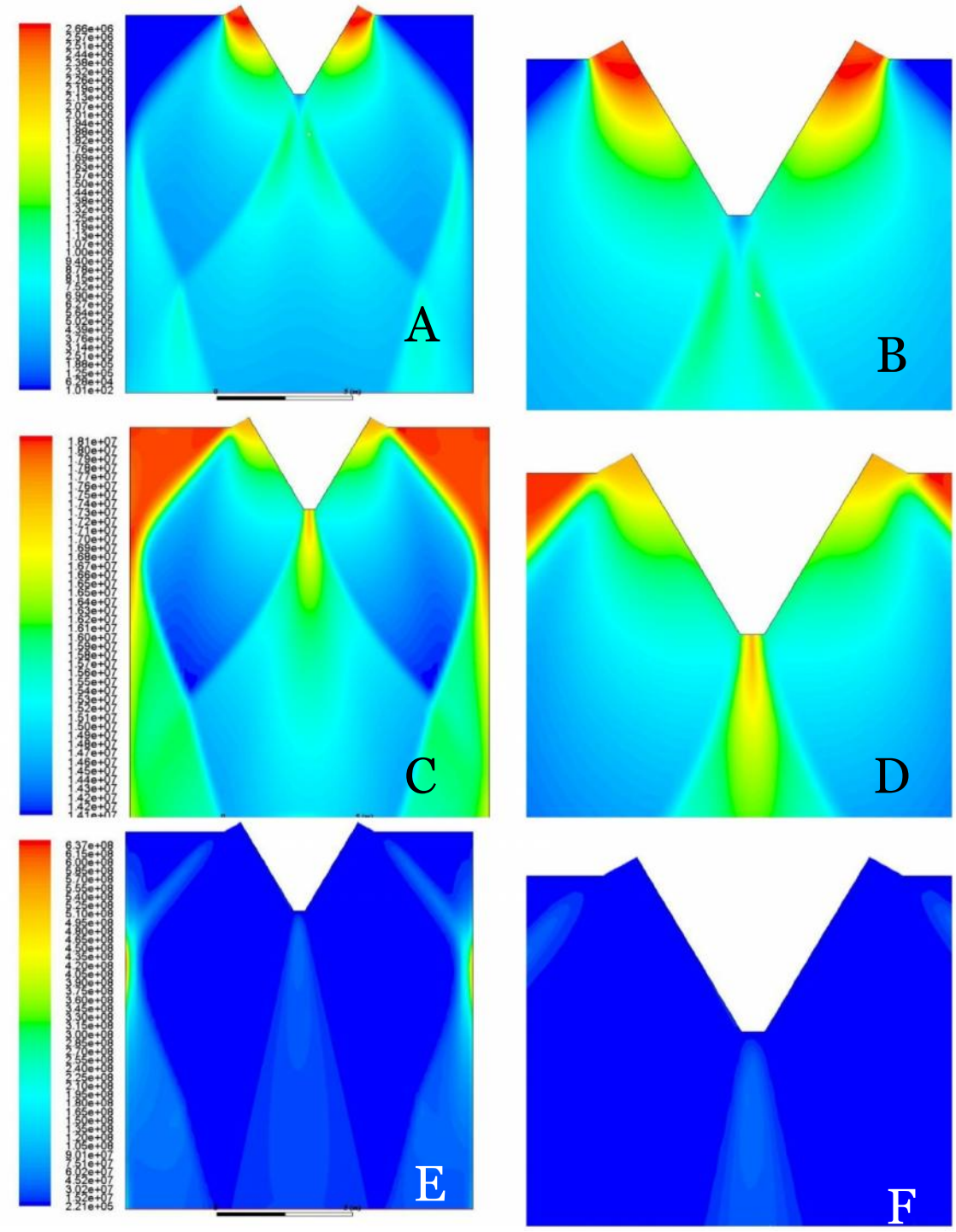

Figure3.5. Contours of Dynamic Pressure (A,B) , Enthalpy (C,D) & Turbulent Dissipation Rate (E,F) for 10 % Truncation with a Base Bleed Mass Flow Rate of 50kg/s.

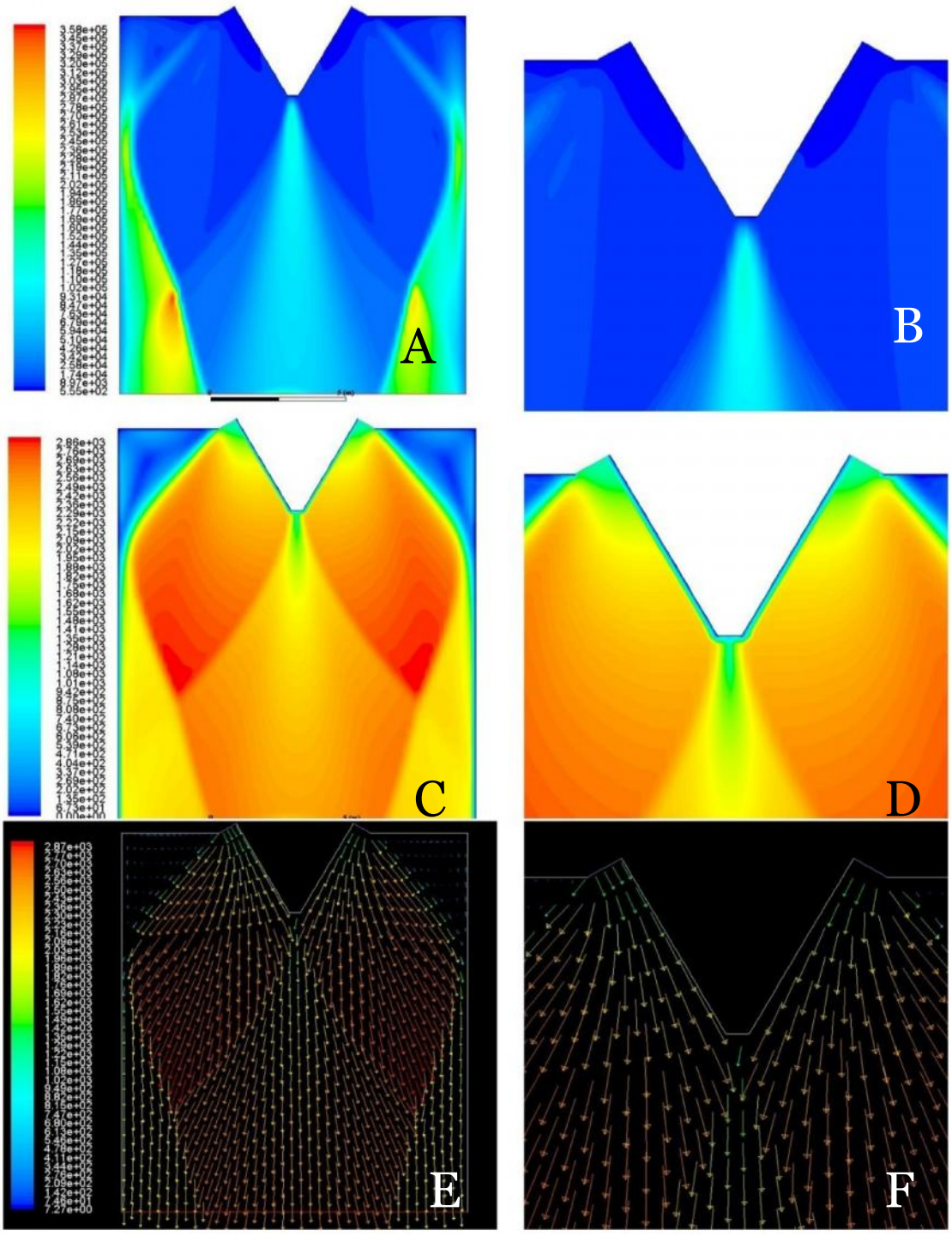

Figure3.6. Contours of Turbulent Kinetic Energy (A,B) , Velocity Magnitude (C,D) & Velocity Vector (E,F) for 10 % Truncation with a Base Bleed Mass Flow Rate of 50kg/s.

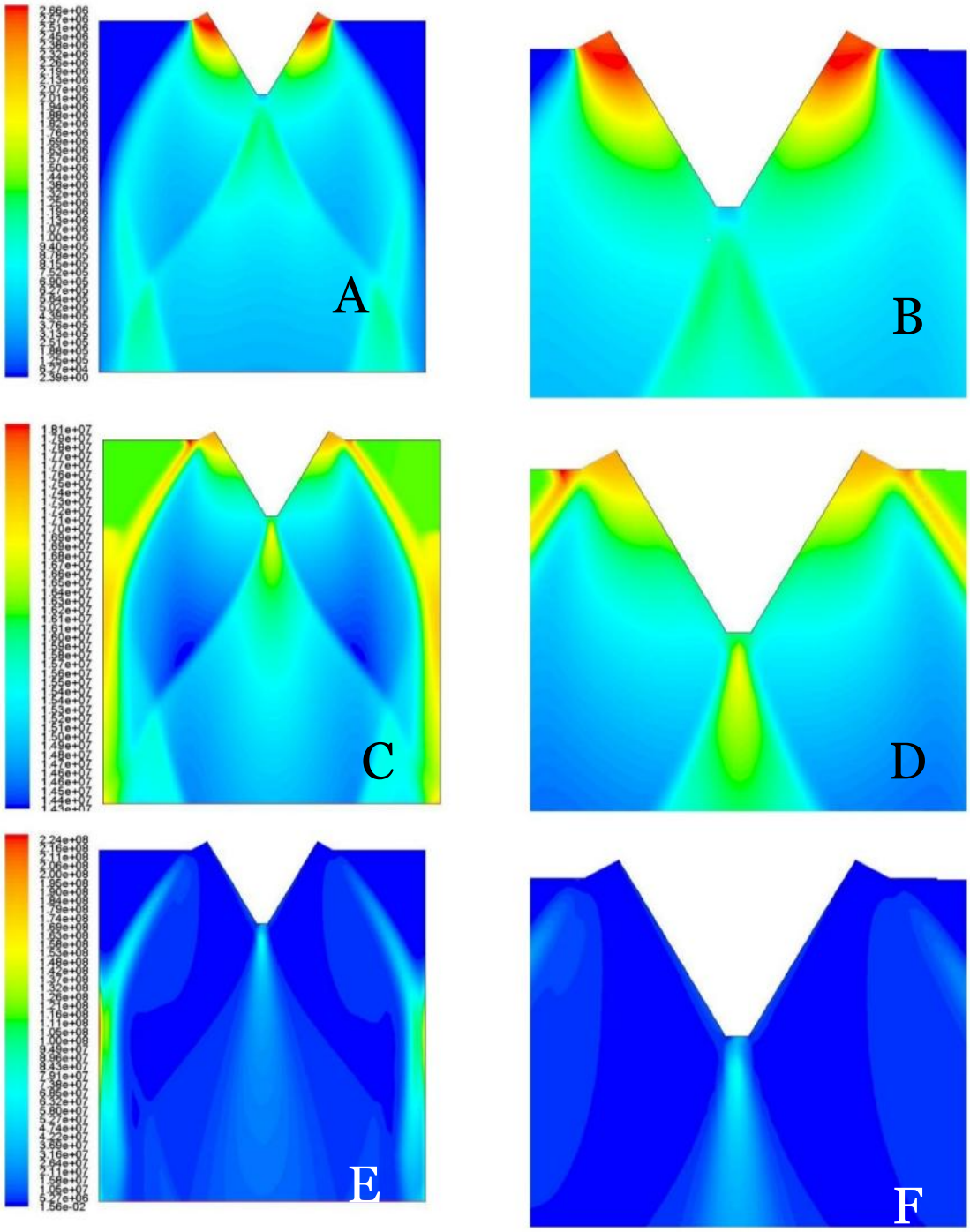

Figure3.7. Contours of Dynamic Pressure (A,B) , Enthalpy (C,D) & Turbulent Dissipation Rate (E,F) for 10 % Truncation with a Base Bleed Mass Flow Rate of 60kg/s.

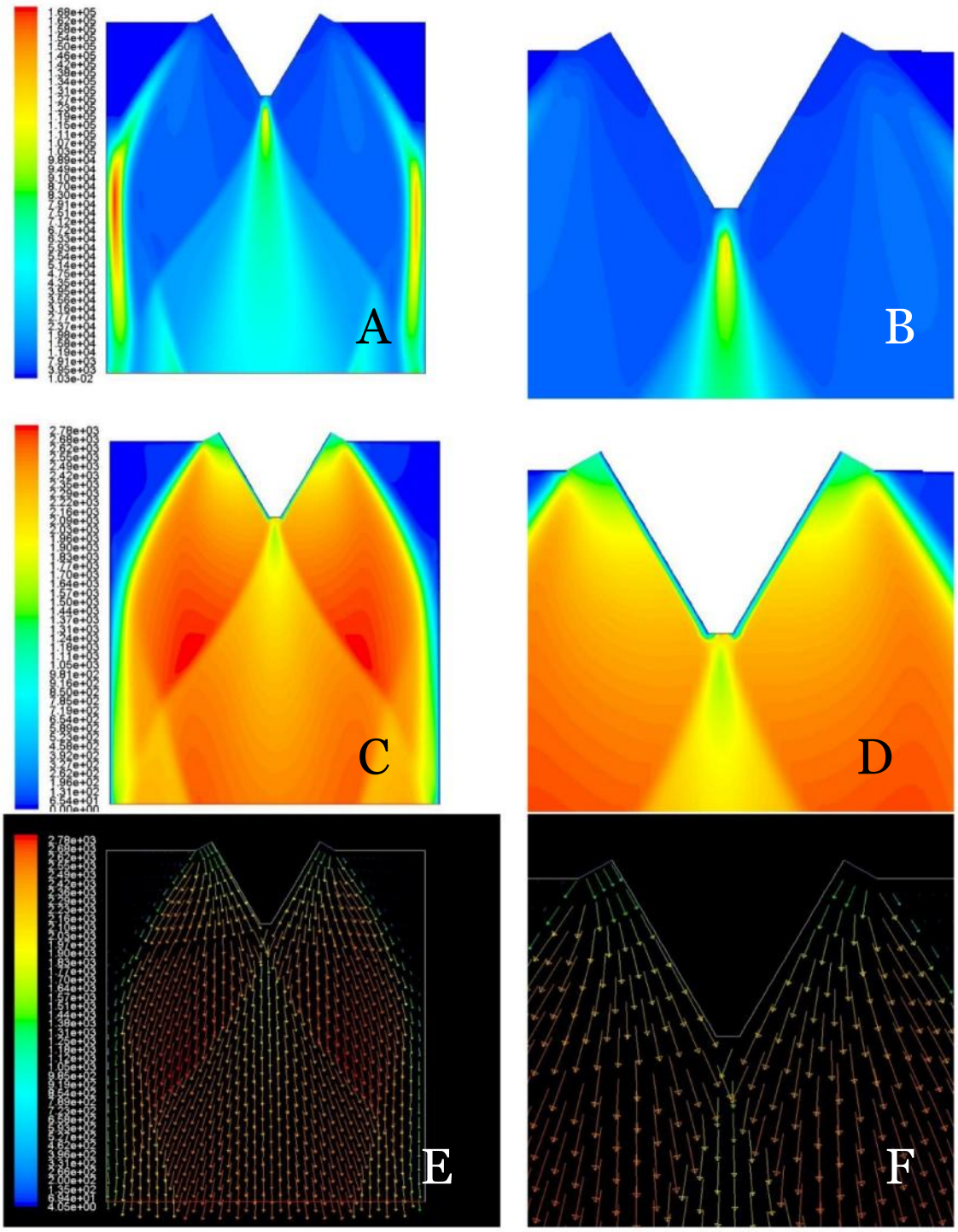

Figure3.8. Contours of Turbulent Kinetic Energy (A,B) , Velocity Magnitude (C,D) & Velocity Vector (E,F) for 10 % Truncation with a Base Bleed Mass Flow Rate of 60kg/s.

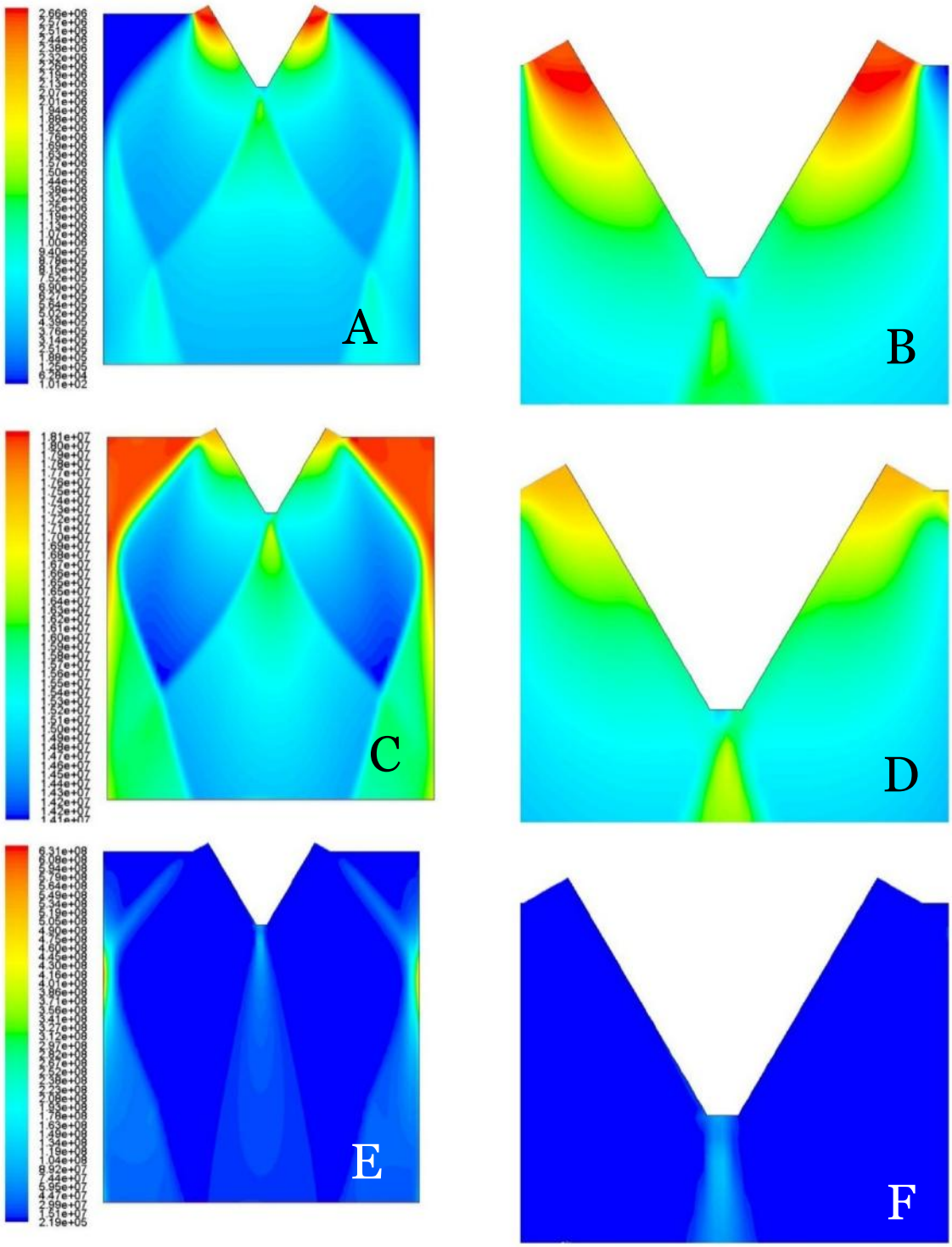

Figure3.9. Contours of Dynamic Pressure (A,B) , Enthalpy (C,D) & Turbulent Dissipation Rate (E,F) for 10 % Truncation with a Base Bleed Mass Flow Rate of 70kg/s.

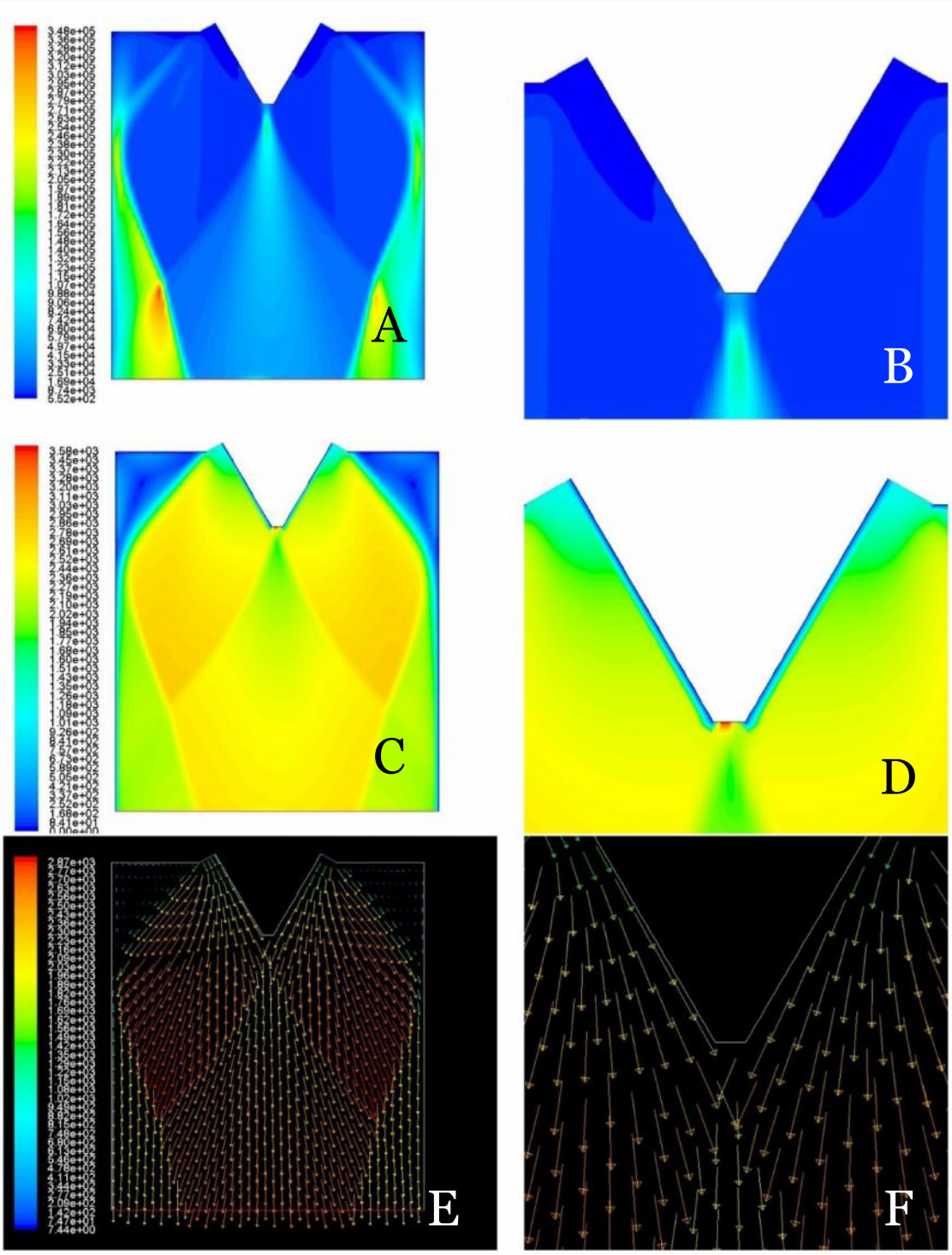

Figure3.10. Contours of Turbulent Kinetic Energy (A,B) , Velocity Magnitude (C,D) & Velocity Vector (E,F) for 10 % Truncation with a Base Bleed Mass Flow Rate of 70kg/s.

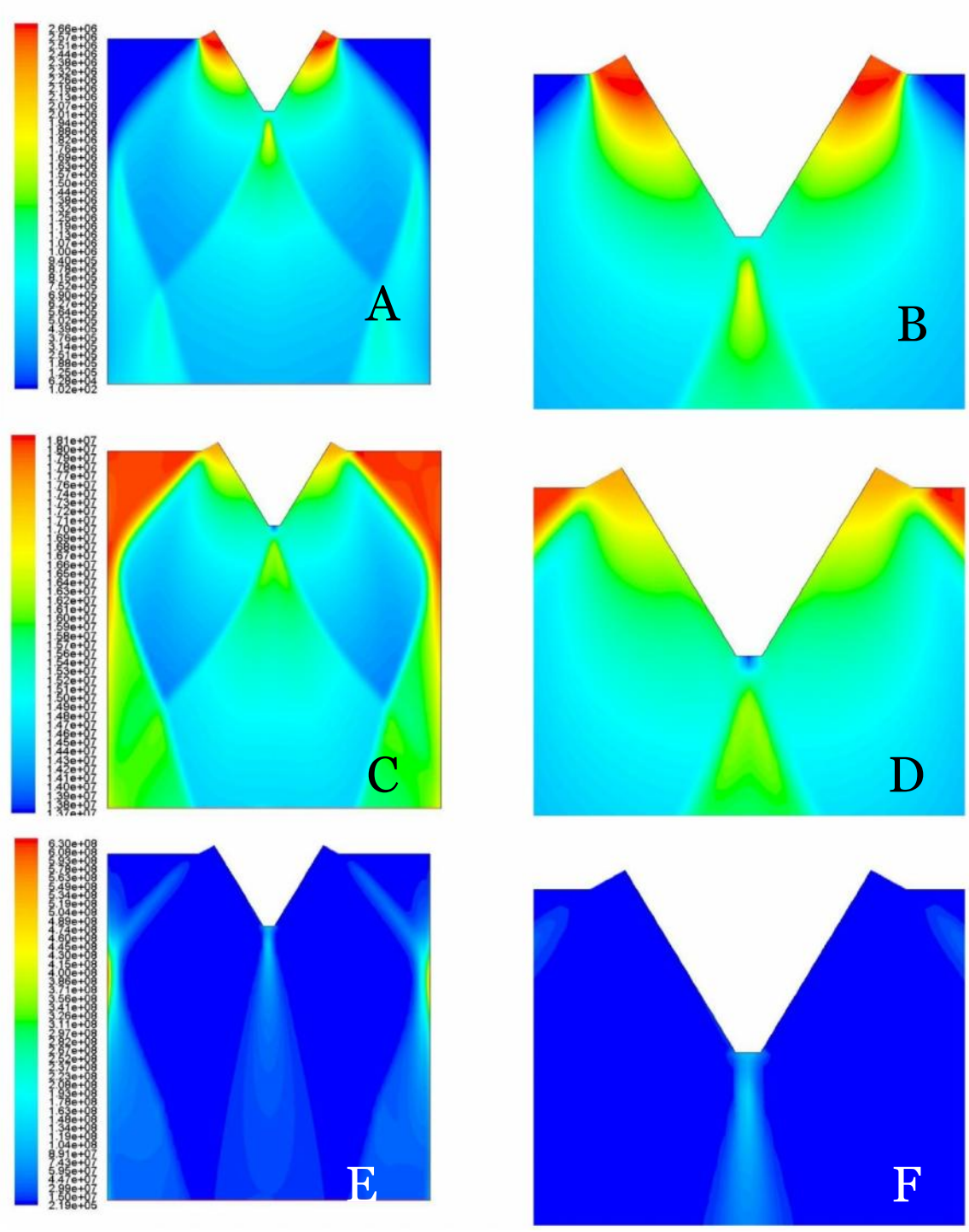

Figure3.11. Contours of Dynamic Pressure (A,B), Enthalpy (C,D) & Turbulent Dissipation Rate (E,F) for 10 % Truncation with a Base Bleed Mass Flow Rate of 80kg/s.

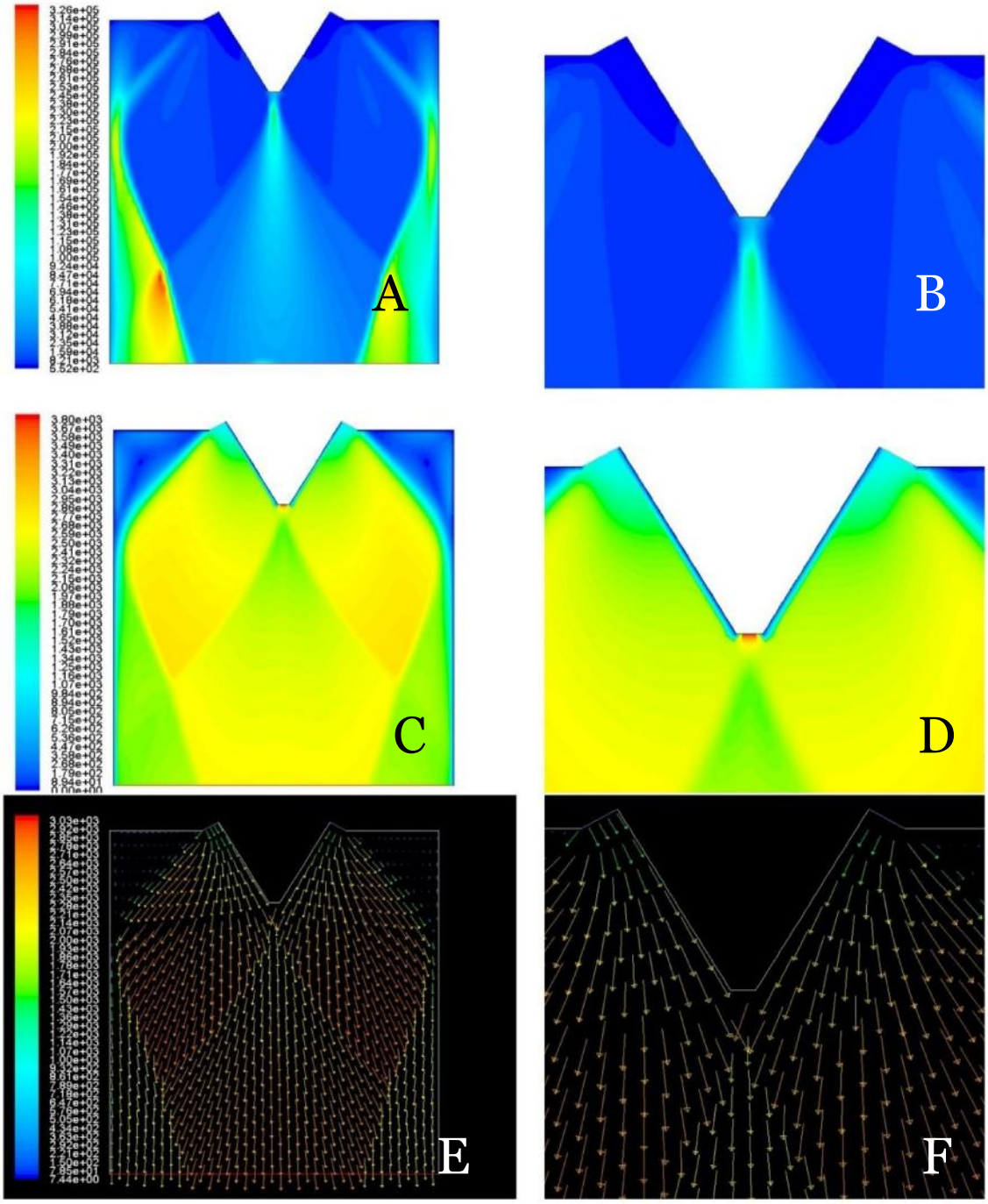

Figure3.12. Contours of Turbulent Kinetic Energy (A,B), Velocity Magnitude (C,D)& Velocity Vector(E,F) for 10 % Truncation with a Base Bleed Mass Flow Rate of 80kg/s.

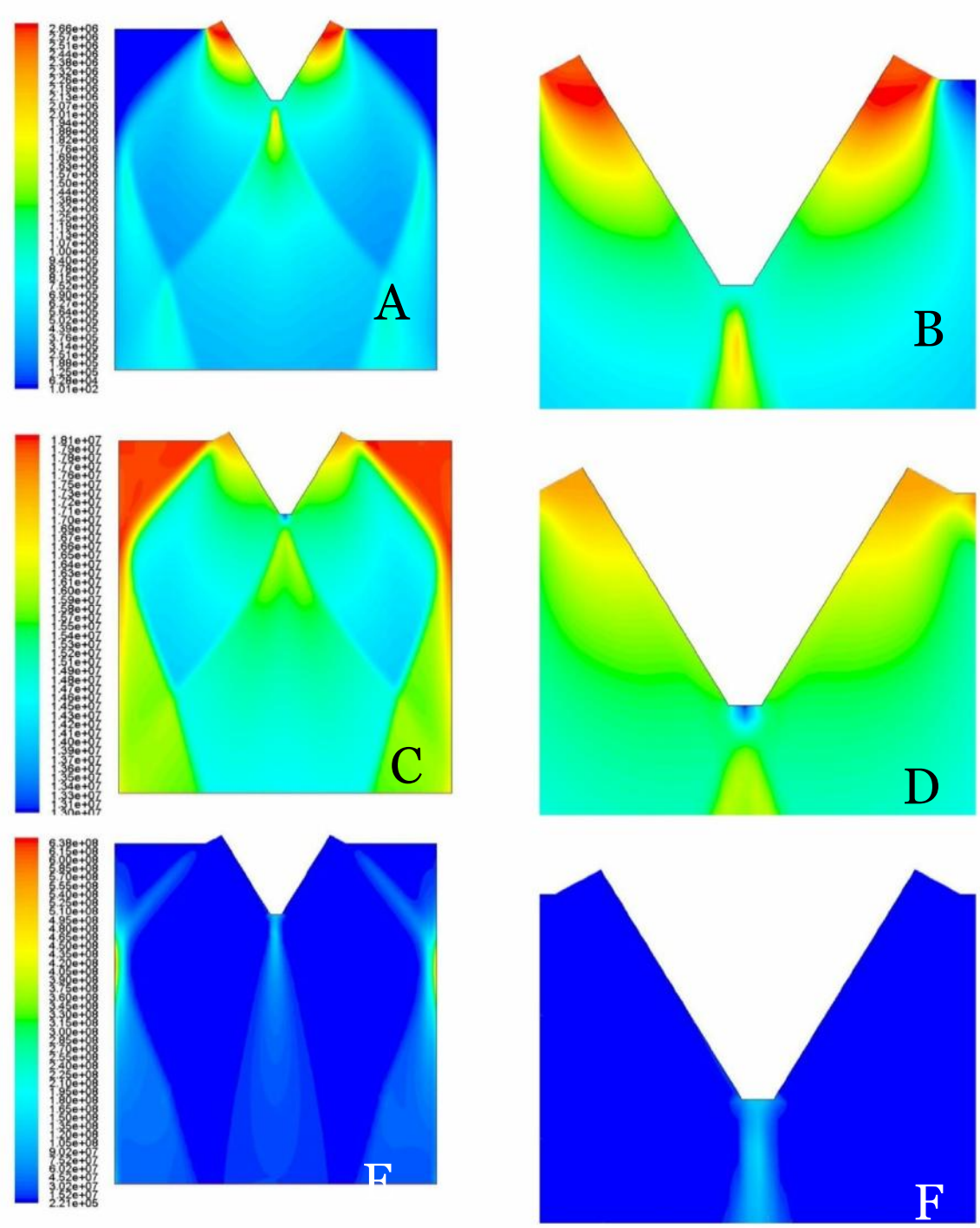

Figure3.13. Contours of Dynamic Pressure (A,B), Enthalpy (C,D) & Turbulent Dissipation Rate (E,F) for 10 % Truncation with a Base Bleed Mass Flow Rate of 90kg/s.

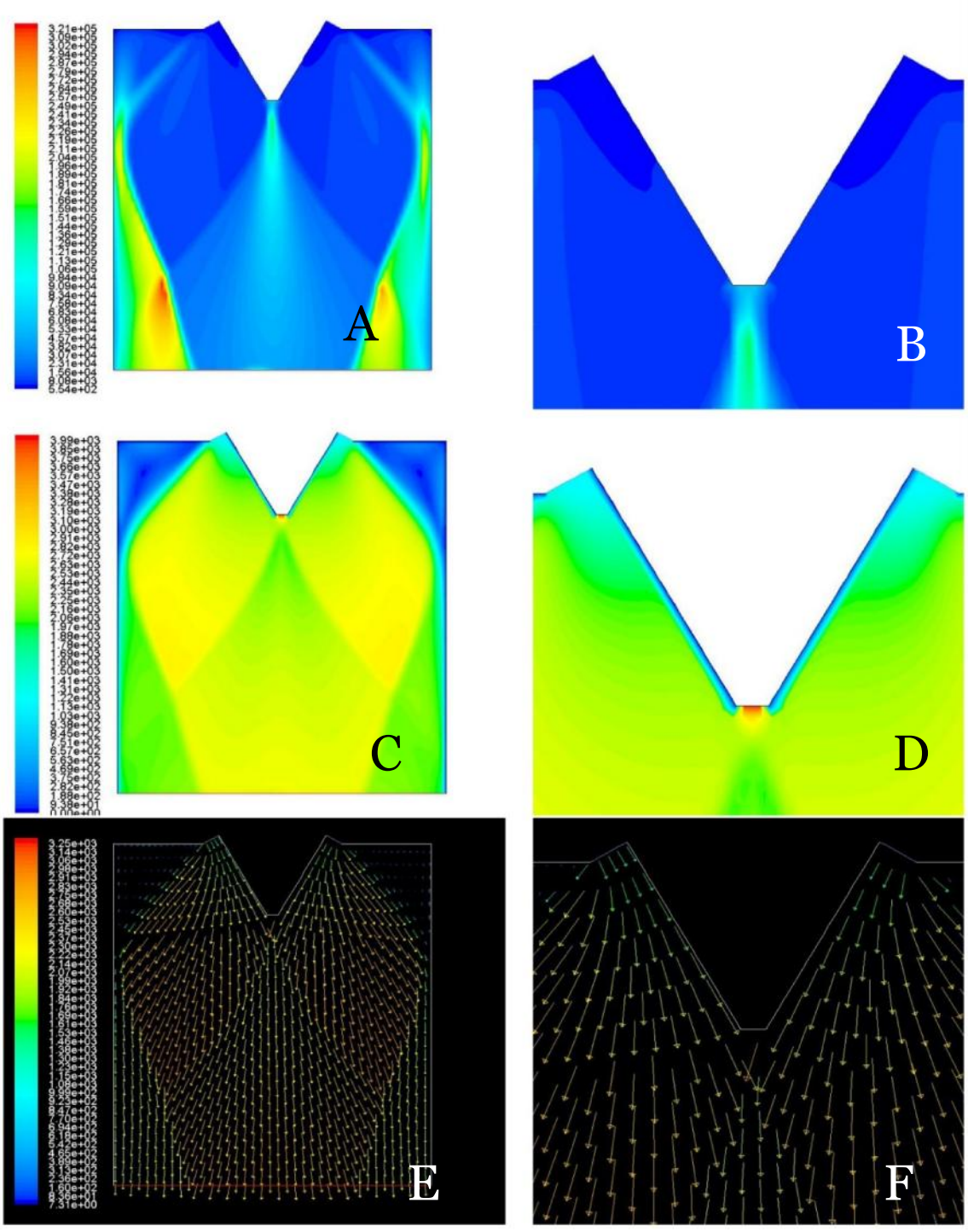

Figure3.14. Contours of Turbulent Kinetic Energy(A,B), Velocity Magnitude (C,D) & Velocity Vector (E,F) for 10 % Truncation with a Base Bleed Mass Flow Rate of 90kg/s.

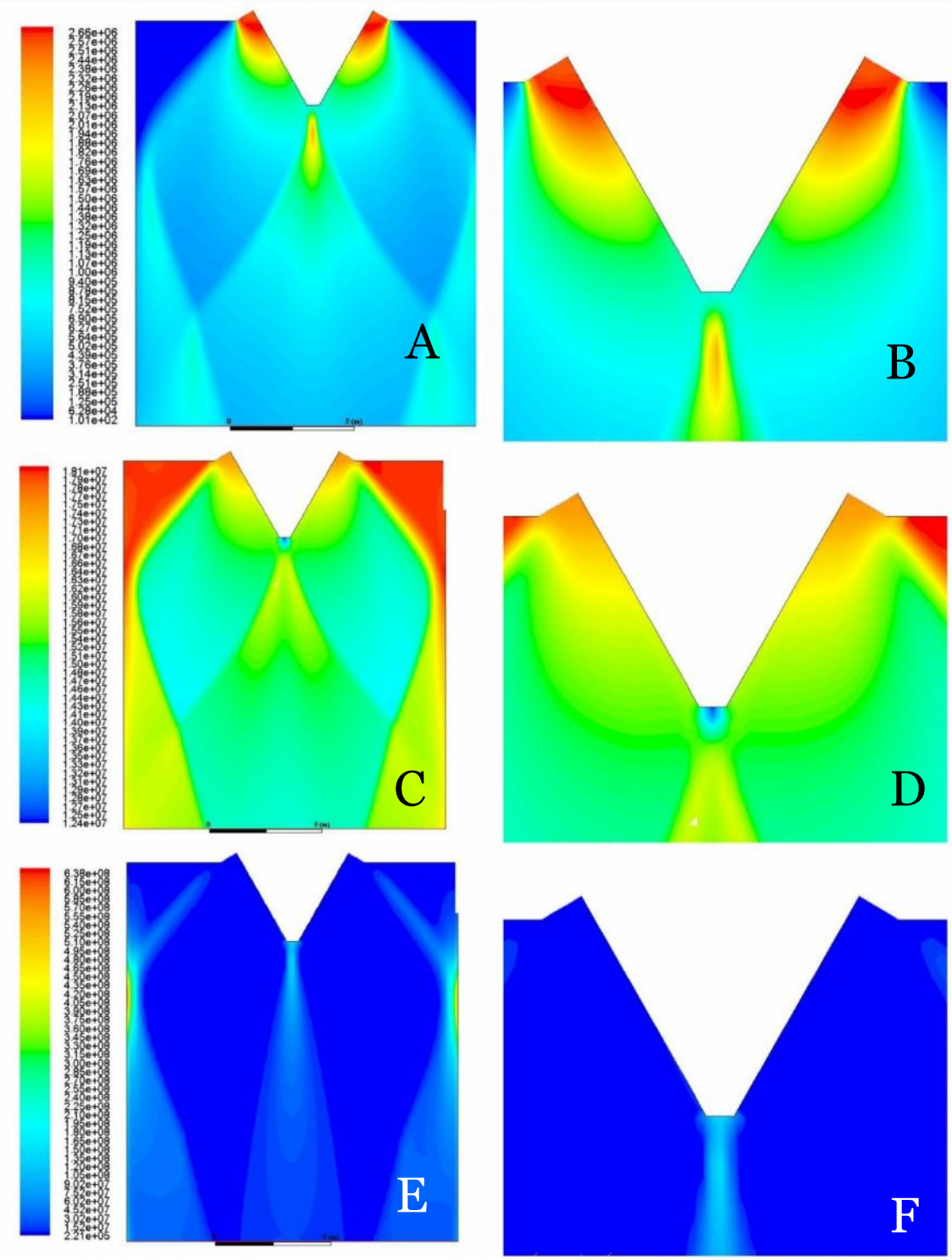

Figure3.15. Contours of Dynamic Pressure (A,B), Enthalpy (C,D)& Turbulent Dissipation Rate (E,F) for 10 % Truncation with a Base Bleed Mass Flow Rate of 100kg/s.

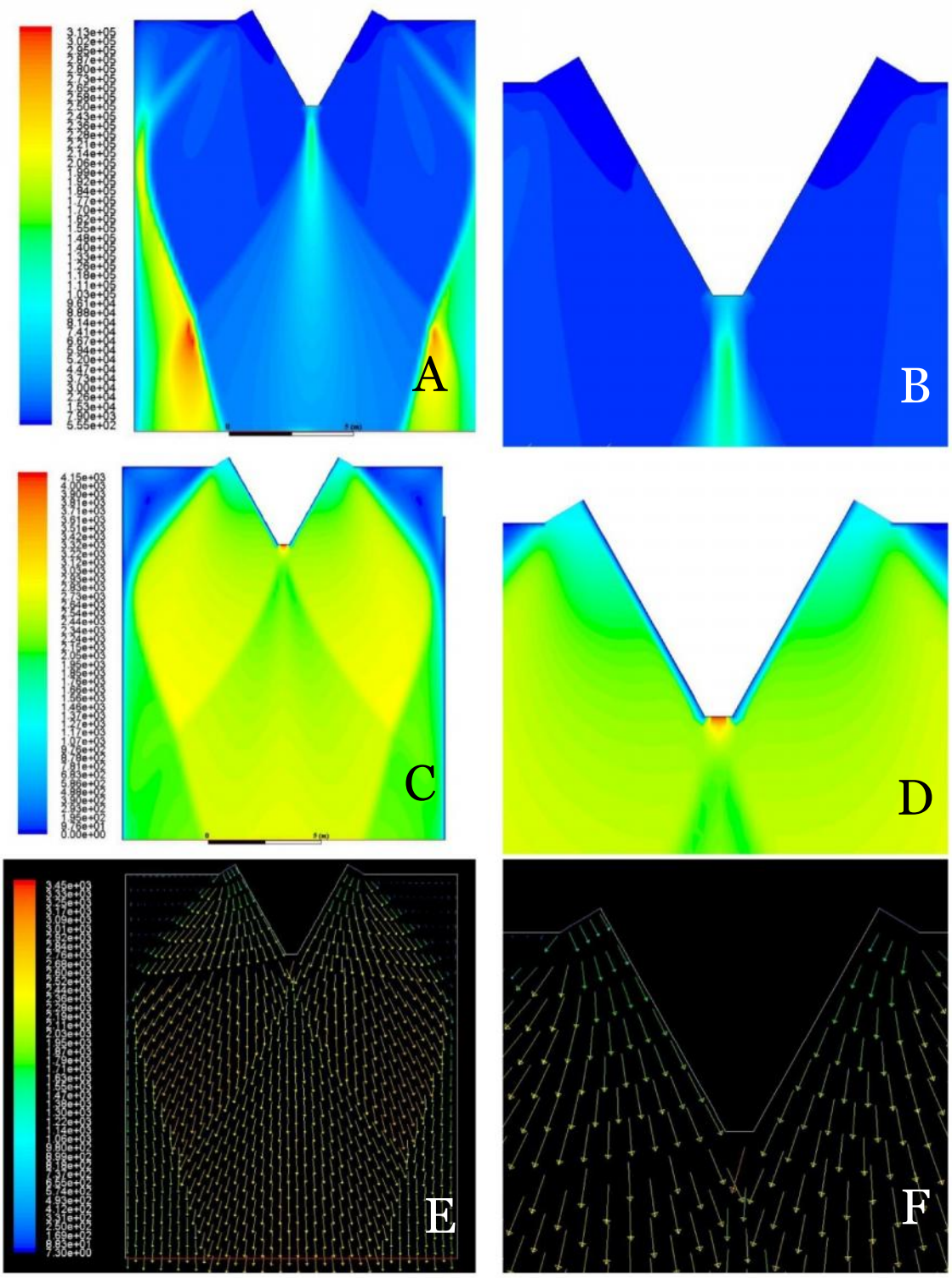

Figure3.16 Contours of Turbulent Kinetic Energy (A,B), Velocity Magnitude (C,D)& Velocity Vector (E,F) for 10 % Truncation with a Base Bleed Mass Flow Rate of 100kg/s.

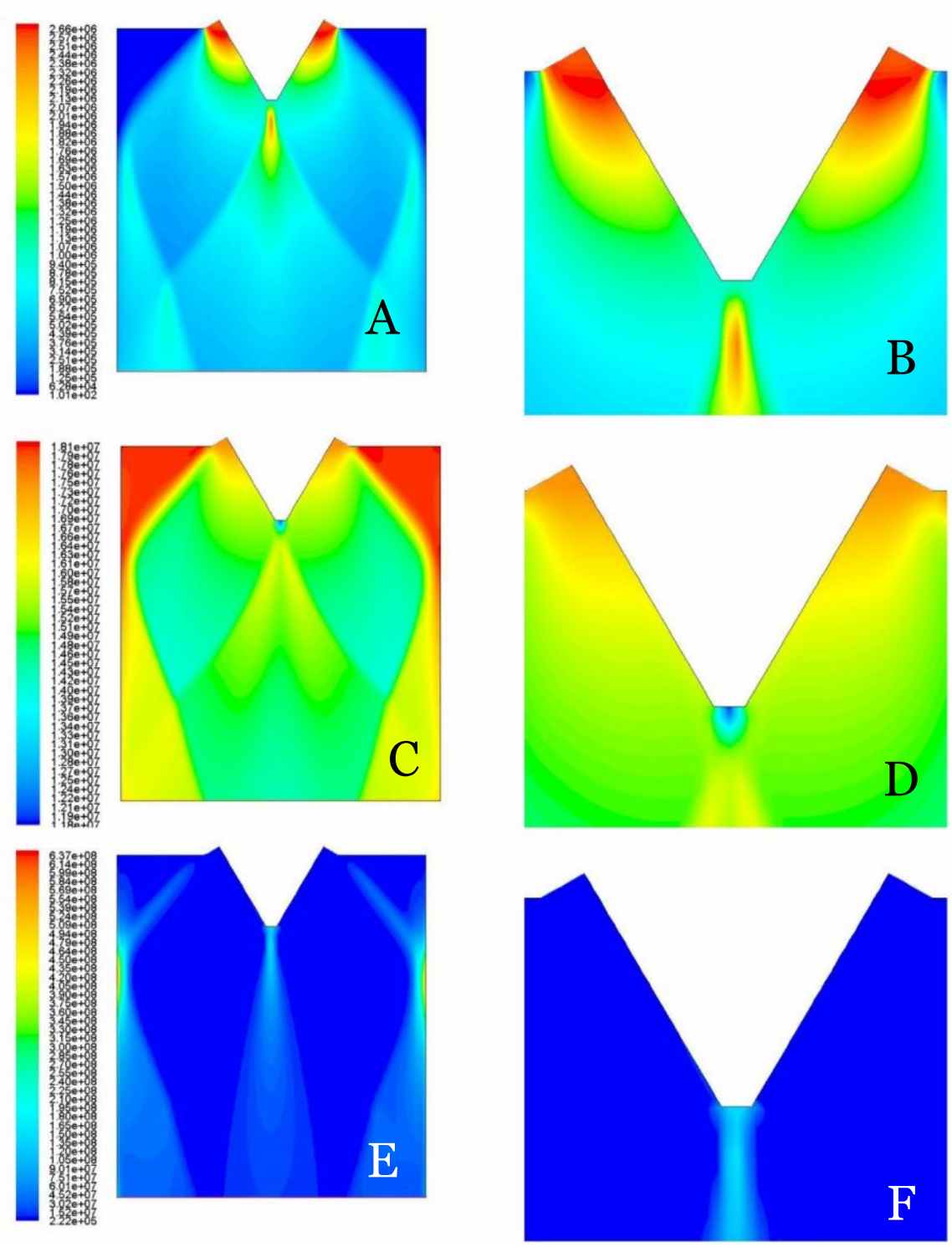

*Figure3.17.*Contours of Dynamic Pressure (A,B), Enthalpy (C,D) & Turbulent Dissipation Rate(E,F) for 10 % Truncation with a Base Bleed Mass Flow Rate of 110kg/s.

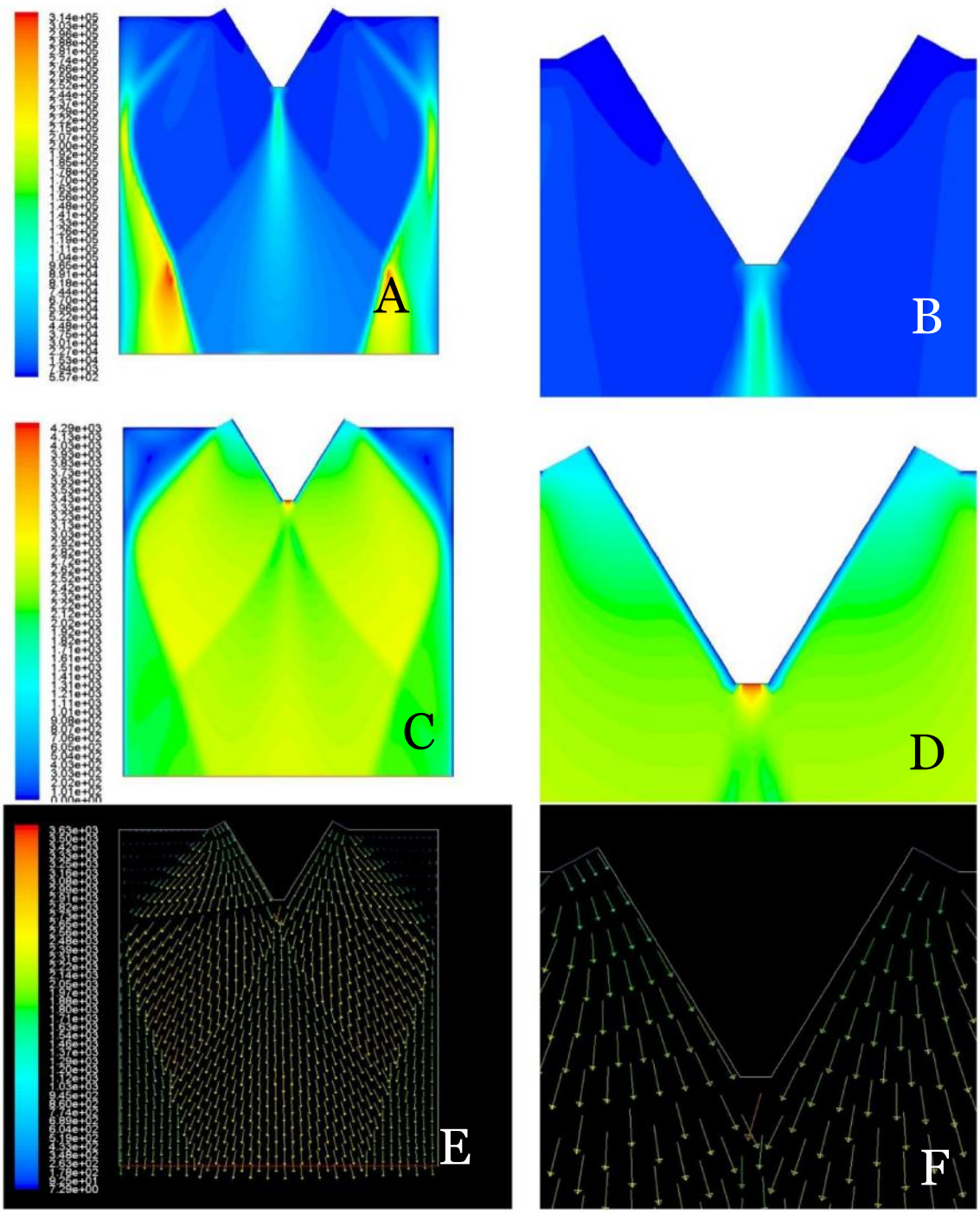

Figure3.18.Contours of Turbulent Kinetic Energy (A,B), Velocity Magnitude (C,D) & Velocity Vector (E,F) for 10 % Truncation with a Base Bleed Mass Flow Rate of 110kg/s.

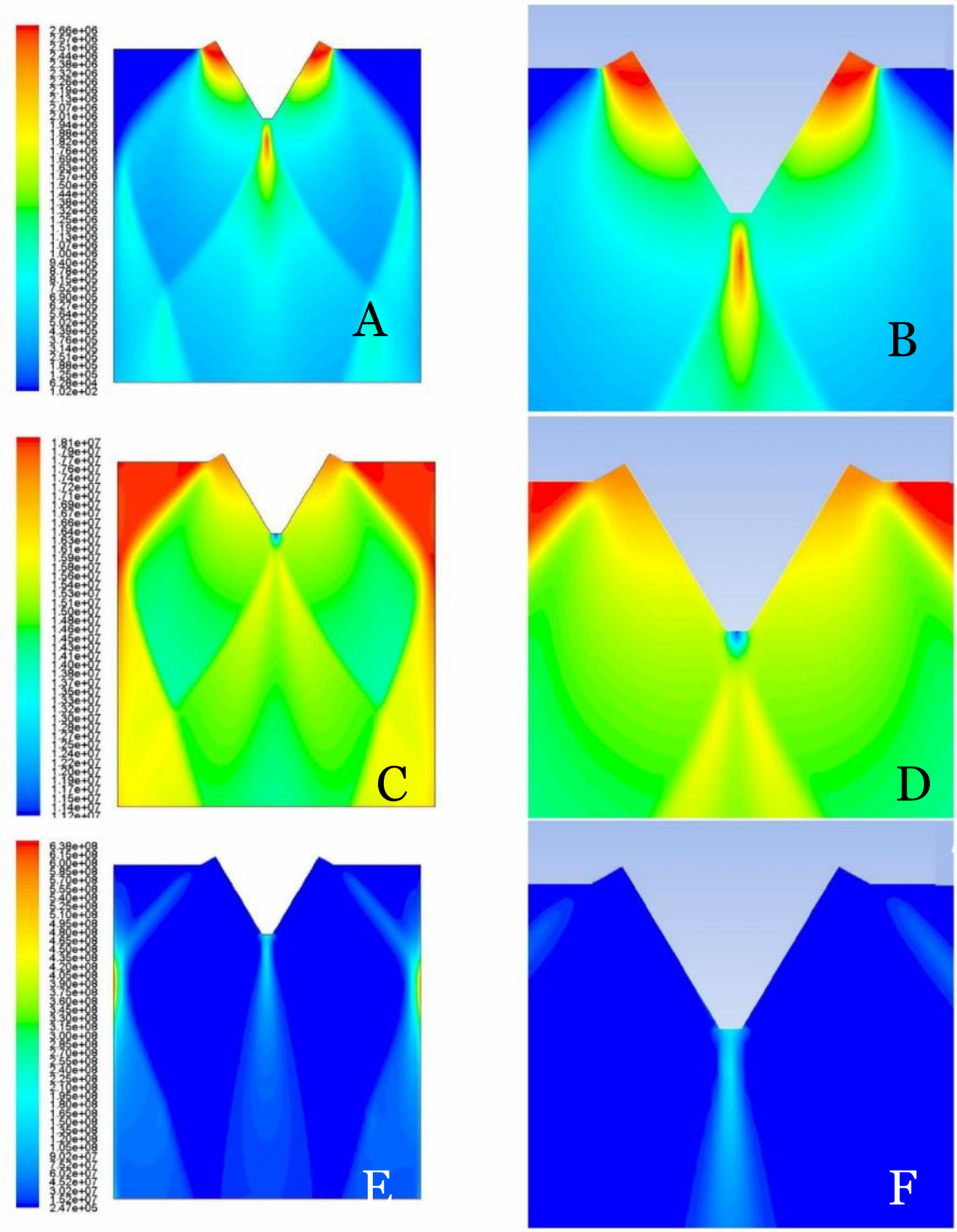

*Figure3.19.*Contours of Dynamic Pressure(A,B), Enthalpy (C,D) & Turbulent Dissipation Rate (E,F) for 10 % Truncation with a Base Bleed Mass Flow Rate of 120kg/s.

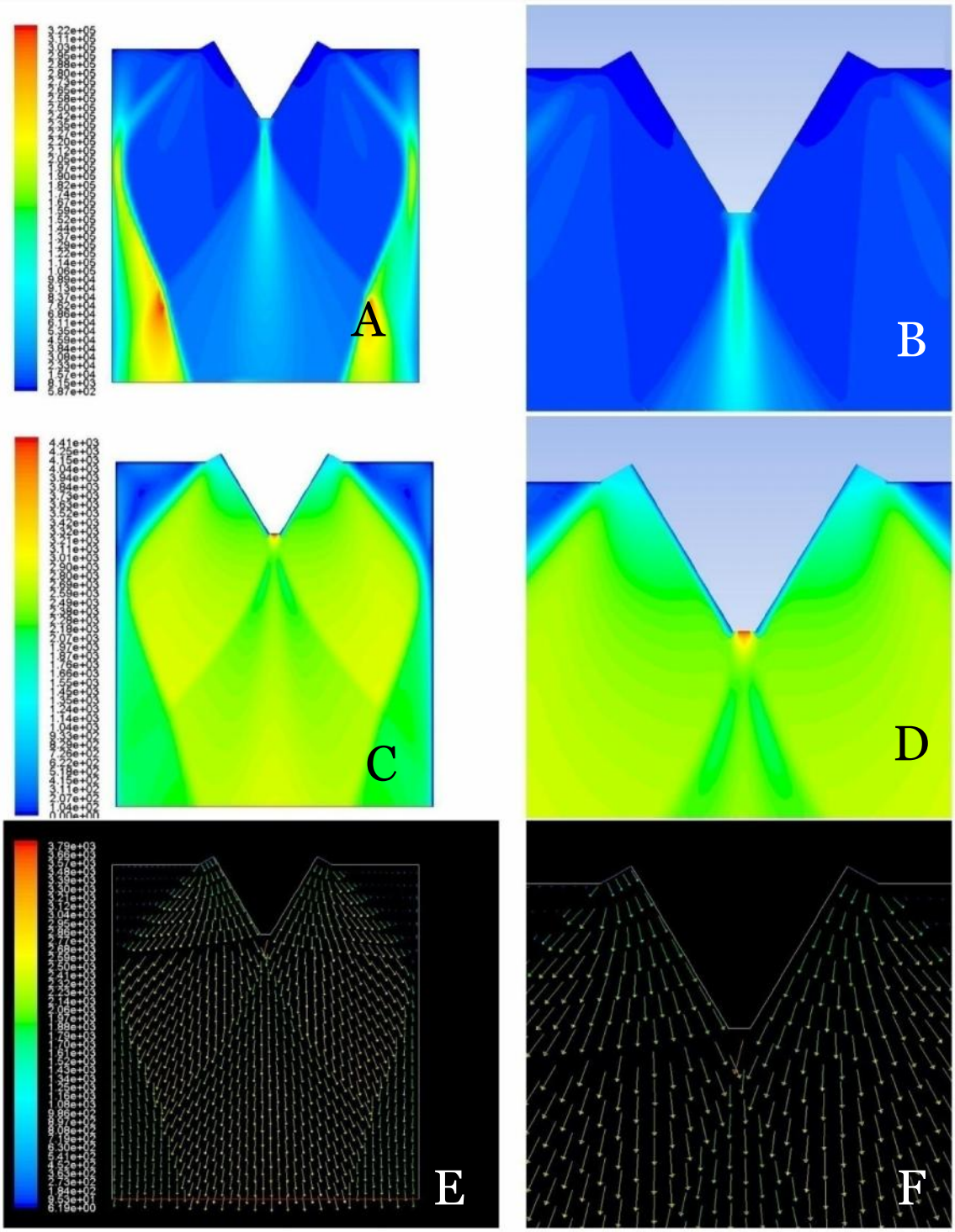

Figure3.20.Contours of Turbulent Kinetic Energy (A,B), Velocity Magnitude (C,D)& Velocity Vector (E,F) for 10 % Truncation with a Base Bleed Mass Flow Rate of 120kg/s.

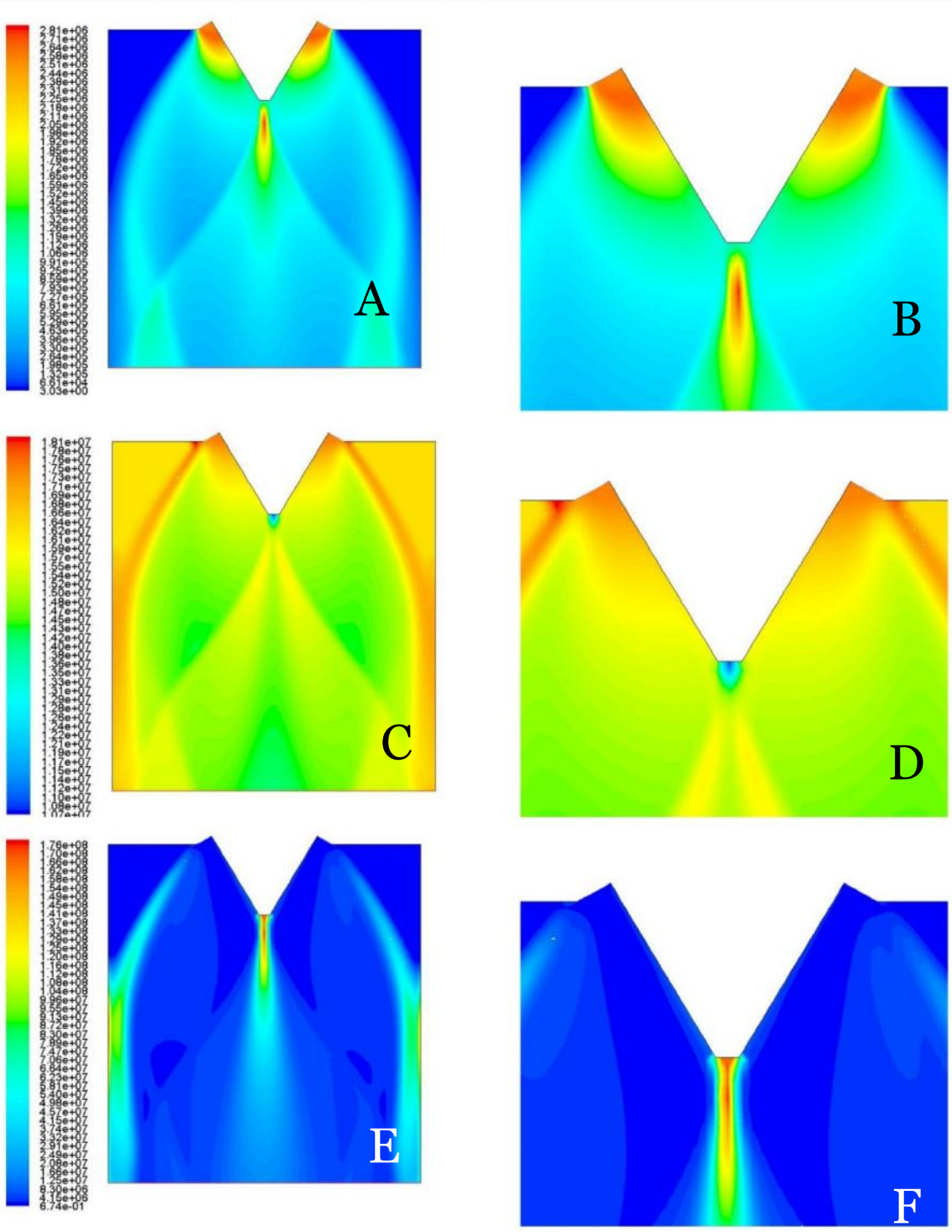

*Figure3.21.*Contours of Dynamic Pressure (A,B), Enthalpy (C,D) & Turbulent Dissipation Rate (E,F) for 10 % Truncation with a Base Bleed Mass Flow Rate of 130kg/s.

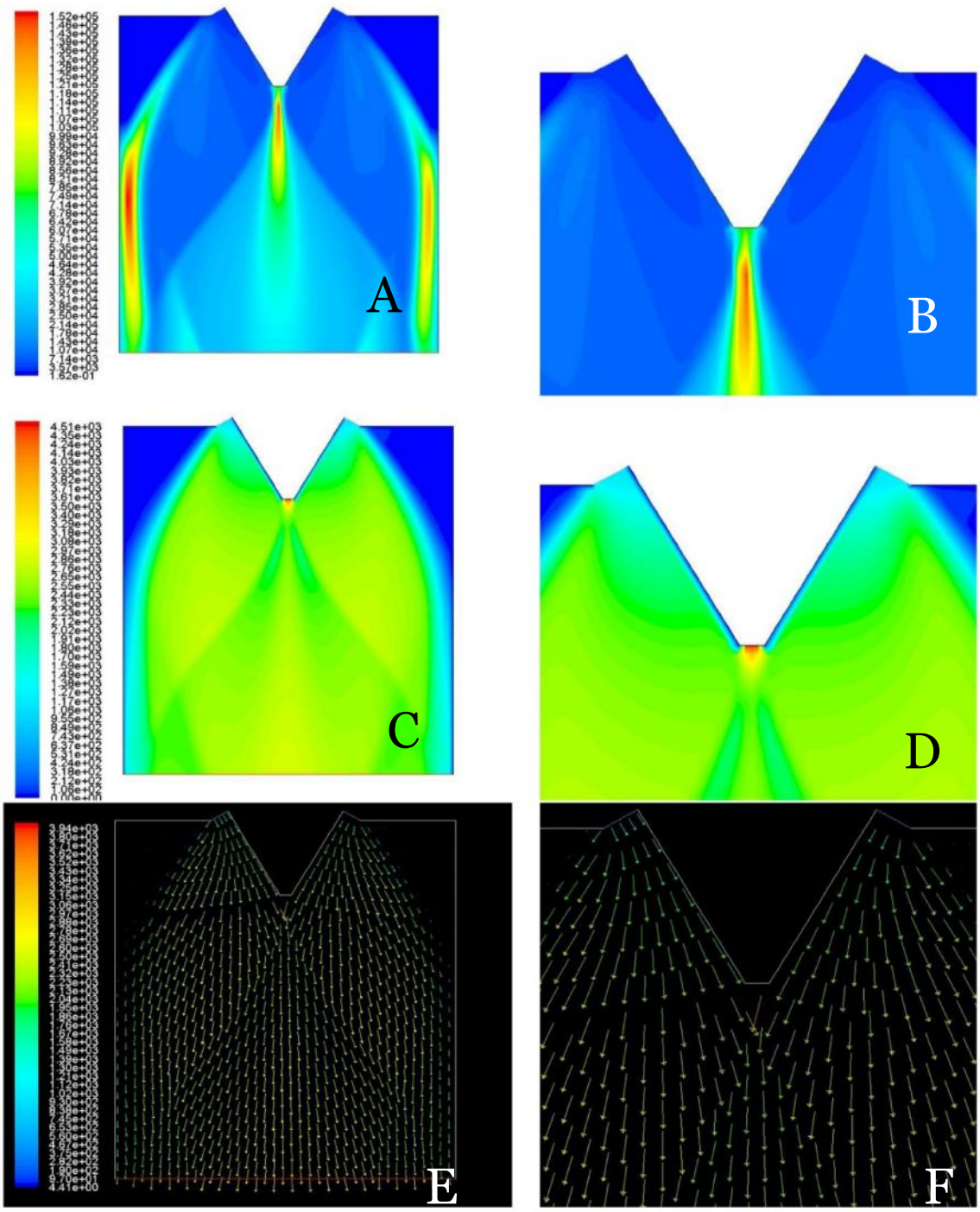

Figure3.22.Contours of Turbulent Kinetic Energy (A,B), Velocity Magnitude (C,D)& Velocity Vector (E,F) for 10 % Truncation with a Base Bleed Mass Flow Rate of 130kg/s.

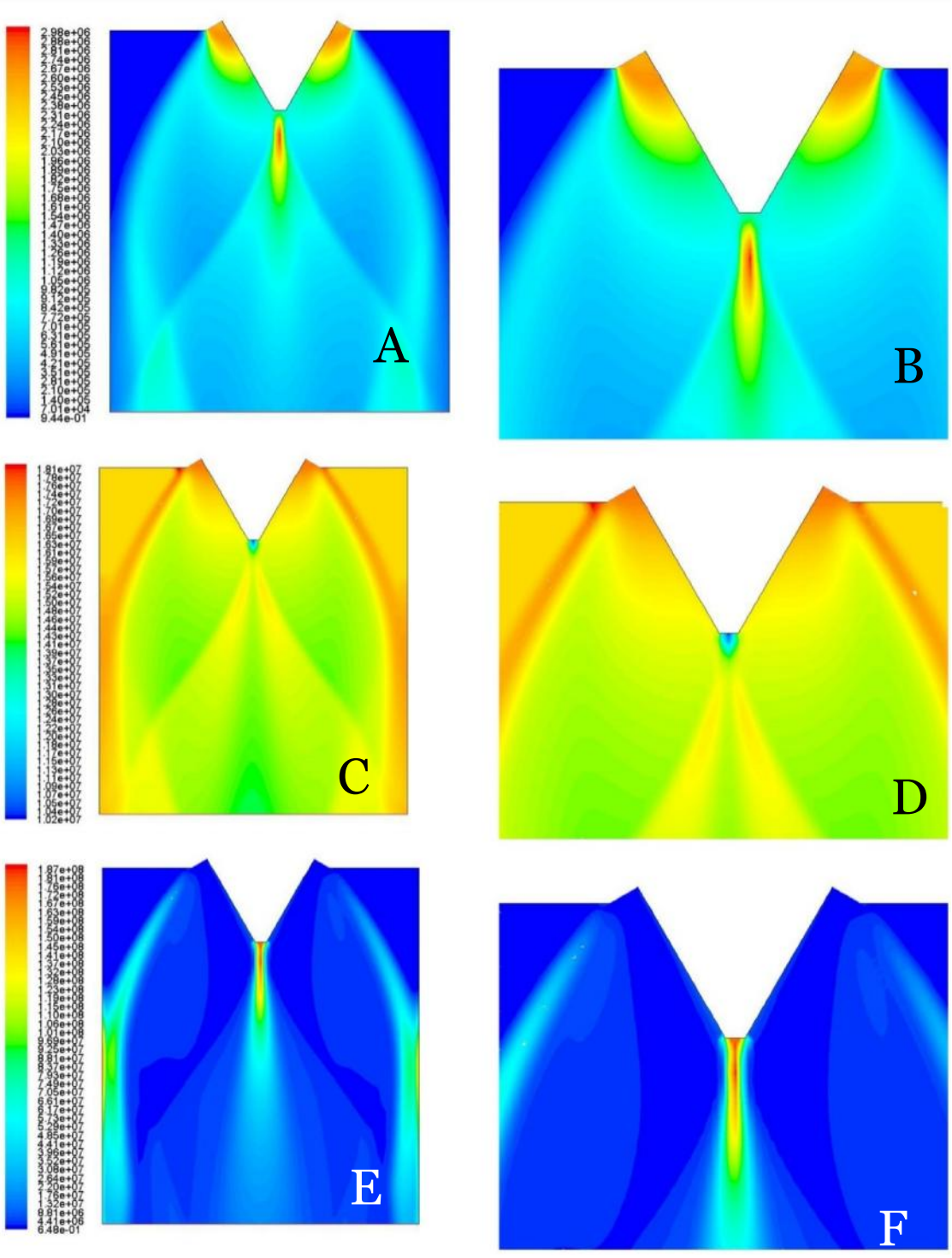

Figure3.23.Contours of Dynamic Pressure (A,B), Enthalpy (C,D) & Turbulent Dissipation Rate (E,F) for 10 % Truncation with a Base Bleed Mass Flow Rate of 140kg/s.

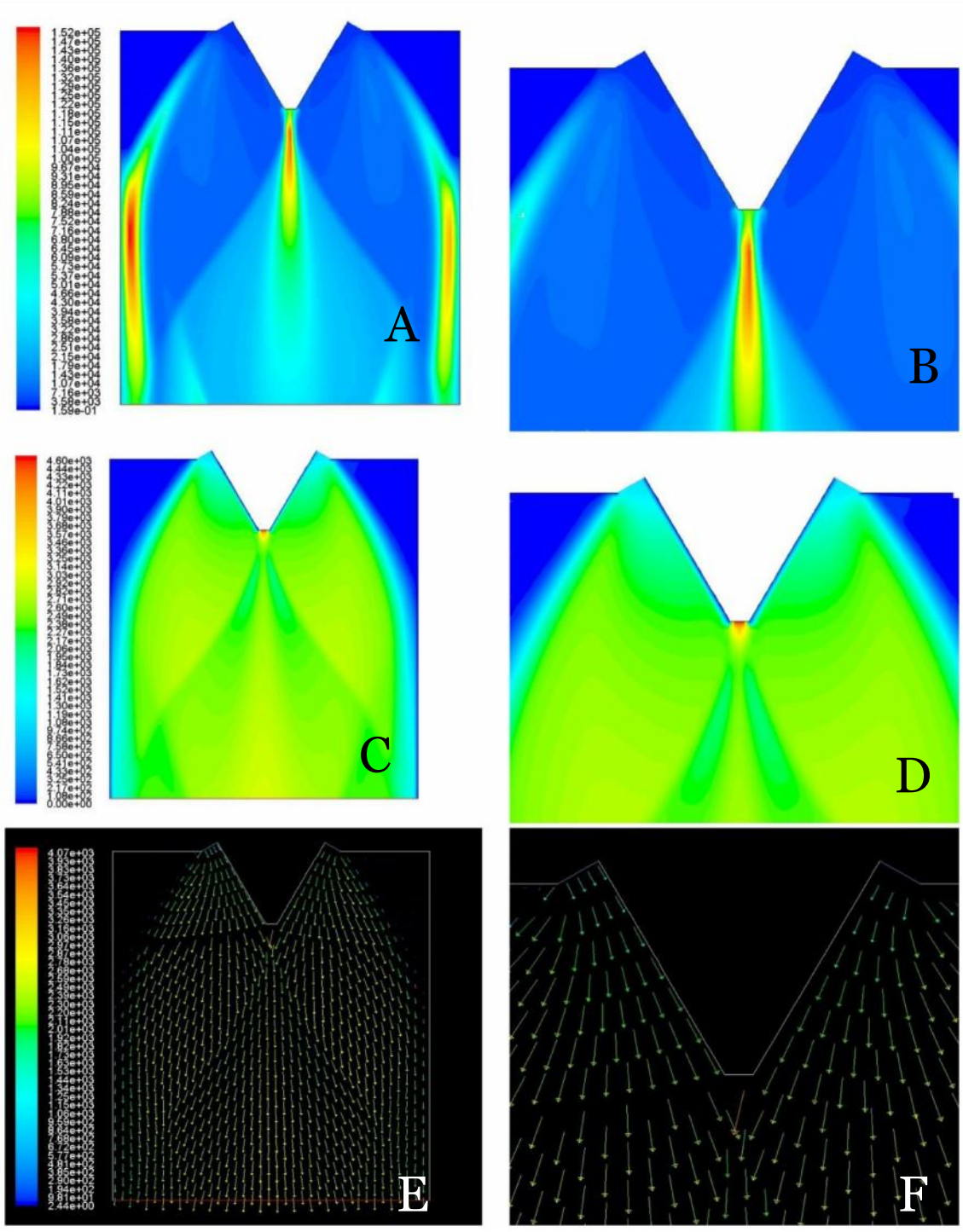

*Figure3.24.*Contours of Turbulent Kinetic Energy (A,B), Velocity Magnitude (C,D)& Velocity Vector (E,F) for 10 % Truncation with a Base Bleed Mass Flow Rate of 140kg/s.

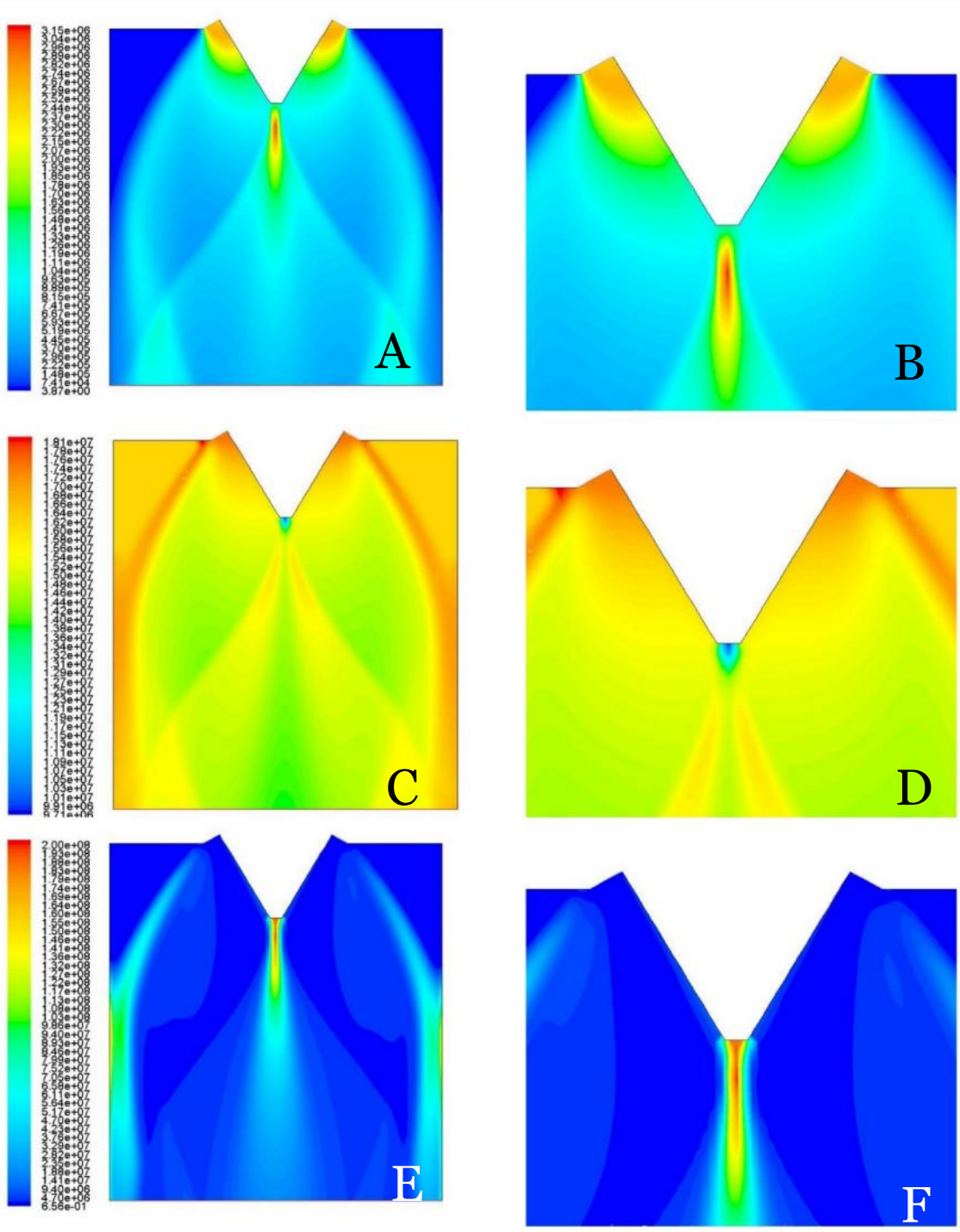

*Figure3.25.*Contours of Dynamic Pressure (A,B), Enthalpy (C,D) & Turbulent Dissipation Rate (E,F) for 10 % Truncation with a Base Bleed Mass Flow Rate of 150kg/s.

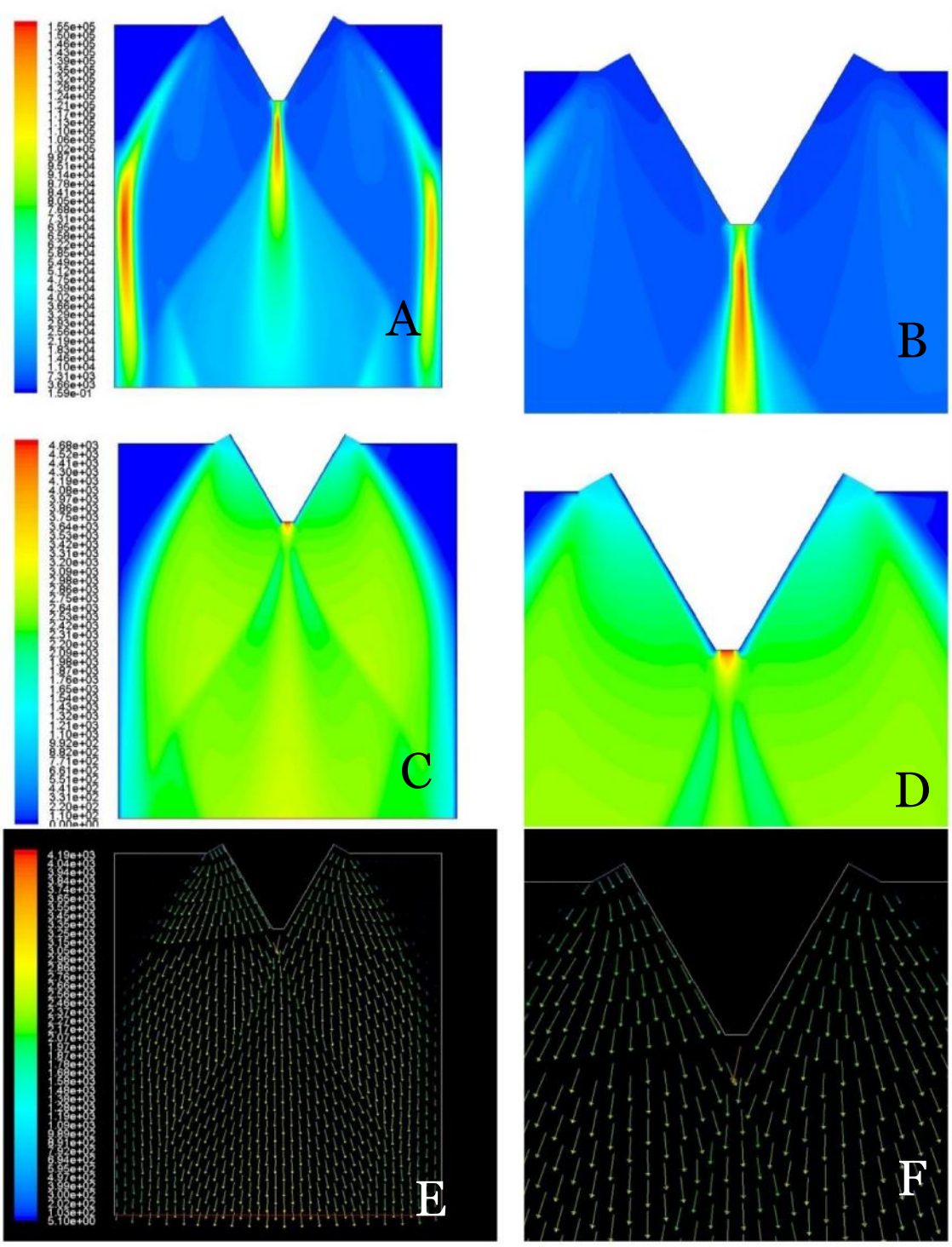

*Figure3.26.*Contours of Turbulent Kinetic Energy (A,B), Velocity Magnitude (C,D) & Velocity Vector (E,F) for 10 % Truncation with a Base Bleed Mass Flow Rate of 150kg/s.

Thus it is observed that 150kg/s is the optimum base bleed mass flow rate for the 10% truncated case. A uniform pressure field near the base of the truncation is seen for this base bleed mass flow rate. The enthalpy seems to be at a minimum near the truncated portion for all base bleed mass flow rates. As for the turbulent kinetic energy and turbulent dissipation rate, they seem to increase in magnitude (maximum at the base of truncation) proportional to the base bleed mass flow rate.

The following pages (48-61) contain contour plots for the 20 % truncated cases.A 20% truncated nozzle is lighter and more compact compared to a 10 % truncated nozzle but recirculation losses are higher. The base bleed mass flow rates used for simulating the 20 % truncated case are thus higher than the ones used for 10 % truncated case.

The enthalpy, turbulent kinetic energy and total dissipation rate for the 20 % truncated follow similar trends as with the 10 % truncated case. The enthalpy is at a minimum near the base of the truncation. The turbulent kinetic energy and turbulent dissipation rate near the truncated portion increases in magnitude proportional to the base bleed mass flow rate.

The optimum base bleed mass flow rate for the 20 % is found out to be 300 kg /s for which the dynamic pressure profile appears to be uniform near the truncated portion.

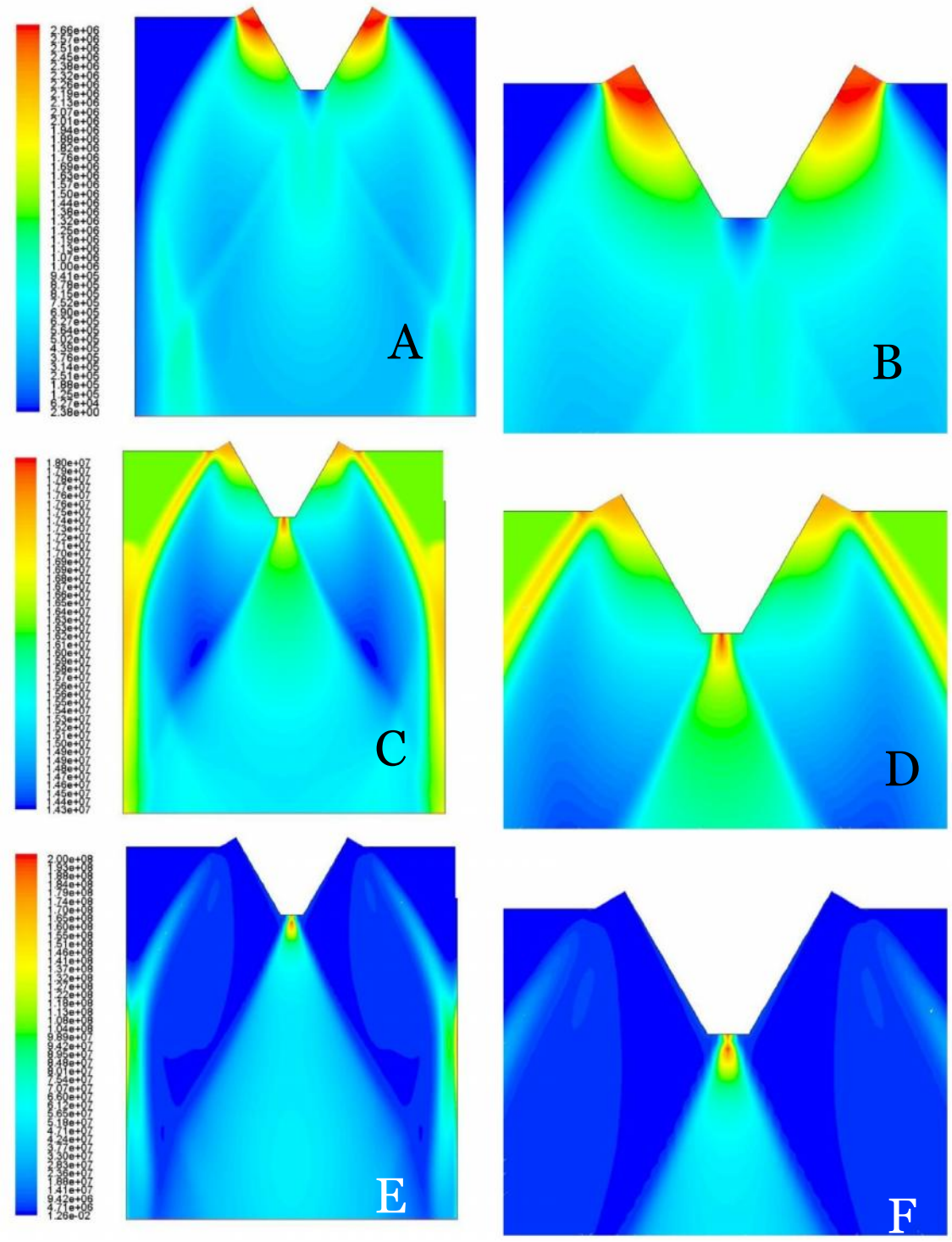

*Figure3.27.*Contours of Dynamic Pressure (A,B), Enthalpy (C,D) & Turbulent Dissipation Rate (E,F) for 20 % Truncation without Base Bleed.

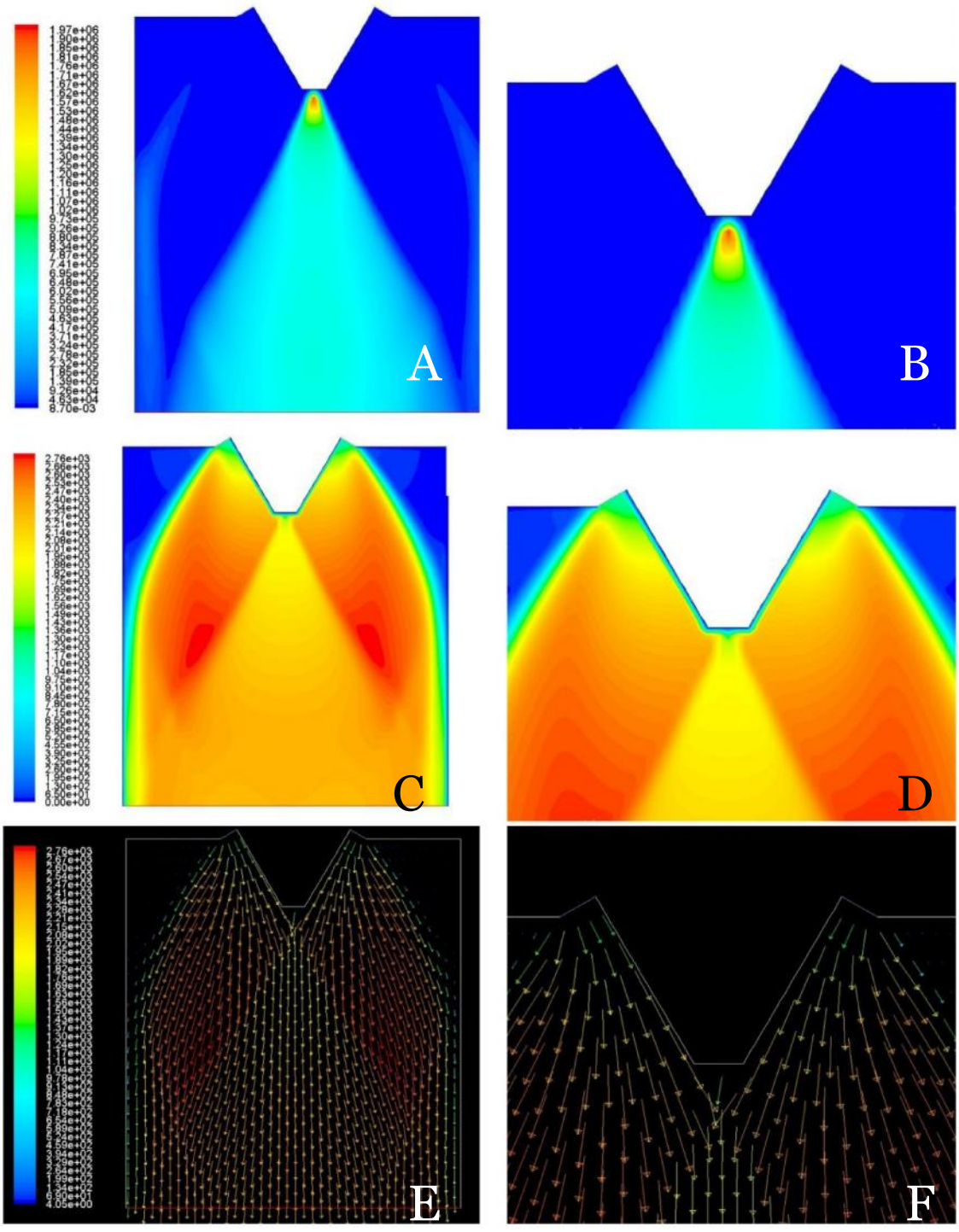

Figure3.28.Contours of Turbulent Kinetic Energy (A,B) , Velocity Magnitude (C,D)& Velocity Vector (E,F) for 20 % Truncation without Base Bleed.

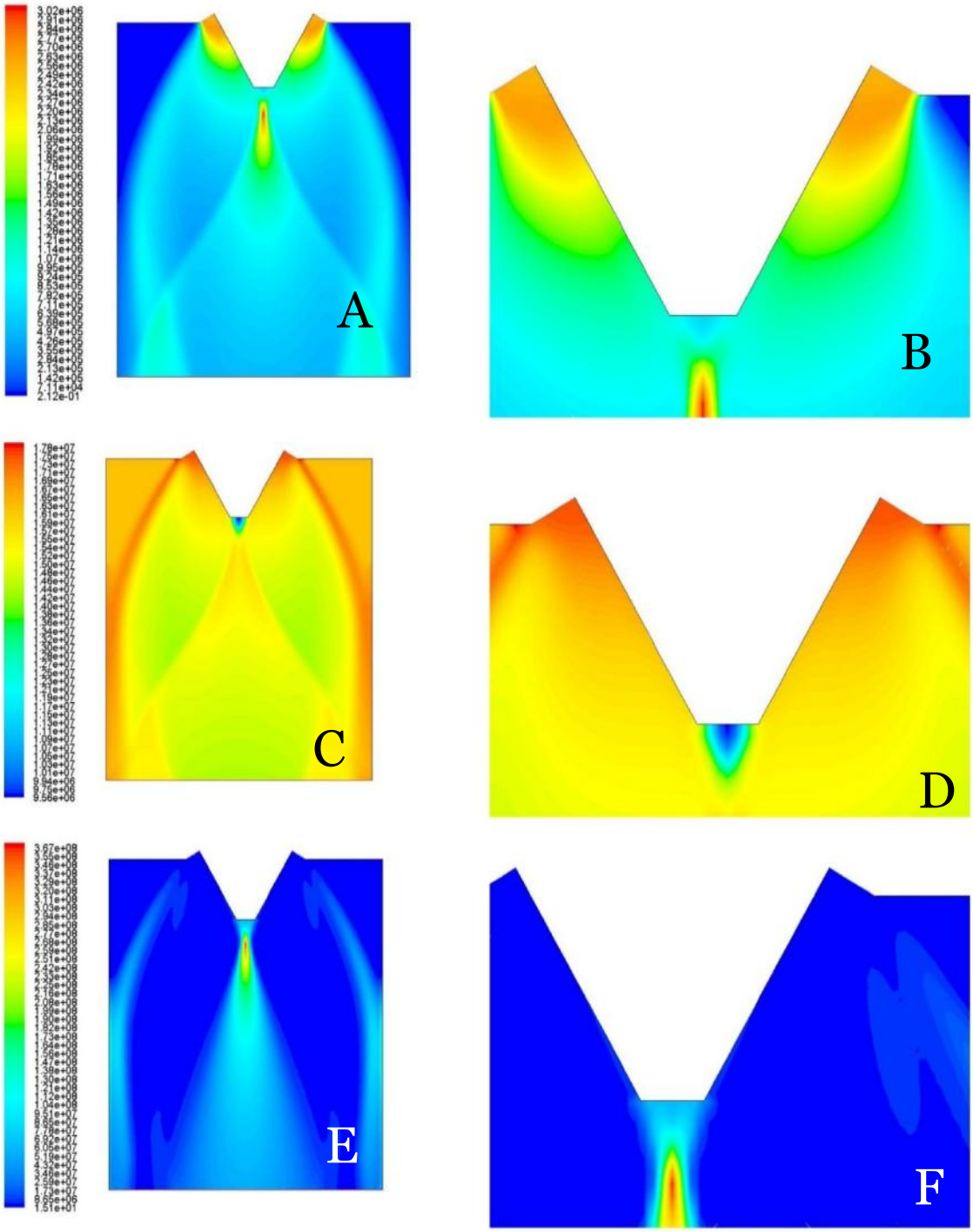

*Figure3.29.*Contours of Dynamic Pressure (A,B), Enthalpy (C,D) & Turbulent Dissipation Rate (E,F) for 20 % Truncation with a Base Bleed Mass Flow Rate of 200 kg/s.

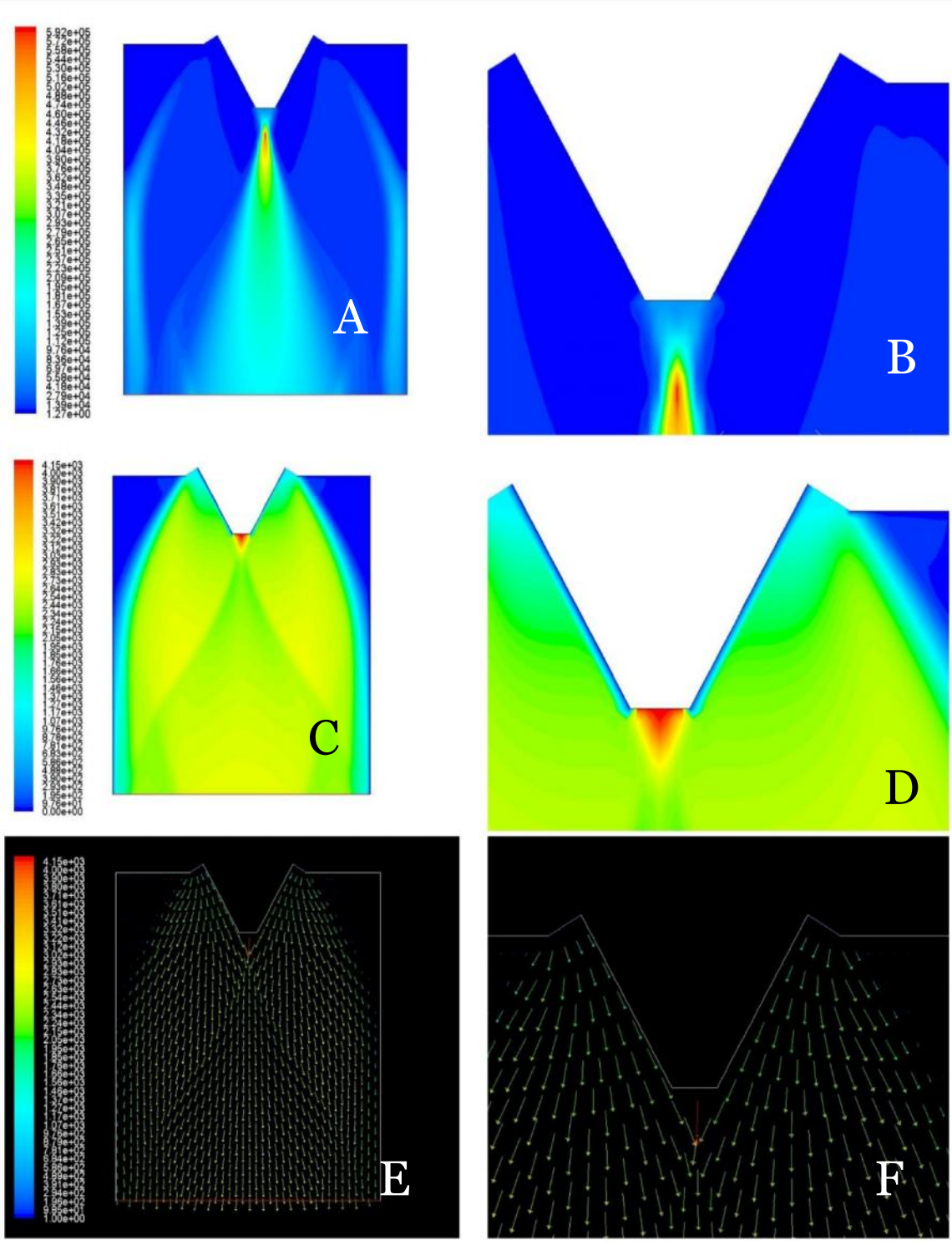

Figure3.30.Contours of Turbulent Kinetic Energy (A,B), Velocity Magnitude (C,D) & Velocity Vector (E,F) for 20 % Truncation with a Base Bleed Mass Flow Rate of 200 kg/s.

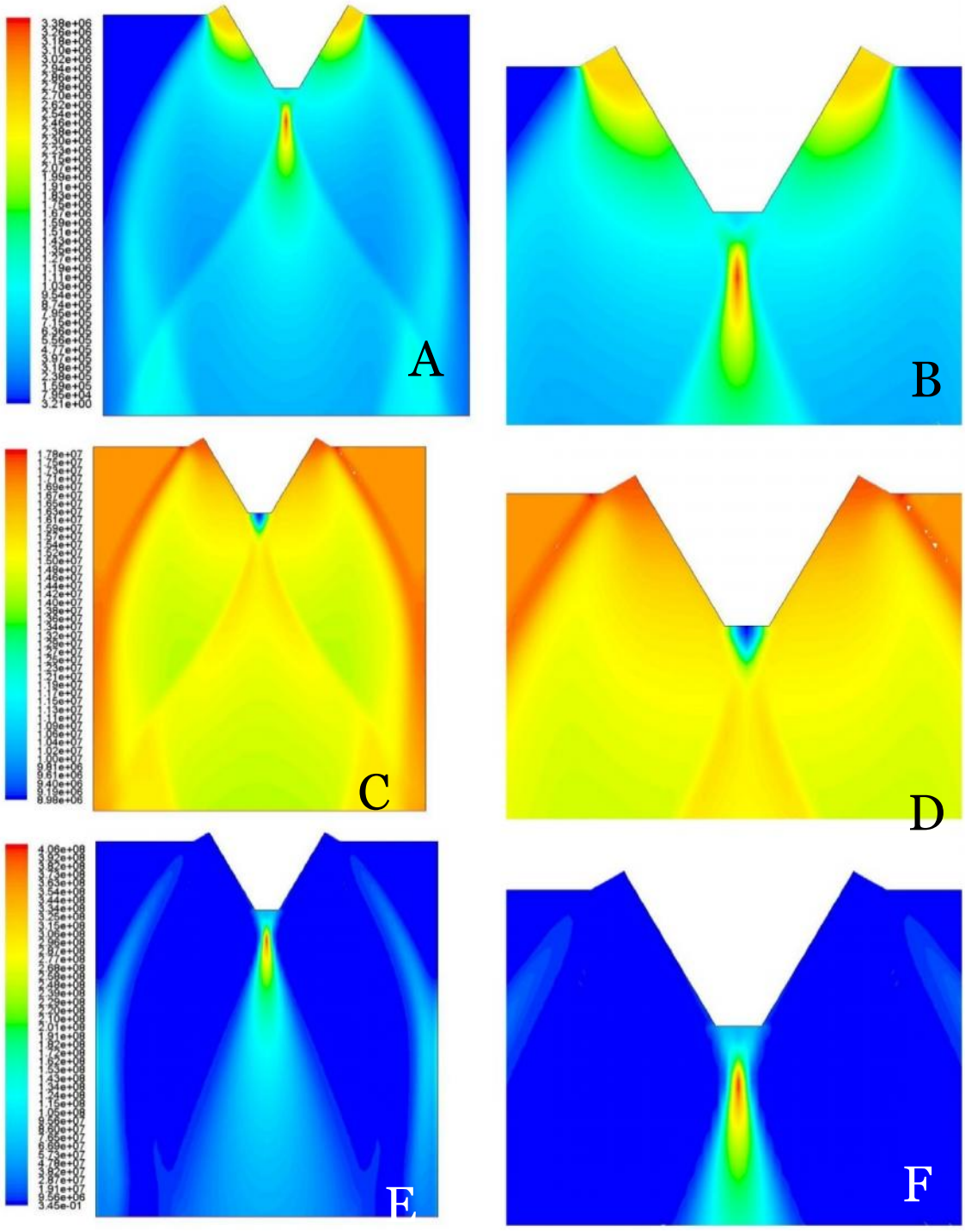

*Figure3.31.*Contours of Dynamic Pressure (A,B), Enthalpy (C,D) & Turbulent Dissipation Rate (E,F) for 20 % Truncation with a Base Bleed Mass Flow Rate of 220 kg/s.

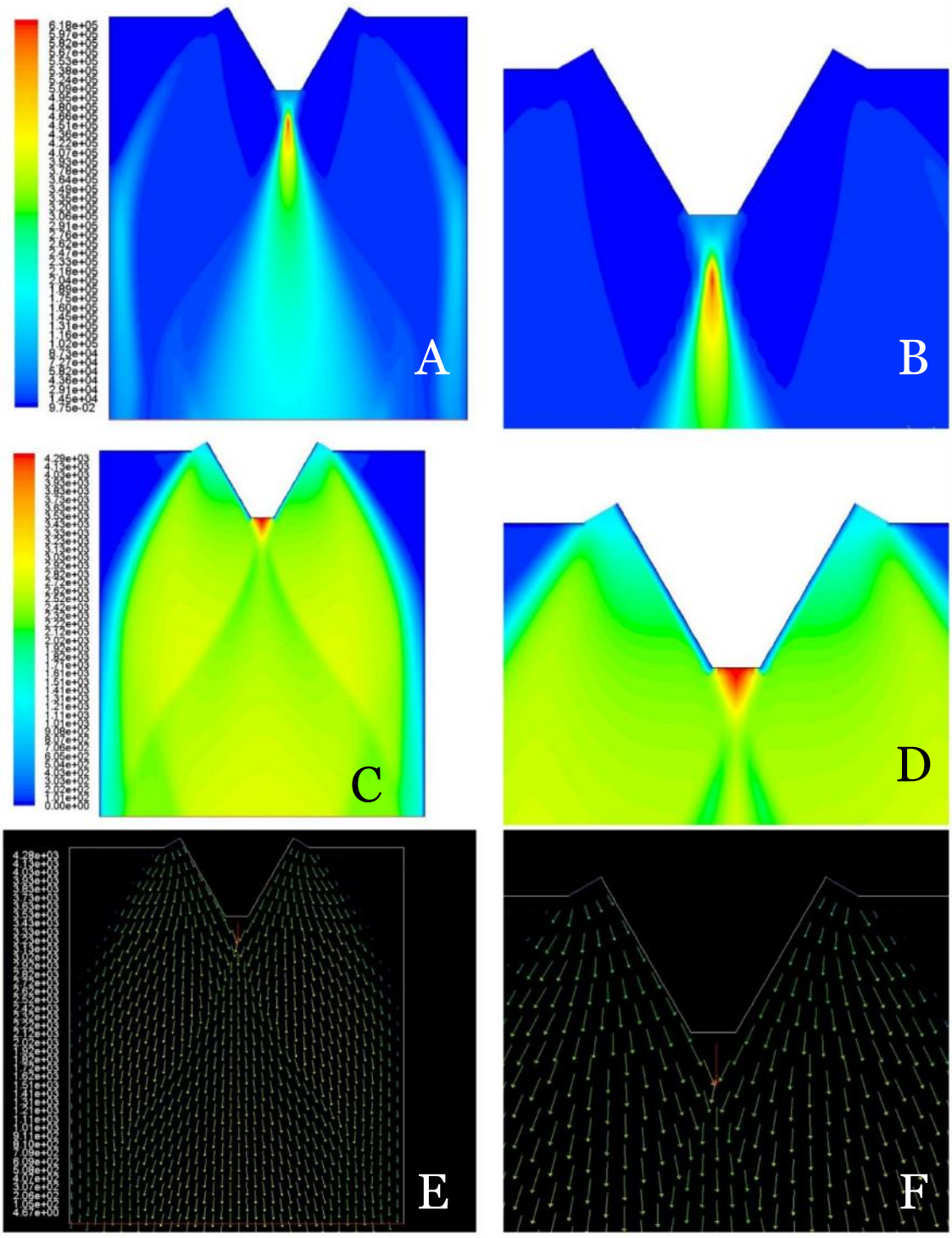

Figure3.32.Contours of Turbulent Kinetic Energy (A,B), Velocity Magnitude (C,D) & Velocity Vector (E,F) for 20 % Truncation with a Base Bleed Mass Flow Rate of 220 kg/s.

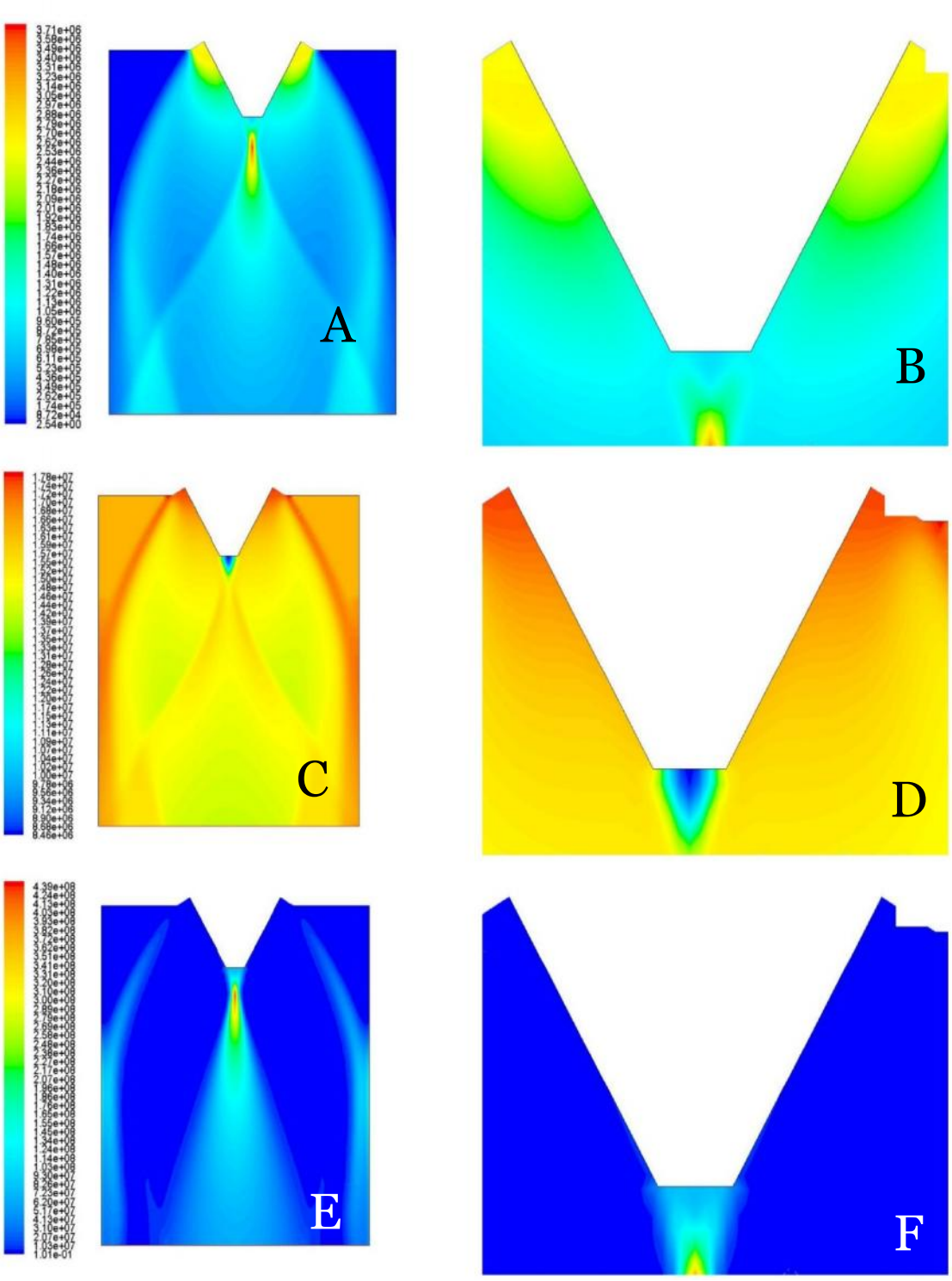

Figure3.33.Contours of Dynamic Pressure (A,B), Enthalpy(C,D) & Turbulent Dissipation Rate (E,F) for 20 % Truncation with a Base Bleed Mass Flow Rate of 240 kg/s.

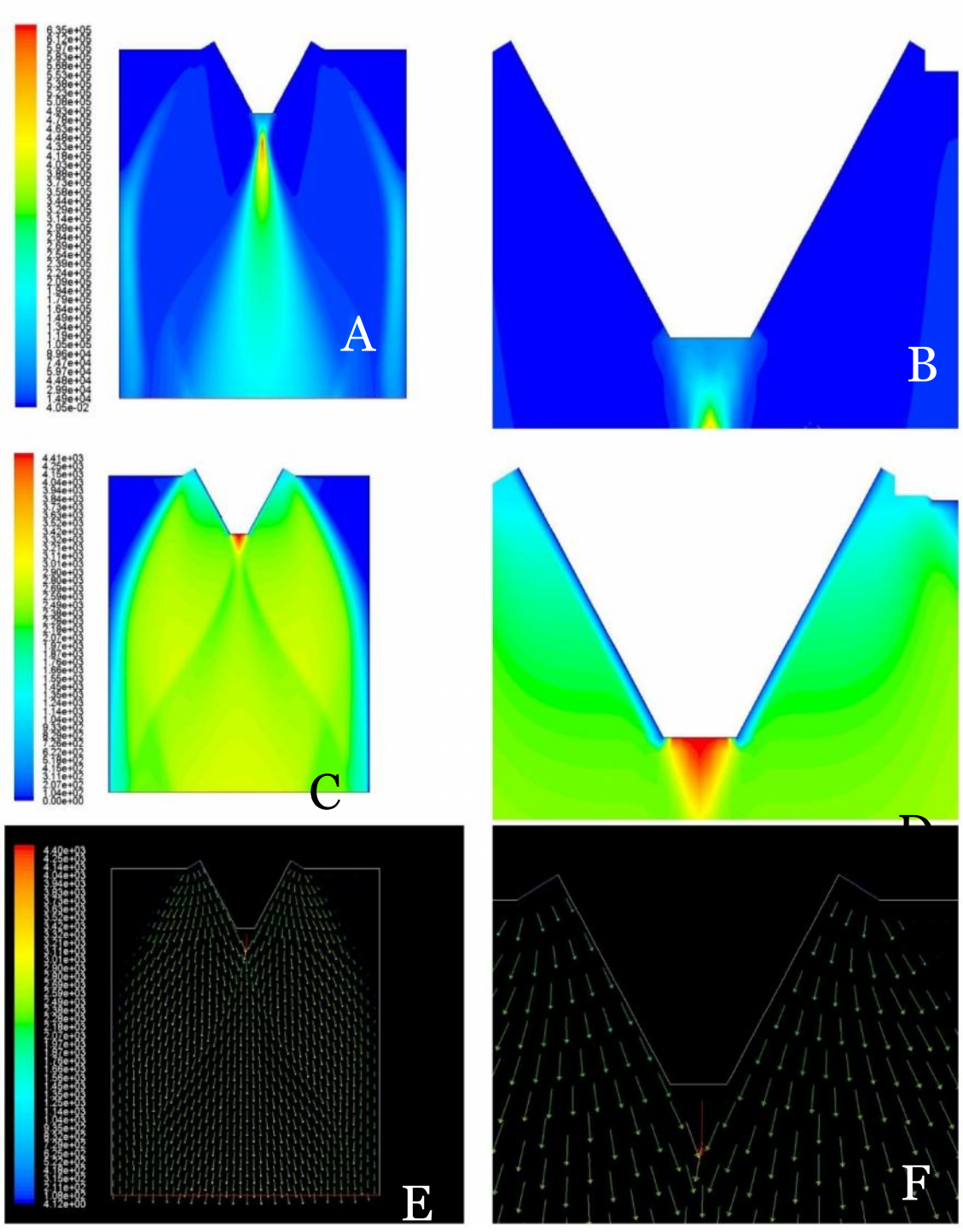

*Figure3.34.*Contours of Turbulent Kinetic Energy (A,B), Velocity Magnitude (C,D) & Velocity Vector (E,F) for 20 % Truncation with a Base Bleed Mass Flow Rate of 240 kg/s.

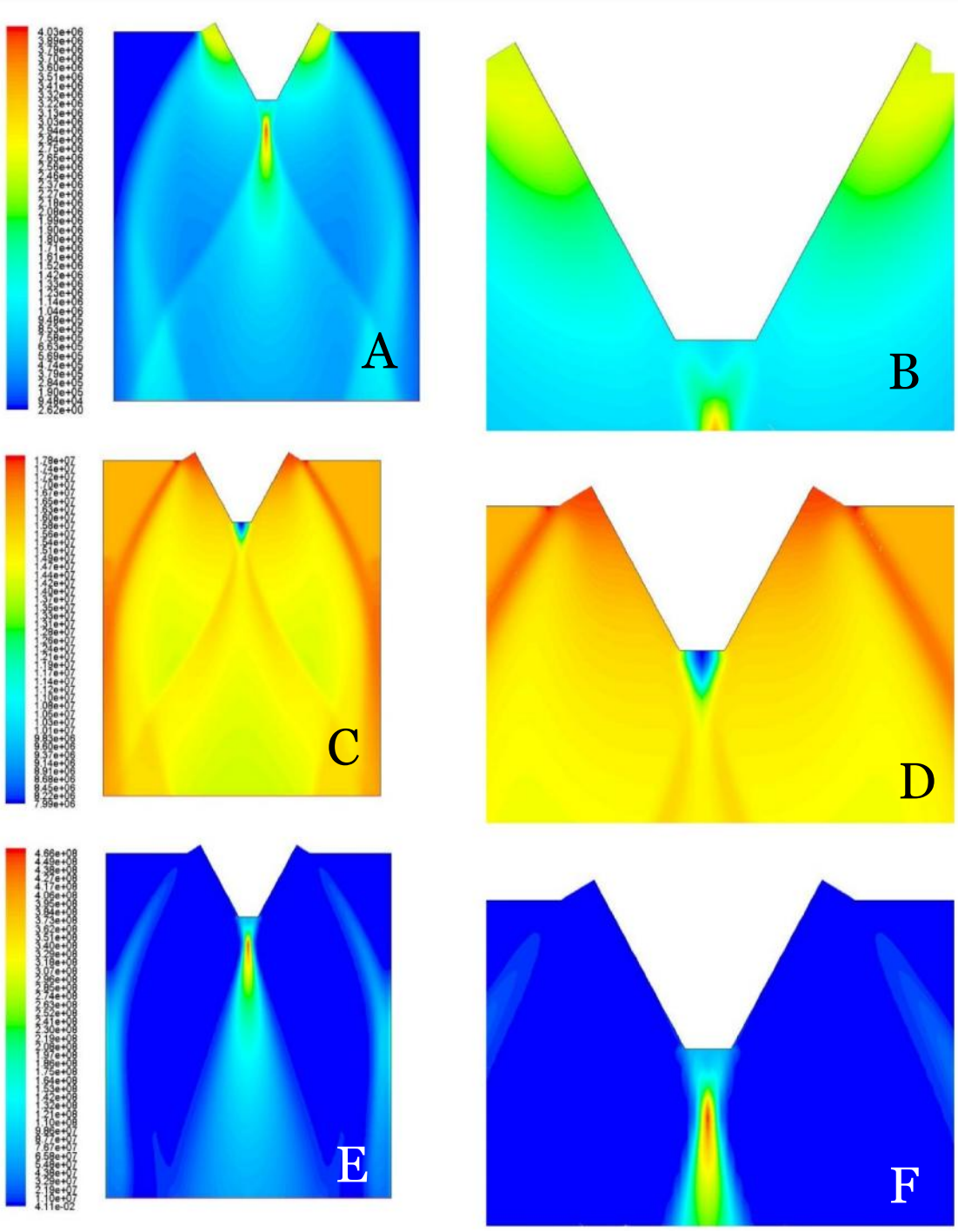

Figure3.35.Contours of Dynamic Pressure (A,B), Enthalpy (C,D) & Turbulent Dissipation Rate (E,F) for 20 % Truncation with a Base Bleed Mass Flow Rate of 260 kg/s.

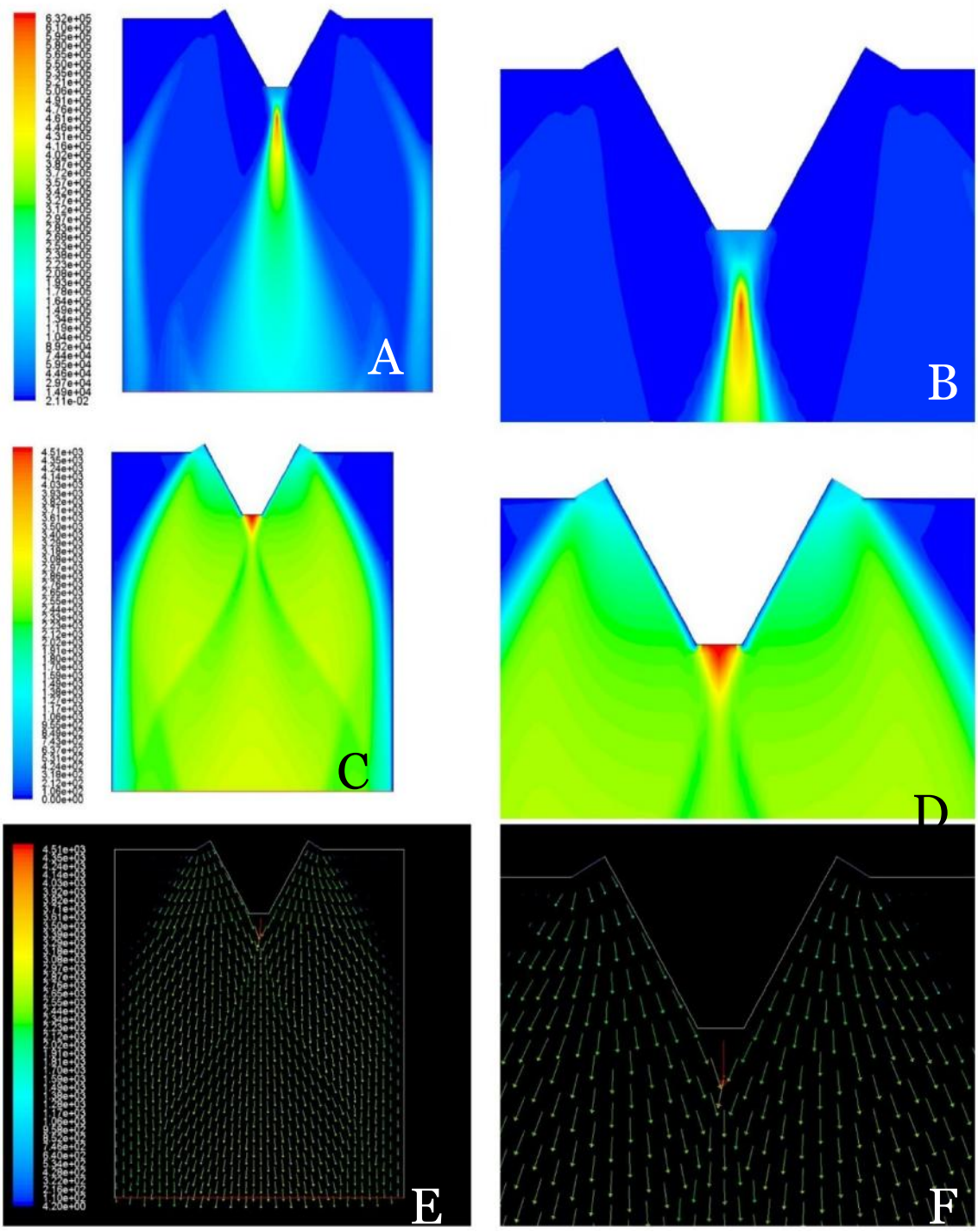

*Figure3.36.*Contours of Turbulent Kinetic Energy (A,B), Velocity Magnitude (C,D) & Velocity Vector (E,F) for 20 % Truncation with a Base Bleed Mass Flow Rate of 260 kg/s.

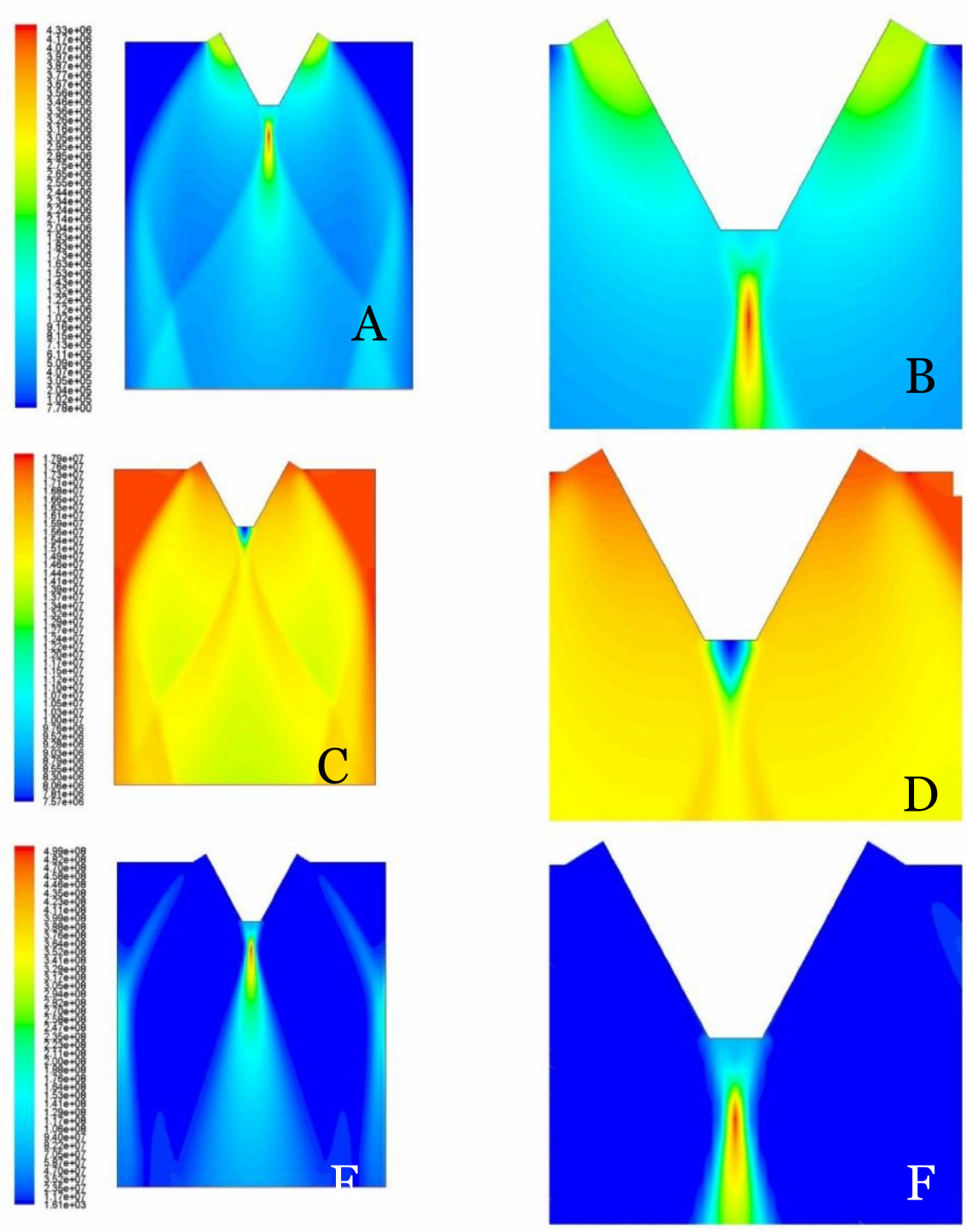

*Figure3.37.*Contours of Dynamic Pressure (A,B), Enthalpy (C,D) & Turbulent Dissipation Rate (E,F) for 20 % Truncation with a Base Bleed Mass Flow Rate of 280 kg/s.

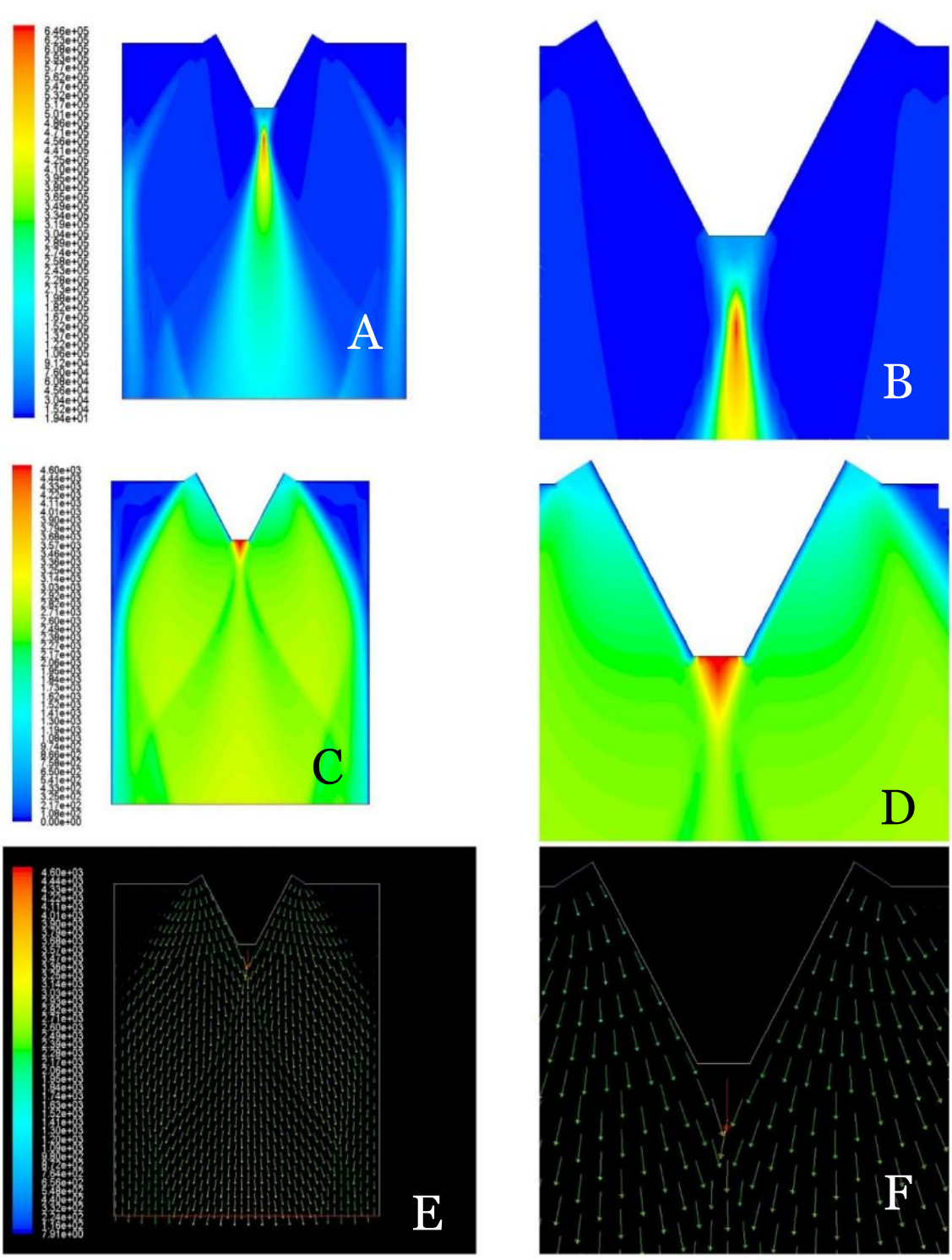

Figure3.38.Contours of Turbulent Kinetic Energy (A,B), Velocity Magnitude (C,D) & Velocity Vector (E,F) for 20 % Truncation with a Base Bleed Mass Flow Rate of 280 kg/s.

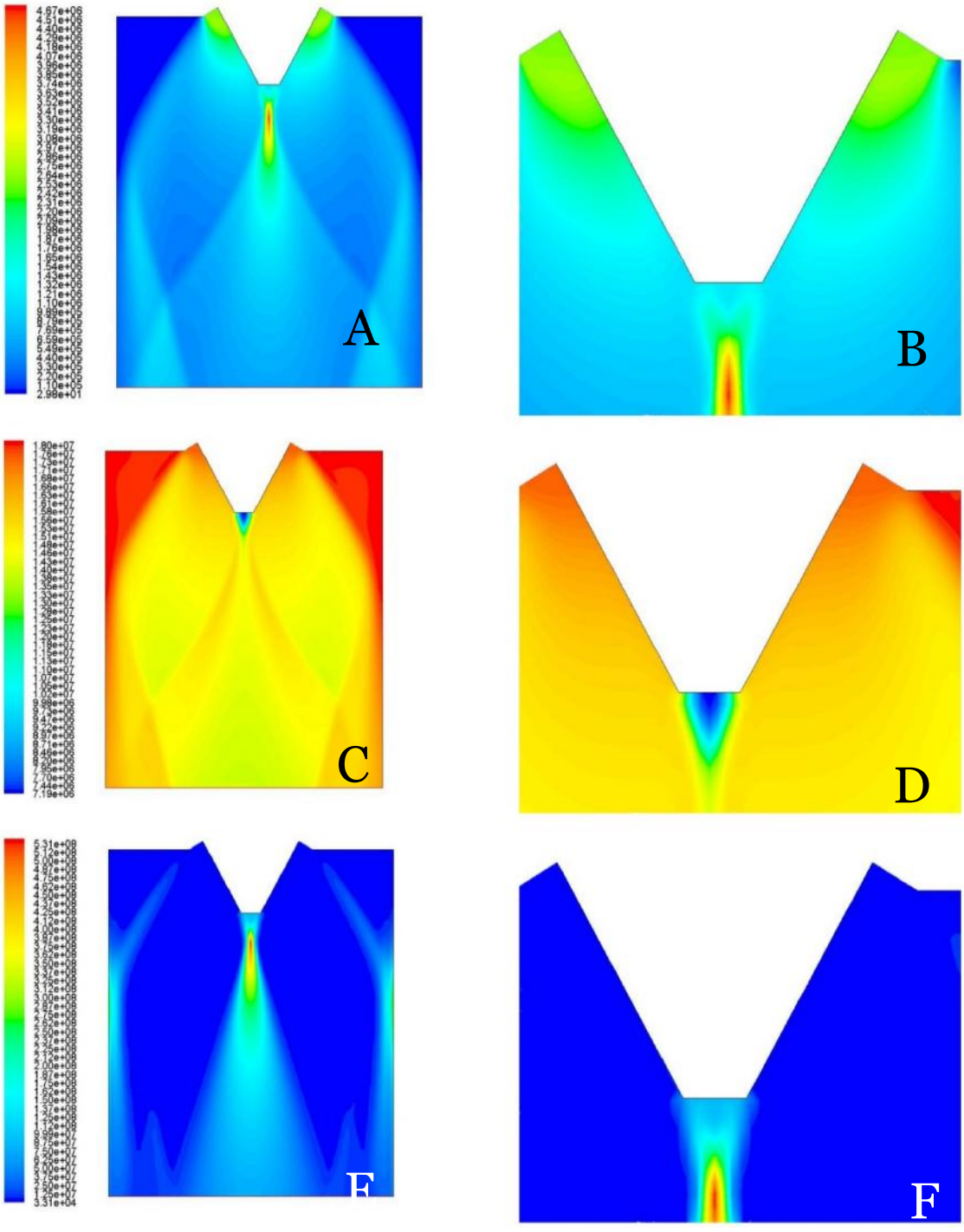

*Figure3.39.*Contours of Dynamic Pressure(A,B), Enthalpy (C,D) & Turbulent Dissipation Rate (E,F) for 20 % Truncation with a Base Bleed Mass Flow Rate of 300 kg/s.

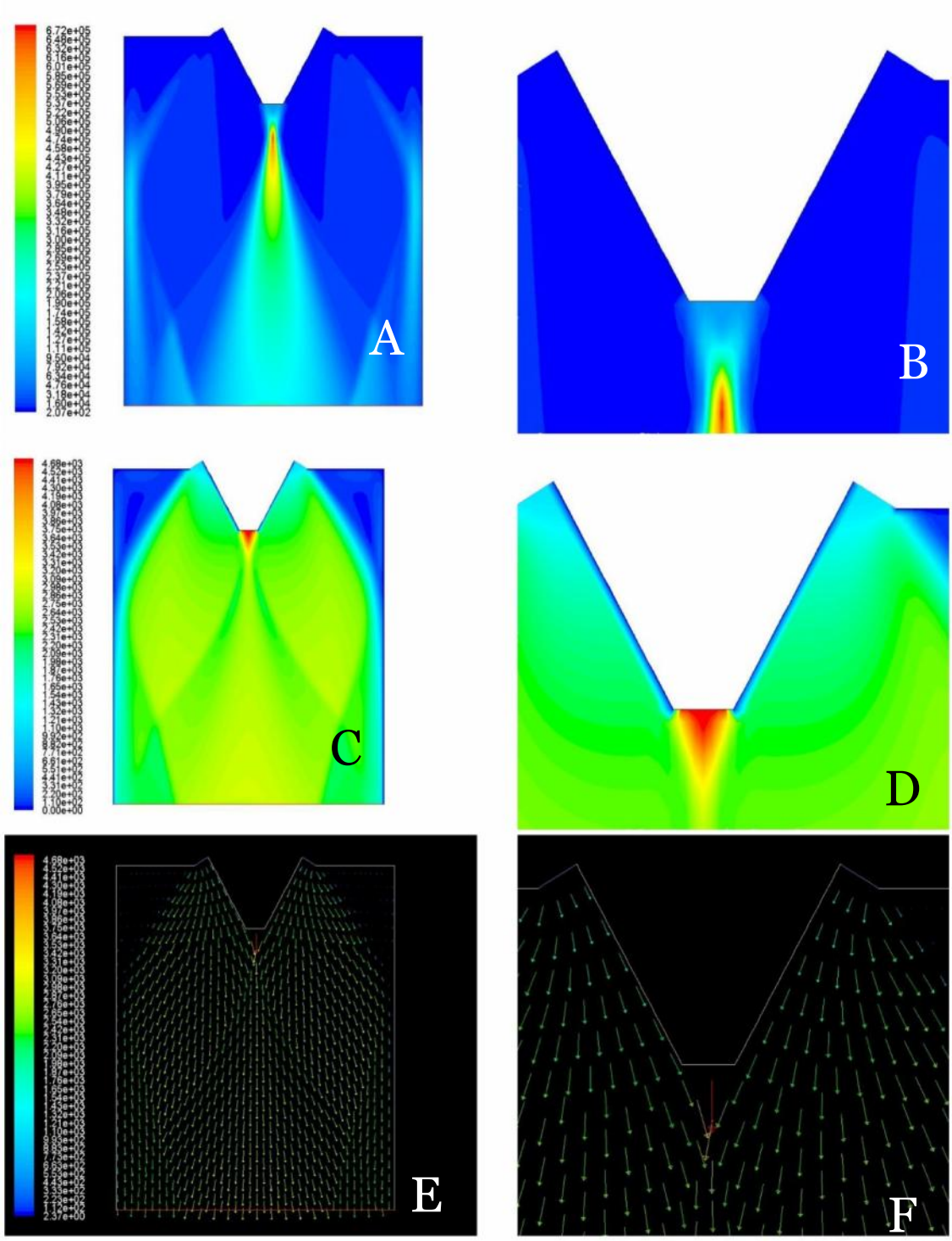

Figure3.40.Contours of Turbulent Kinetic Energy (A,B) , Velocity Magnitude (C,D) & Velocity Vector(E,F) for 20 % Truncation with a Base Bleed Mass Flow Rate of 300 kg/s.

The following pages (62-76) contain the contour plots for the 30 % truncated case. A 30 % truncated nozzle is lighter and more compact than a 20 % truncated nozzle but produces more thrust loss than a 20 % truncated case. Therefore higher values of base bleed mass flow rates were used to simulate the 30 % truncated case. The parameters follow a similar trend as with the 10 % and the 20 % truncated cases. Enthalpy is at a minimum near the truncated portion. The turbulent kinetic energy and the turbulent dissipation rate increase in magnitude proportional to the base bleed mass flow rate. The dynamic pressure profile appears to be uniform for a base bleed mass flow rate of 480 kg/s. Therefore it was concluded that optimum thrust is obtained for this mass flow rate.

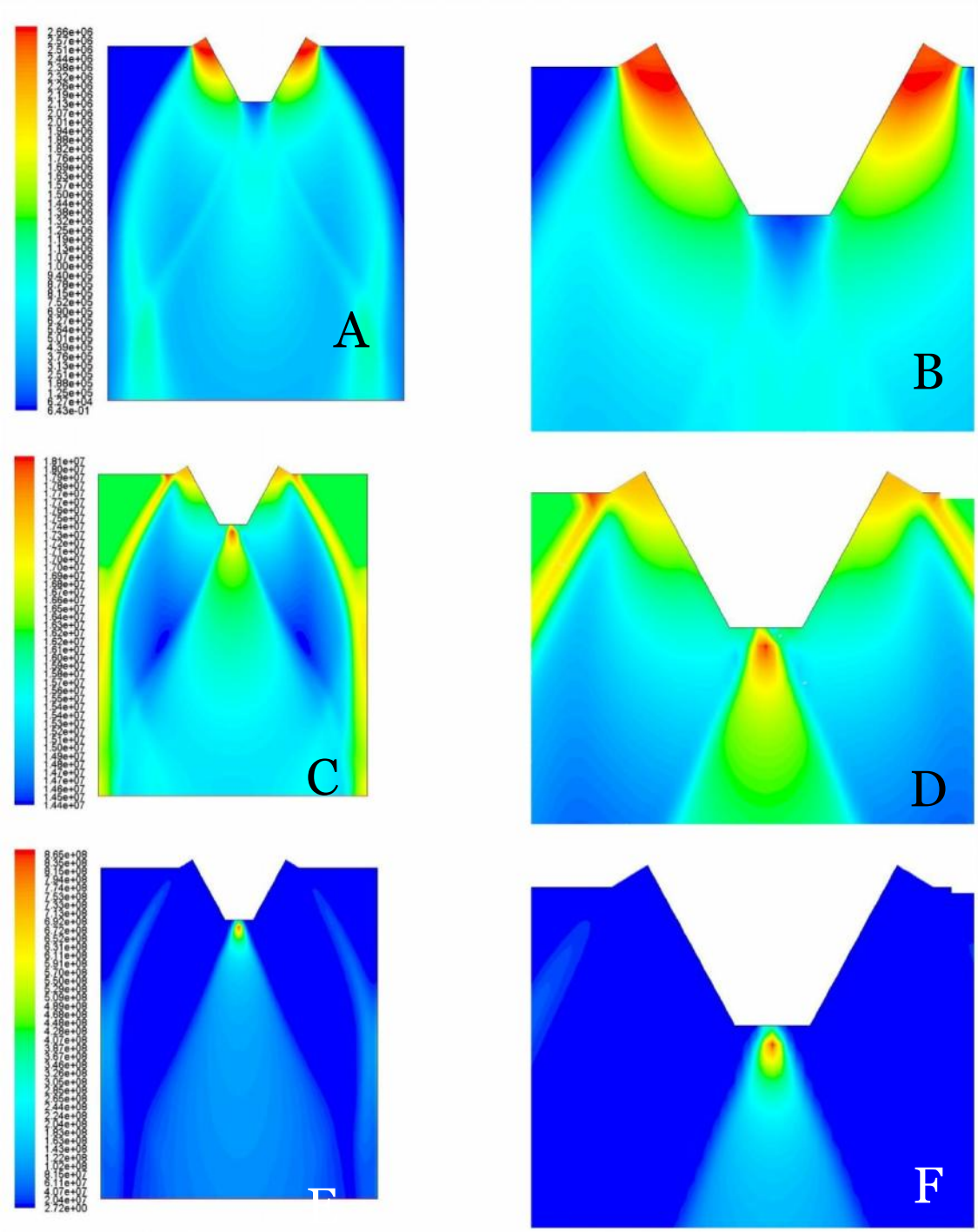

Figrue3.41.Contours of Dynamic Pressure (A,B), Enthalpy (C,D) & Turbulent Dissipation Rate (E,F) for 30 % Truncation without Base Bleed.

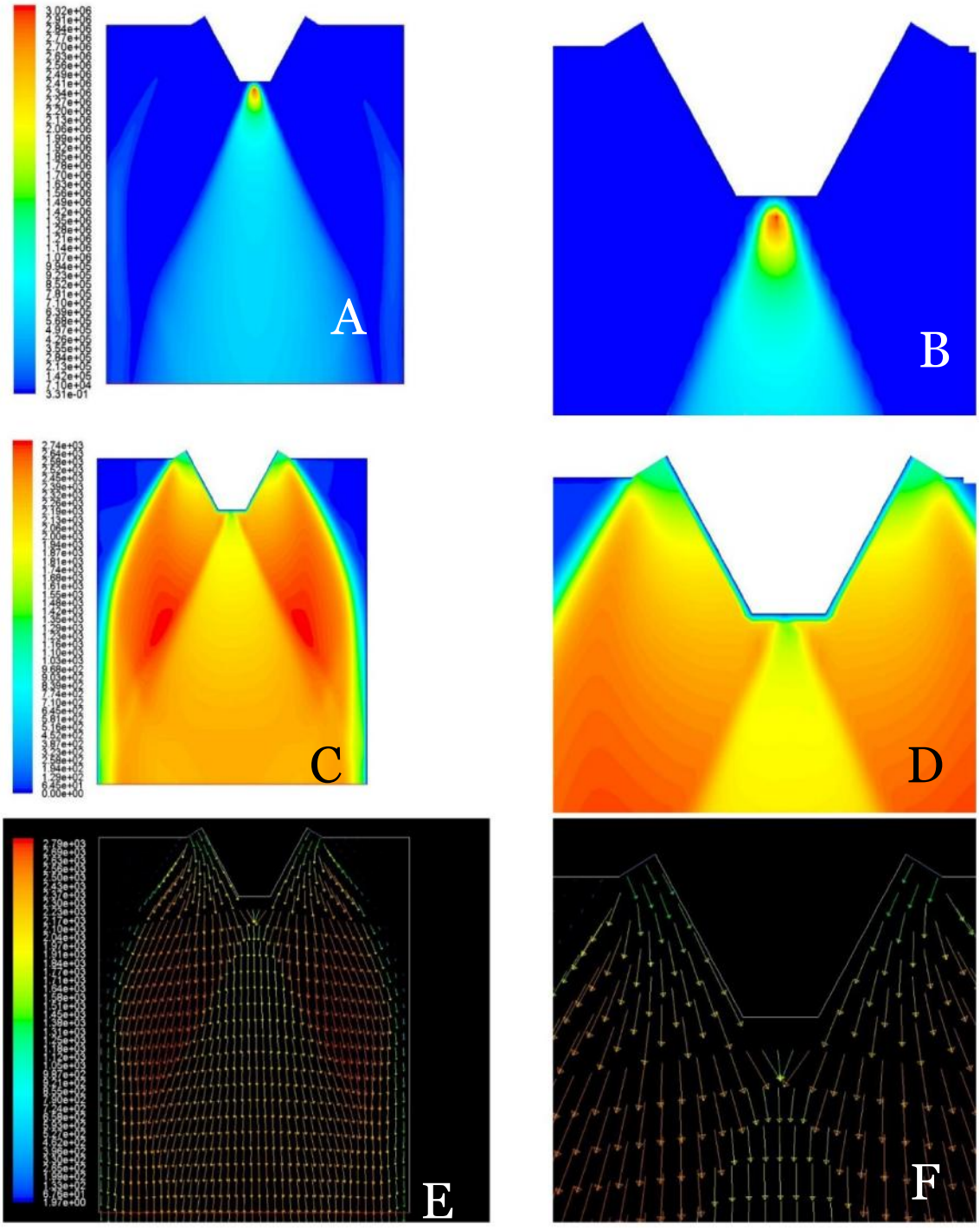

Figure3.42.Contours of Turbulent Kinetic Energy (A,B), Velocity Magnitude (C,D) & Velocity Vector (E,F) for 30 % Truncation without Base Bleed.

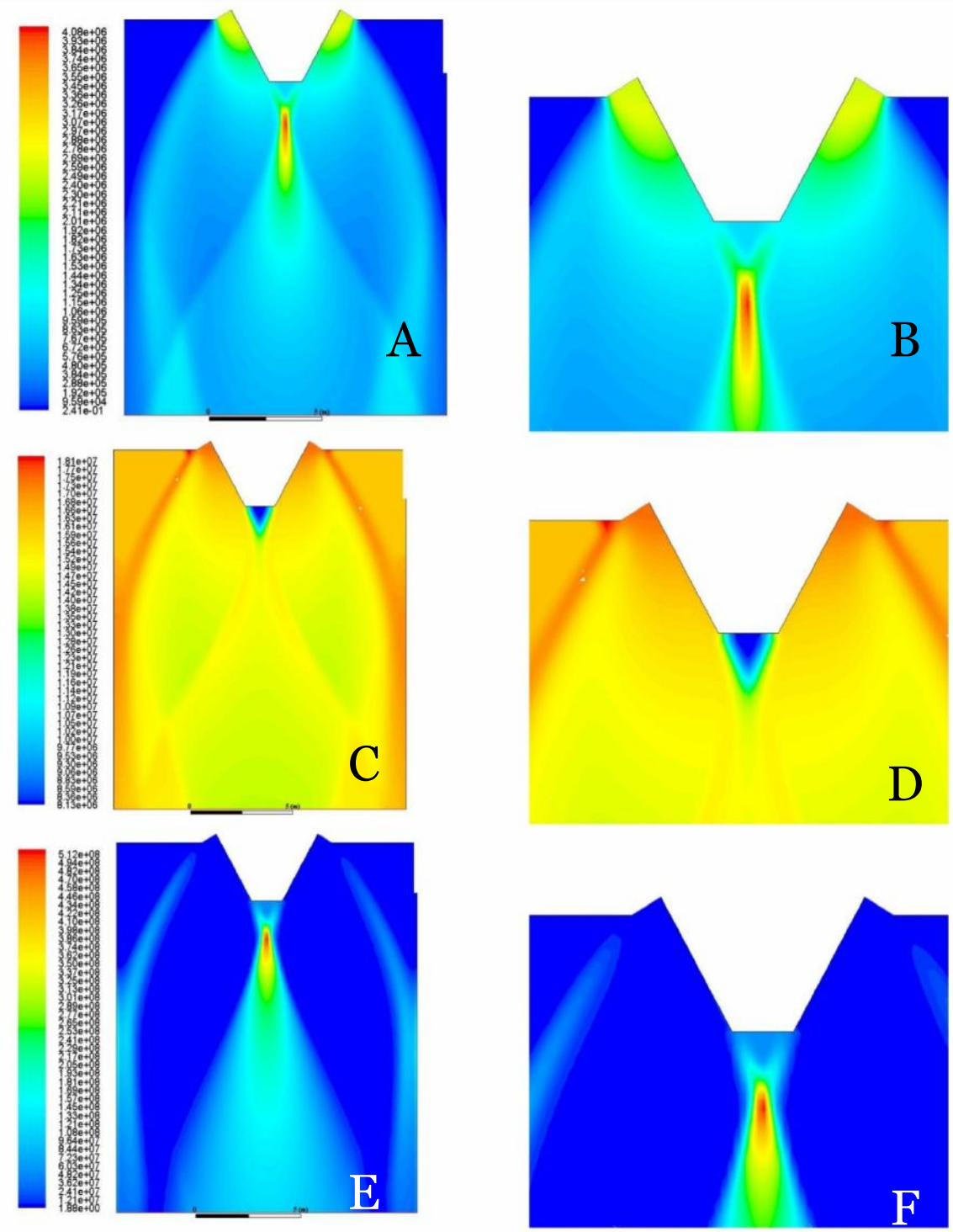

Figure3.43.Contours of Dynamic Pressure (A,B), Enthalpy (C,D)& Turbulent Dissipation Rate (E,F) for 30 % Truncation with a Base Bleed Mass Flow Rate of 380 kg/s.

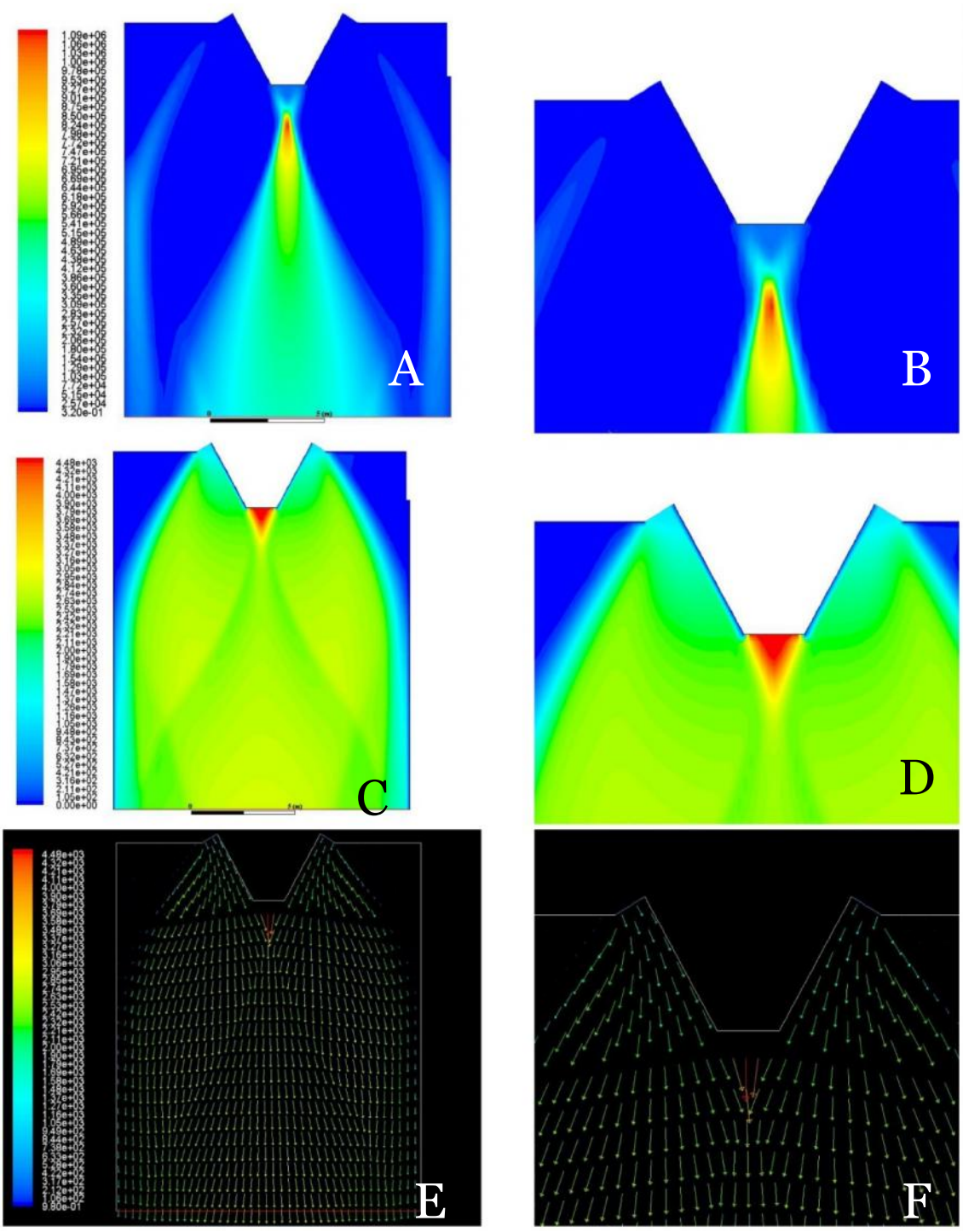

*Figure3.44.*Contours of Turbulent Kinetic Energy (A,B), Velocity Magnitude (C,D) & Velocity Vector (E,F) for 30 % Truncation with a Base Bleed Mass Flow Rate of 380 kg/s.

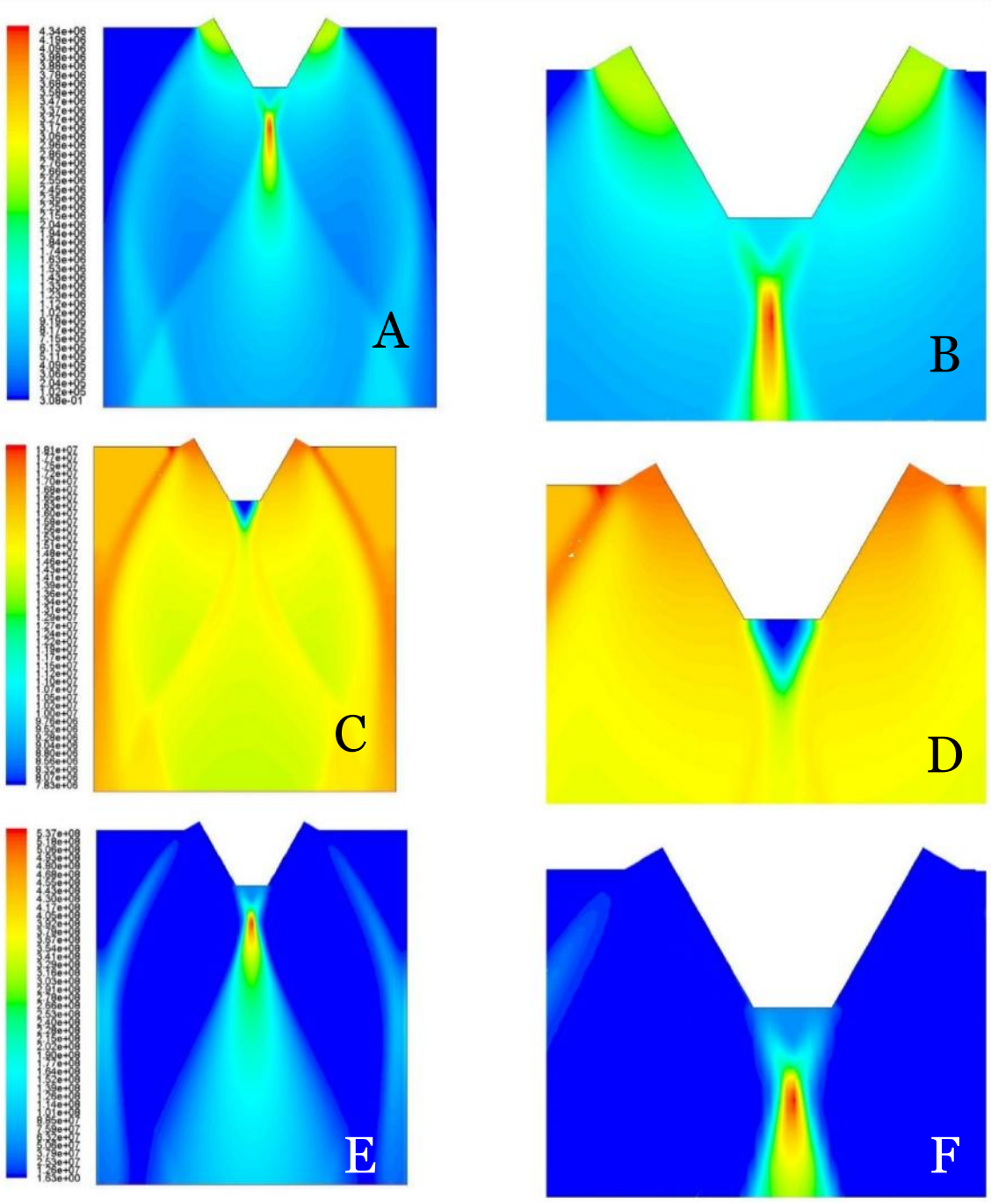

Figure3.45.Contours of Dynamic Pressure (A,B), Enthalpy (C,D)& Turbulent Dissipation Rate (E,F) for 30 % Truncation with a Base Bleed Mass Flow Rate of 400 kg/s.

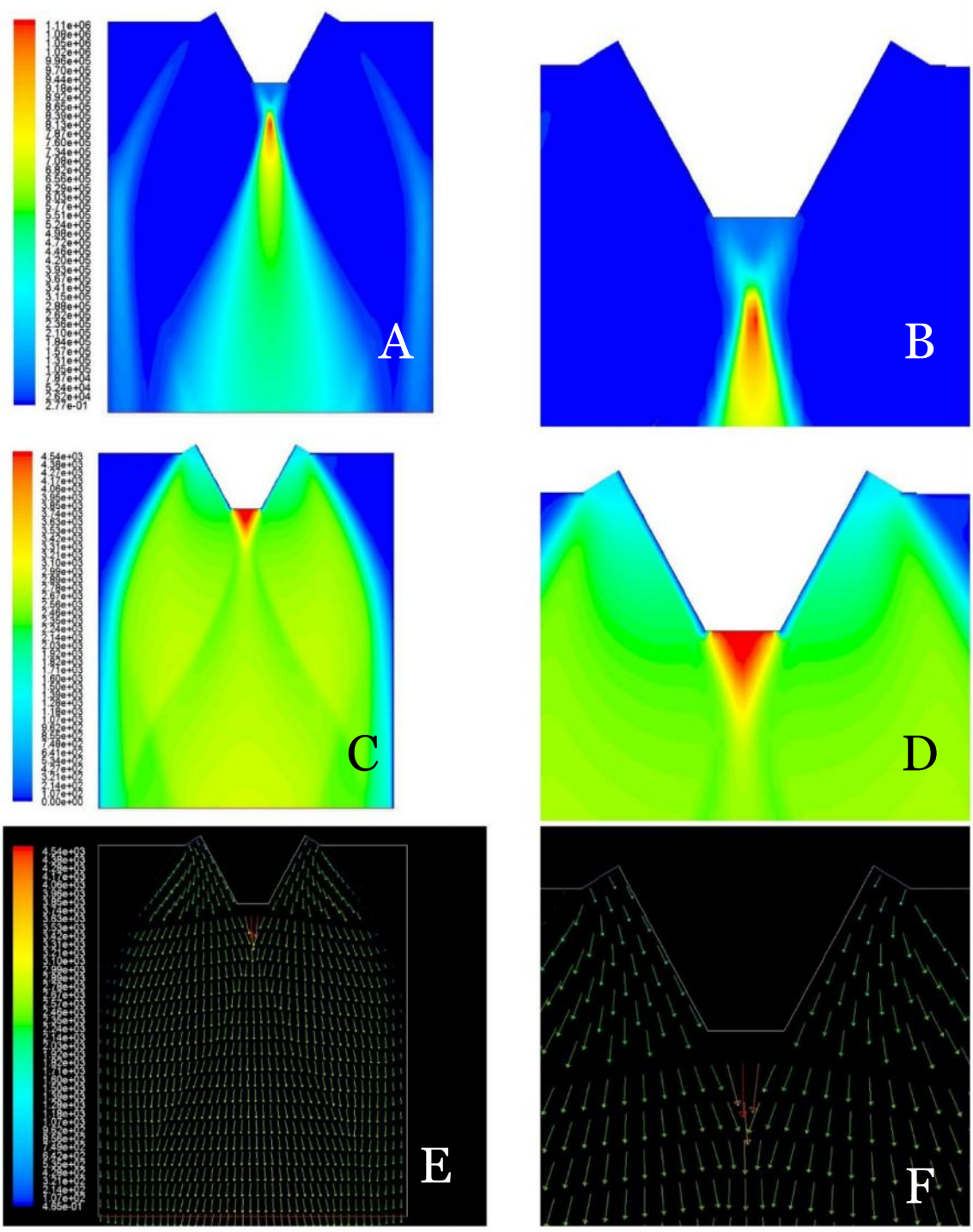

Figure3.46.Contours of Turbulent Kinetic Energy (A,B), Velocity Magnitude (C,D)& Velocity Vector (E,F) for 30 % Truncation with a Base Bleed Mass Flow Rate of 400 kg/s.

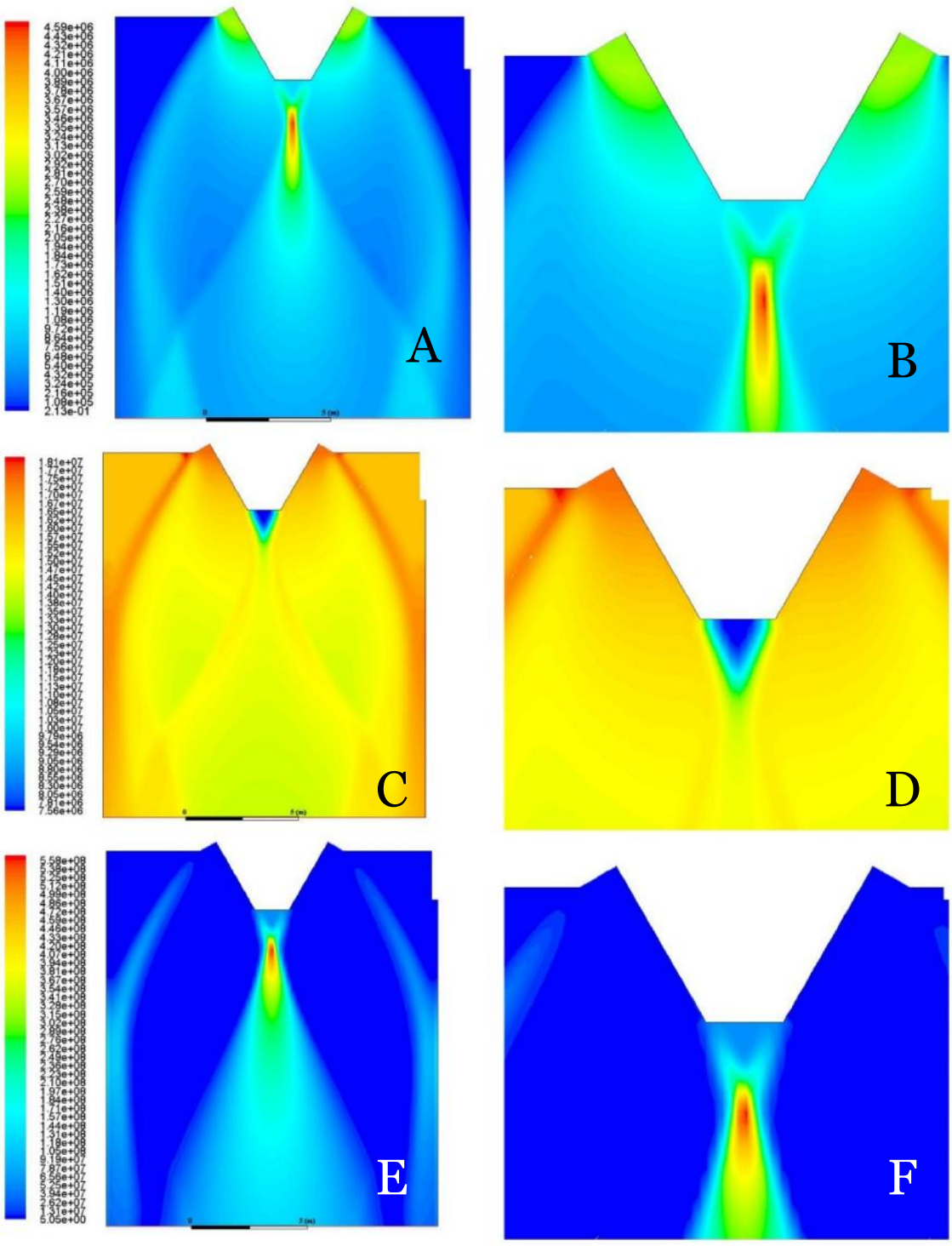

*Figure3.47.*Contours of Dynamic Pressure(A,B), Enthalpy (C,D) & Turbulent Dissipation Rate (E,F) for 30 % Truncation with a Base Bleed Mass Flow Rate of 420 kg/s.

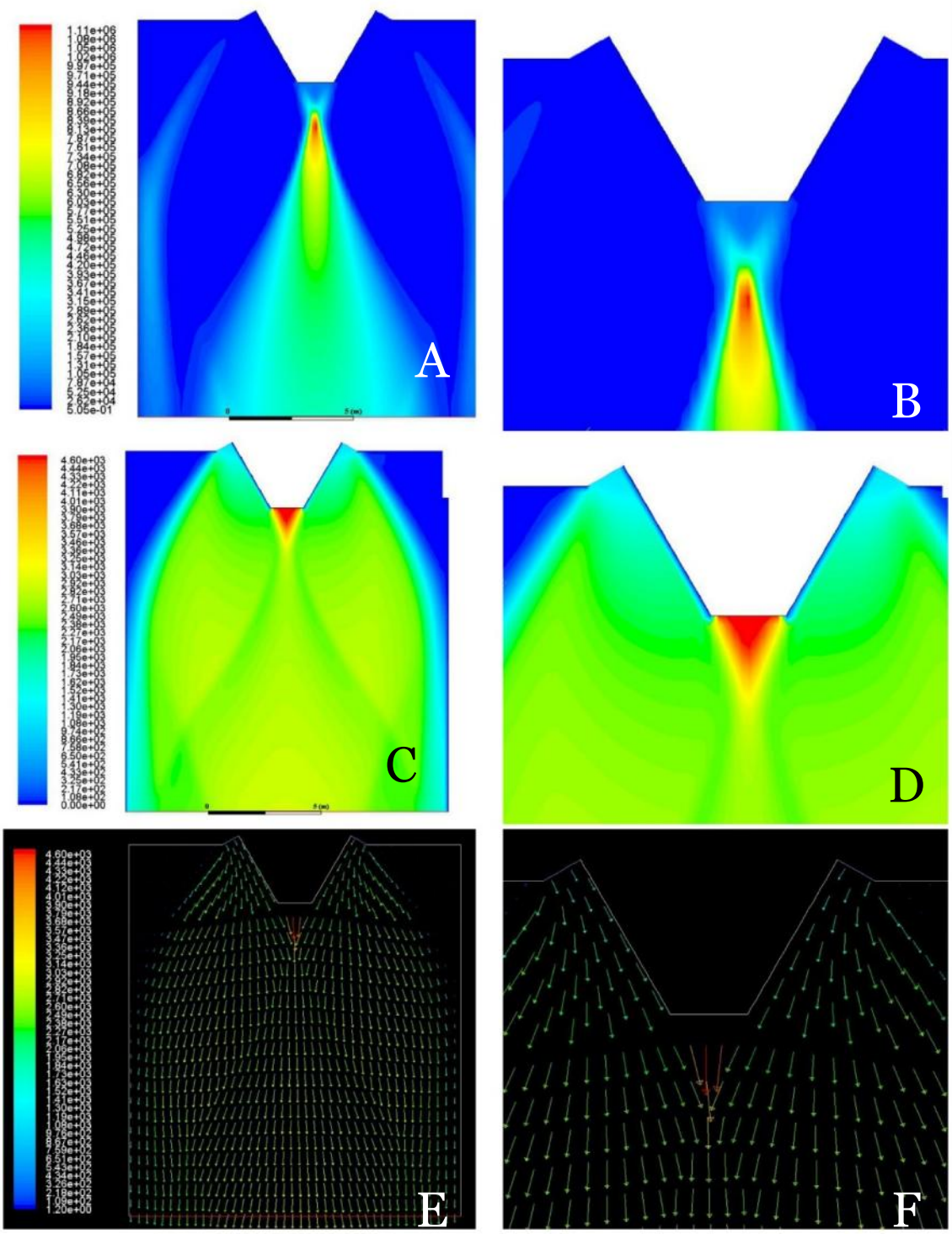

Figure3.48.Contours of Turbulent Kinetic Energy (A,B), Velocity Magnitude (C,D) & Velocity Vector (E,F) for 30 % Truncation with a Base Bleed Mass Flow Rate of 420 kg/s.

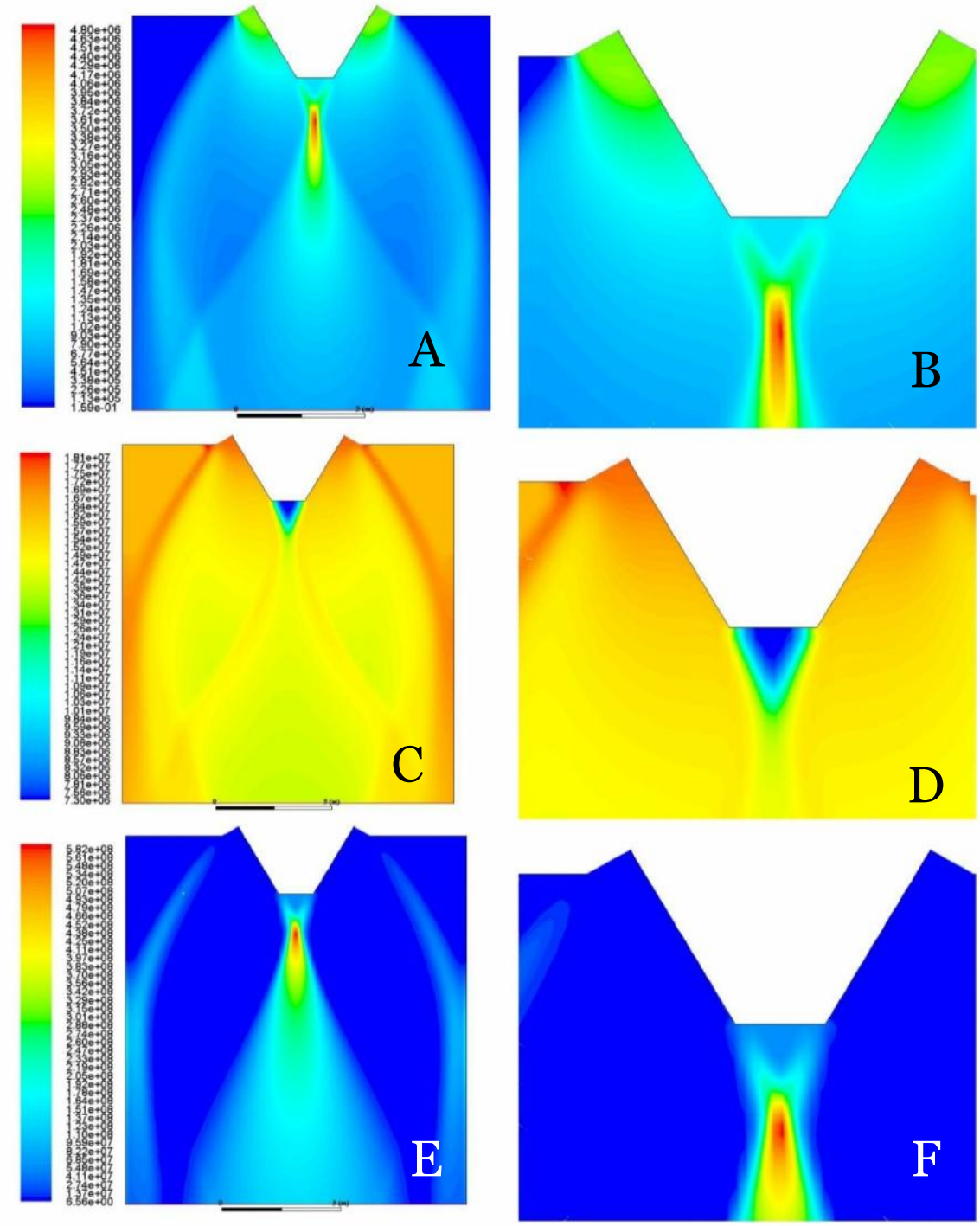

Figure3.49.Contours of Dynamic Pressure (A,B), Enthalpy (C,D) & Turbulent Dissipation Rate (E,F) for 30 % Truncation with a Base Bleed Mass Flow Rate of 440 kg/s.

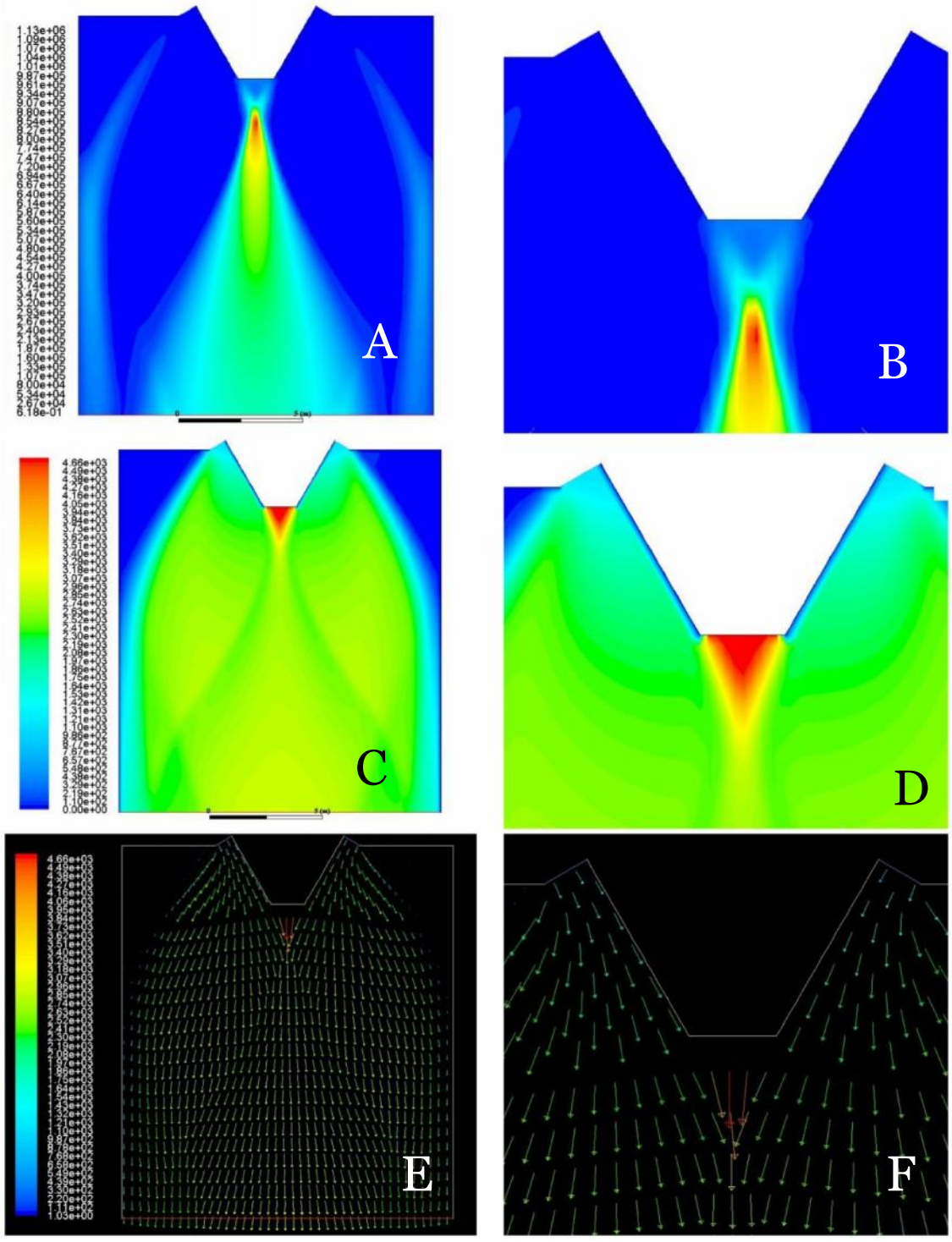

Figure3.50.Contours of Turbulent Kinetic Energy (A,B), Velocity Magnitude (C,D) & Velocity Vector (E,F) for 30 % Truncation with a Base Bleed Mass Flow Rate of 440 kg/s.

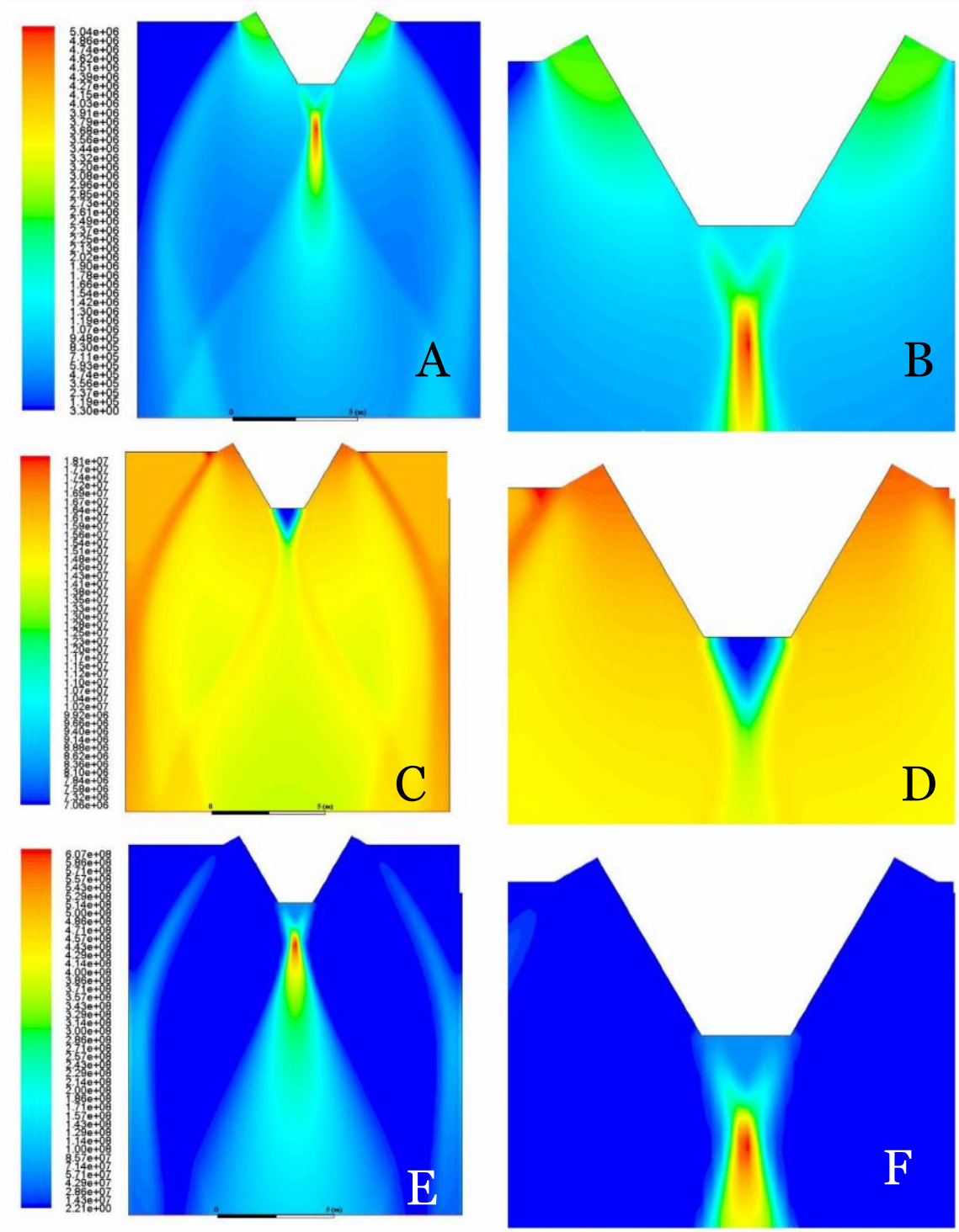

*Figure3.51.*Contours of Dynamic Pressure (A,B), Enthalpy (C,D) & Turbulent Dissipation Rate (E,F) for 30 % Truncation with a Base Bleed Mass Flow Rate of 460 kg/s.

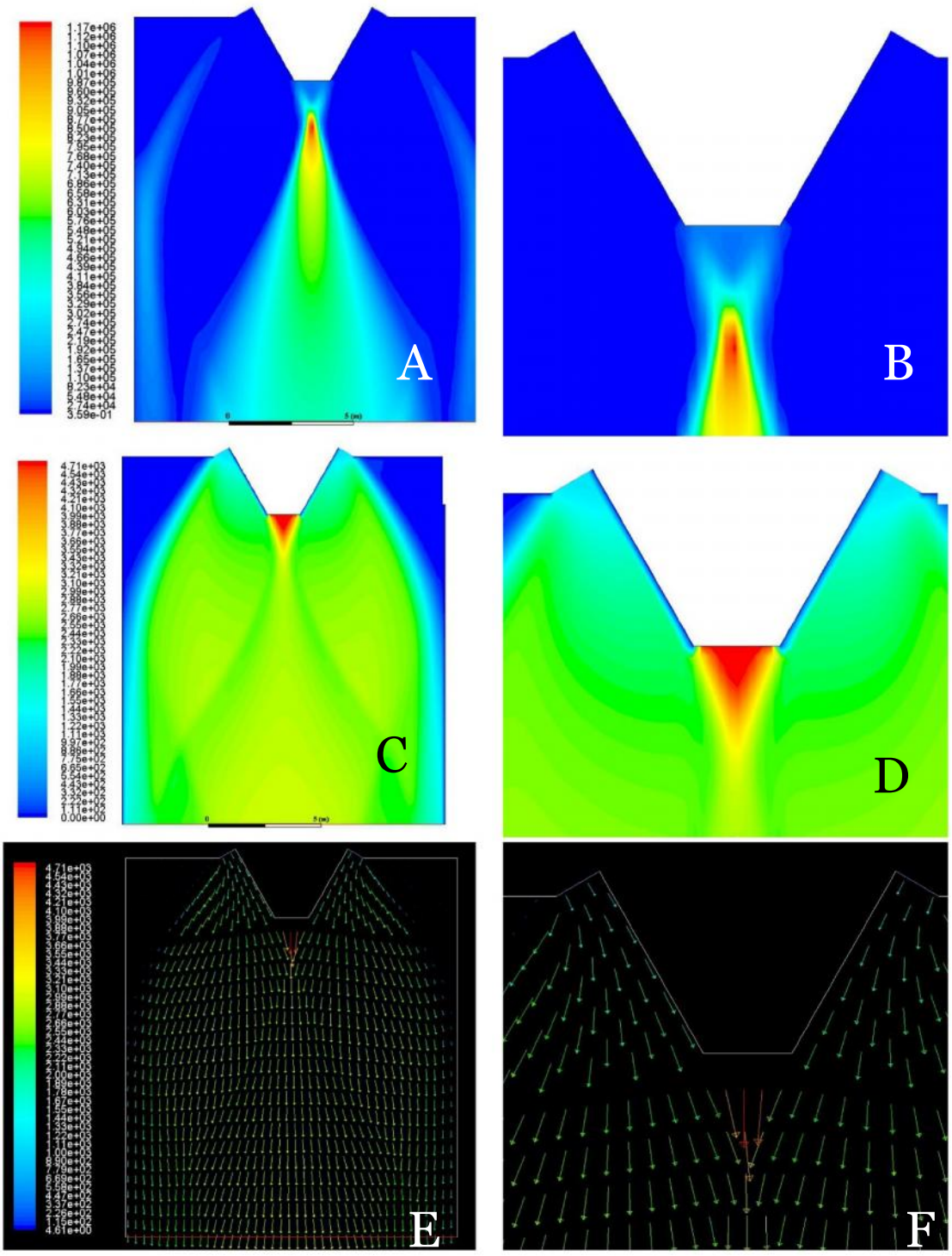

Figure3.52.Contours of Turbulent Kinetic Energy (A,B), Velocity Magnitude (C,D) & Velocity Vector (E,F) for 30 % Truncation with a Base Bleed Mass Flow Rate of 460 kg/s.

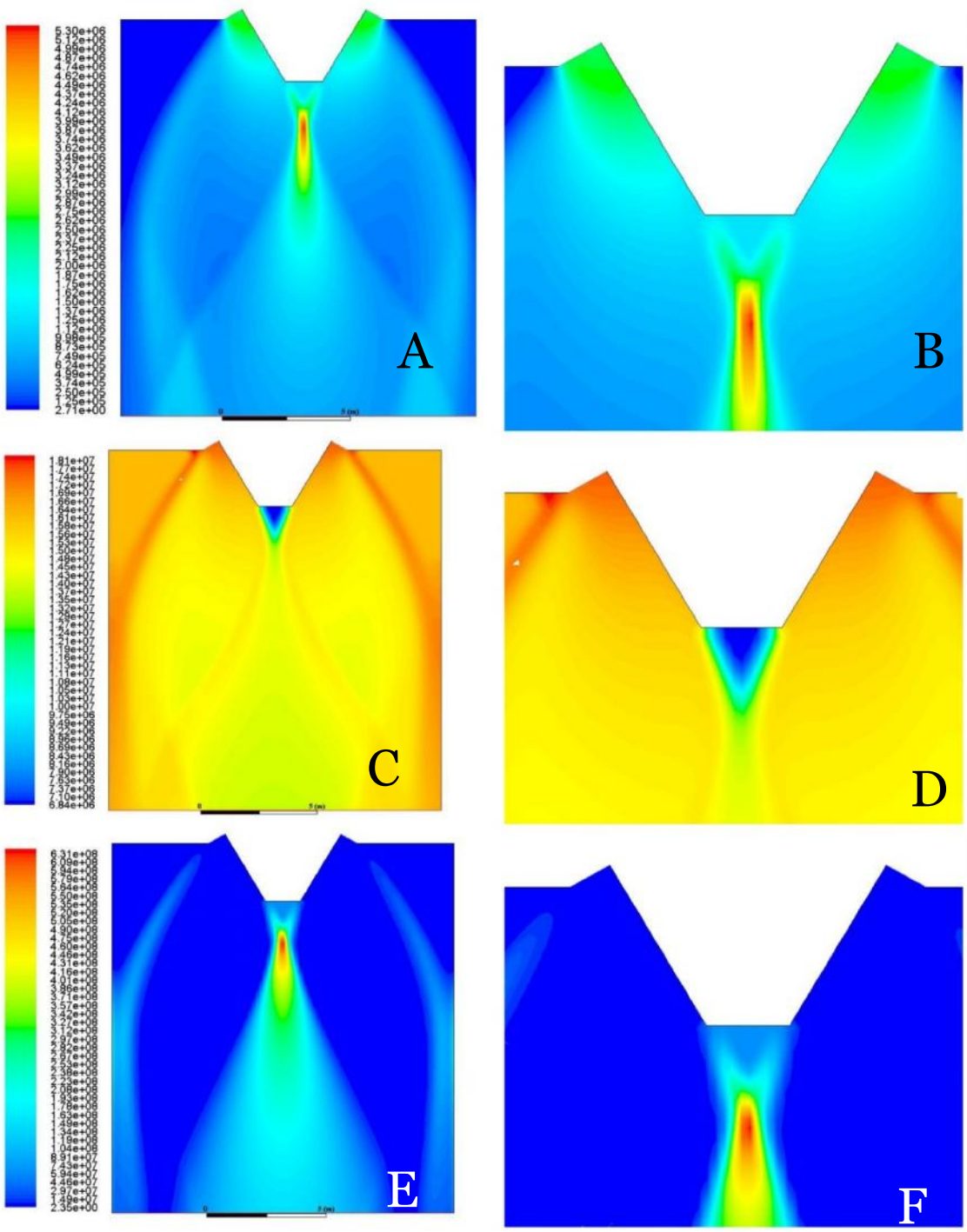

Figure3.53.Contours of Dynamic Pressure (A,B), Enthalpy (C,D) & Turbulent Dissipation Rate (E,F) for 30 % Truncation with a Base Bleed Mass Flow Rate of 480 kg/s.

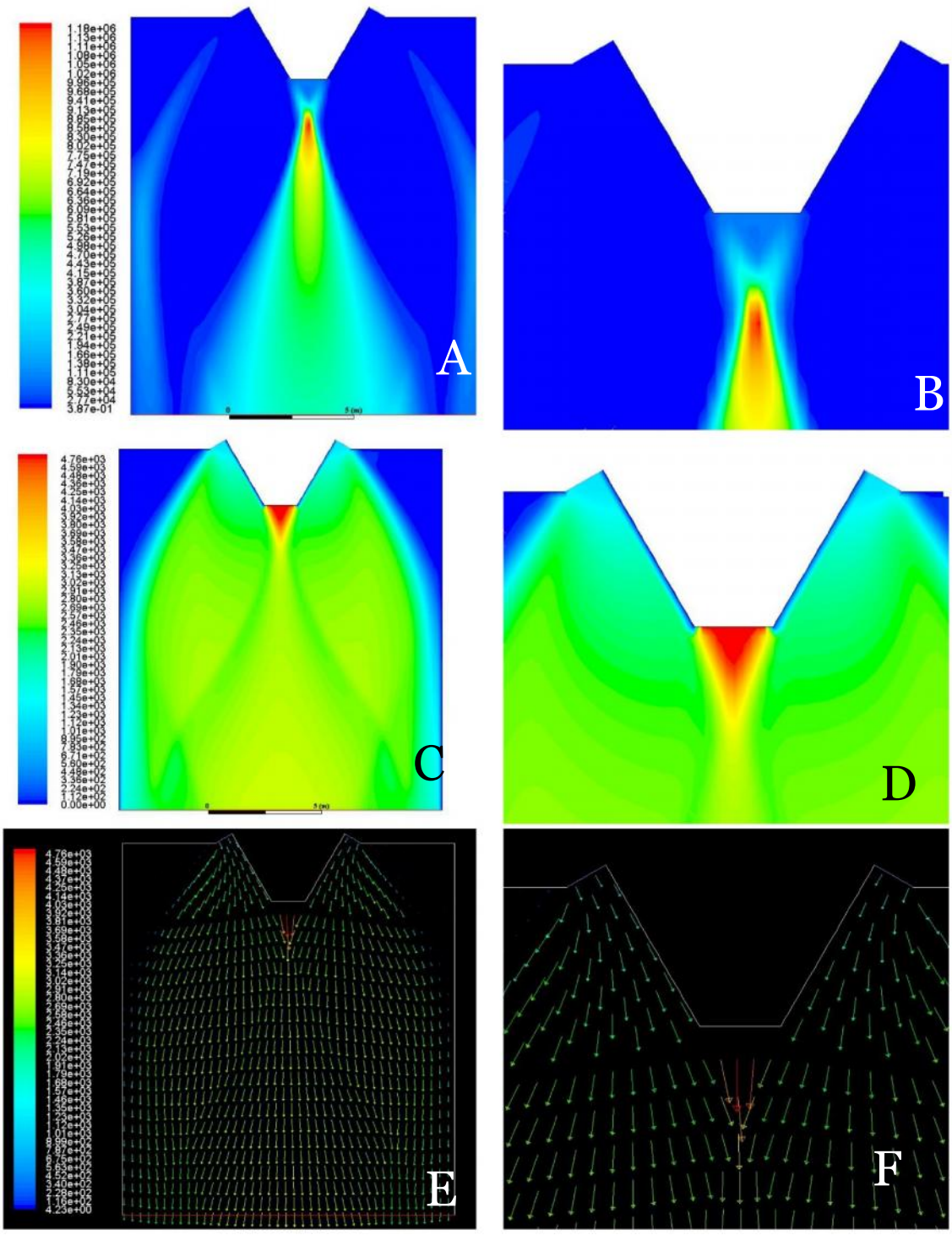

*Figure3.54.*Contours of Turbulent Kinetic Energy (A,B), Velocity Magnitude (C,D) & Velocity Vector (E,F) for 30 % Truncation with a Base Bleed Mass Flow Rate of 480 kg/s.

CHAPTER 4

FUTURE SCOPE

This thesis work aims to identify the optimal base bleed mass flow rate for which there is very little base recirculation under the truncation, which is validated with the help of dynamic pressure plots. The idea behind this thesis could be used to identify optimal base bleed mass flow rates for higher percentages of truncation(35% and above).Furthermore this thesis could serve as a groundwork for future studies about truncated aerospike base bleed mass flow rate and its impact on enthalpy, turbulent kinetic energy and turbulent dissipation rate .

REFERENCES

Baftalovskii, S., Kraiko, A., & Tillyayeva, N. (1999). Optimal design of self-controlled spike nozzles and their thrust determination at start. In *9th International Space Planes and Hypersonic Systems and Technologies Conference*. American Institute of Aeronautics and Astronautics. https://doi.org/10.2514/6.1999-4955

Barrere, M., Jaumotte, A., Fraeijs de Veubeke, B., & Vandenkerckhove, J. (1960). *Rocket propulsion*. LTAS. Retrieved from http://orbi.ulg.ac.be/bitstream/2268/206040/1/ST_Veubeke_025.pdf

Besnard, E., & Garvey, J. (2004). Development and Flight-Testing of Liquid Propellant Aerospike Engines. In *40th AIAA/ASME/SAE/ASEE Joint Propulsion Conference and Exhibit*. American Institute of Aeronautics and Astronautics. https://doi.org/10.2514/6.2004-3354

Calzada, R. (2015, June 29). Skunkworks Technicians Install LASRE on #844 [Text]. Retrieved July 2, 2017, from http://www.nasa.gov/centers/dryden/multimedia/imagegallery/SR-71-LASRE/EC96-43419-21.html

Dai, W.-Y., Liu, Y., Cheng, X.-C., & Ma, B. (2003). Analytical and Experimental Studies of Tile-Shaped Aerospike Nozzles. *Journal of Propulsion and Power*, *19*(4), 640–645. https://doi.org/10.2514/2.6152

Dumnov, G. E., Nikulin, N. B., & Ponomaryov, N. B. (1993). Investigation of advanced nozzles for rocket engines. *Space Rocket Engine Power Plants*, *4*(142), 117–142.

Farley, J. M., & Campbell, C. E. (1960). *Performance of Several Method-of-Characteristics Exhaust Nozzles*. Retrieved from https://ntrs.nasa.gov/search.jsp?R=19980227854

Fick, M., & Schmucker, R. H. (1996). Performance aspects of plug cluster nozzles. *Journal of Spacecraft and Rockets*, *33*(4), 507–512. https://doi.org/10.2514/3.26792

Frey, M., & Hagemann, G. (1999). Flow Separation and Side-Loads in Rocket Nozzles (PDF Download Available). Retrieved July 2, 2017, from https://www.researchgate.net/publication/224789711_Flow_Separation_and_Side-Loads_in_Rocket_Nozzles

Geron, M., Paciorri, R., Nasuti, F., & Sabetta, F. (2007a). Flowfield analysis of a linear clustered plug nozzle with round-to-square modules. *Aerospace Science and Technology*, *11*(2), 110–118. https://doi.org/10.1016/j.ast.2006.08.004

Gibbs, Y. (2014, February 28). NASA Dryden Fact Sheet - LASRE Project. Retrieved July 2, 2017, from http://www.nasa.gov/centers/armstrong/news/FactSheets/FS-043-DFRC.html

Hagemann, G., Immich, H., & Dumnov, G. (n.d.). Critical assessment of the linear plug nozzle concept. In *37th Joint Propulsion Conference and Exhibit*. American Institute of Aeronautics and Astronautics. https://doi.org/10.2514/6.2001-3683

Hagemann, G., Immich, H., Nguyen, T. V., & Dumnov, G. E. (1998). Advanced Rocket Nozzles. *Journal of Propulsion and Power*, *14*(5), 620–634. https://doi.org/10.2514/2.5354

HOFFMAN, J. D. (1987). Design of compressed truncated perfect nozzles. *Journal of Propulsion and Power*, *3*(2), 150–156. https://doi.org/10.2514/3.22967

HUANG, D. (1974). Aerospike engine technology demonstration for space propulsion. In *10th Propulsion Conference*. American Institute of Aeronautics and Astronautics. https://doi.org/10.2514/6.1974-1080

KIRBY, F., & MARTINEZ, A. (1977). Linear aerospike engine. In *13th Propulsion Conference*. American Institute of Aeronautics and Astronautics. https://doi.org/10.2514/6.1977-968

Knauber, R. N. (1996). Thrust misalignments of fixed-nozzle solid rocket motors. *Journal of Spacecraft and Rockets*, *33*(6), 794–799. https://doi.org/10.2514/3.26840

Koelle, H. H. (1961). *Handbook of Astronautical Engineering*. McGraw-Hill.

LAMONT, E. (1973). The Aerospike Engine System for the Space Tug - A status report. In *9th Propulsion Conference*. American Institute of Aeronautics and Astronautics. https://doi.org/10.2514/6.1973-1245

Lash, E. (2015a). Trajectory Analysis and Comparison of a Linear Aerospike Nozzle to a Conventional Bell Nozzle for SSTO Flight. *Masters Theses*. Retrieved from http://trace.tennessee.edu/utk_gradthes/3383

Lemieux, P. (2010). Nitrous oxide cooling in hybrid rocket nozzles. *Progress in Aerospace Sciences*, *46*, 106–115. https://doi.org/10.1016/j.paerosci.2009.12.001

LILLEY, J. S. (1986). Design and optimization of propulsion systems employing scarfed nozzles. *Journal of Spacecraft and Rockets*, *23*(6), 597–604. https://doi.org/10.2514/3.25853

LILLEY, J. S. (1987). Experimental validation of a performance model for scarfed nozzles. *Journal of Spacecraft and Rockets*, *24*(5), 474–480. https://doi.org/10.2514/3.25941

Liu, Y., Zhang, G., Dai, W., Ma, B., Cheng, X., Wang, Y., … Li, J. (2001). Experimental investigation on aerospike nozzle in different structures and working conditions. In *37th Joint Propulsion Conference and Exhibit*. American Institute of Aeronautics and Astronautics. https://doi.org/10.2514/6.2001-3704

Meiss, J.-H., & Besnard, E. (2013). Advanced Design of a Multi-Thruster LOX/Propylene Aerospike Engine. In *49th AIAA/ASME/SAE/ASEE Joint Propulsion Conference*. American Institute of Aeronautics and Astronautics. https://doi.org/10.2514/6.2013-3955

Muss, J., Nhuyen, T., Reske, E., McDaniels, D., Muss, J., Nhuyen, T., … McDaniels, D. (1997). Evaluation of altitude compensating nozzle concepts for RLV. In *33rd Joint Propulsion Conference and Exhibit*. American Institute of Aeronautics and Astronautics. https://doi.org/10.2514/6.1997-3222

NASA - Dryden Flight Research Center - News Room: News Releases: LINEAR AEROSPIKE SR-71 EXPERIMENT COMPLETES SUCCESSFUL FIRST FLIGHT. (1997). Retrieved July 2, 2017, from https://www.nasa.gov/centers/dryden/news/NewsReleases/1997/97-41.html

Nasuti, F., & Onofri, M. (1999). Theoretical Analysis and Engineering Modeling of Flowfields in Clustered Module Plug Nozzles. *Journal of Propulsion and Power*, *15*(4), 544–551. https://doi.org/10.2514/2.5477

Onofri, M., Calabro, M., Hagemann, G., Immich, H., Sacher, P., Nasuti, F., & Reijasse, P. (2006). Plug nozzles: summary of flow features and engine performance - Overview of RTO/AVT WG 10 subgroup 1. *40th AIAA Aerospace Sciences Meeting & Exhibit*. Retrieved from http://www.academia.edu/29610801/Plug_nozzles_summary_of_flow_features_and_engine_performance_-_Overview_of_RTO_AVT_WG_10_subgroup_1

Rao, G. V. R. (1958). Exhaust Nozzle Contour for Optimum Thrust. *Journal of Jet Propulsion*, *28*(6), 377–382. https://doi.org/10.2514/8.7324

Rao, G. V. R. (1961). Recent Developments in Rocket Nozzle Configurations. *ARS Journal*, *31*(11), 1488–1494. https://doi.org/10.2514/8.5837

Ryan, H., Solano, W., Holland, R., & Rahman, S. (2001). The future of full-scale propulsion testing. In *39th Aerospace Sciences Meeting and Exhibit*. American Institute of Aeronautics and Astronautics. https://doi.org/10.2514/6.2001-746

Sakamoto, H., Takahashi, M., Sasaki, M., Tomita, T., Kusaka, K., & Tamura, H. (1999). An experimental study on a 14 kN linear aerospike-nozzle combustor. In *35th Joint Propulsion Conference and Exhibit*. American Institute of Aeronautics and Astronautics. https://doi.org/10.2514/6.1999-2761

Shapiro, A. H. (1954). *The dynamics and thermodynamics of compressible fluid flow*. Ronald Press Co.

Sutton, G. P. (1998, July 14). Stepped nozzle. Retrieved from http://www.google.com/patents/US5779151

Sutton, G. P., & Biblarz, O. (2016). *Rocket Propulsion Elements*. John Wiley & Sons.

Tomita, T., Takahashi, M., Tamura, H., Tomita, T., Takahashi, M., & Tamura, H. (1997). Flow field of clustered plug nozzles. In *33rd Joint Propulsion Conference and Exhibit*. American Institute of Aeronautics and Astronautics. https://doi.org/10.2514/6.1997-3219

Tsutsumi, S., Yamaguchi, K., Teramoto, S., & Nagashima, T. (n.d.). Clustering Effects on Performance and Heating of a Linear Aerospike Nozzle. In *45th AIAA Aerospace Sciences Meeting and Exhibit*. American Institute of Aeronautics and Astronautics. https://doi.org/10.2514/6.2007-122

Wang, C. H. (2005). Experimental and Numerical Investigation of Aerospike Nozzle Aerodynamic Characteristics. *Beijing University of Aeronautics and Astronautics, Beijing*. Retrieved from http://scholar.google.com/scholar?cluster=3902001646482863962&hl=en&oi=scholarr

Wang, C.-H., Liu, Y., & Qin, L.-Z. (2009). Aerospike nozzle contour design and its performance validation. *Acta Astronautica*, *64*(11), 1264–1275. https://doi.org/10.1016/j.actaastro.2008.01.045

Wang, T.-S., Droege, A., D'Agostino, M., Lee, Y.-C., & Williams, R. (2004). Asymmetric Base-Bleed Effect on Aerospike Plume-Induced Base-Heating Environment. *Journal of Propulsion and Power*, *20*(3), 385–393. https://doi.org/10.2514/1.10385

Williams, F. A., Barrere, M., & Huang, N. C. (1969). *FUNDAMENTAL ASPECTS OF SOLID PROPELLANT ROCKETS* (No. AGARD-OGRAPH-116). ADVISORY GROUP FOR AEROSPACE RESEARCH AND DEVELOPMENT NEUILLY-SUR-SEINE (FRANCE), ADVISORY GROUP FOR AEROSPACE RESEARCH AND DEVELOPMENT NEUILLY-SUR-SEINE (FRANCE). Retrieved from http://www.dtic.mil/docs/citations/AD0701545

Wuye, D., Yu, L., Xianchen, C., & Haibin, T. (2001). Aerospike nozzle performance study and its contour optimization. In *37th Joint Propulsion Conference and Exhibit*. American Institute of Aeronautics and Astronautics. https://doi.org/10.2514/6.2001-3237